Mechanisms of Wave Manipulation in Nonlinear Periodic Structures

A DISSERTATION
SUBMITTED TO THE FACULTY OF THE GRADUATE SCHOOL
OF THE UNIVERSITY OF MINNESOTA
BY

R. Ganesh

IN PARTIAL FULFILLMENT OF THE REQUIREMENTS
FOR THE DEGREE OF

Doctor of Philosophy

Stefano Gonella, Adviser

December, 2015

Acknowledgements

First and foremost, I would like to thank my adviser, Prof. Stefano Gonella for having given me the opportunity to pursue my PhD in the interesting field of nonlinear periodic structures. His immense passion for work, attention to detail, and, never-ending enthusiasm to engage in academic and non-academic conversations have made my interactions with him a memorable experience, and has helped me grow leaps and bounds (professionally and personally) in this period.

I am also indebted to Prof. Ranjan Ganguli (Indian Institute of Science, IISc), who introduced me to the field of academic research. Prof. G. K. Ananthasuresh (IISc) gave me the opportunity to further experience academic research before embarking on my PhD, a venture which has helped my professional and personal development.

I am grateful for the financial support (including travel grants) from the Department of Civil, Environmental, and Geo- Engineering, Council of Graduate Students (UMN), and the National Science Foundation (NSF), which allowed me to attend and present my work at multiple conferences - an opportunity that has given me exposure to the research community at large.

While friends from India have made my stay in Minnesota "warm" and pleasant, my interactions with the technically and culturally diverse graduate student community in the Department of Civil, Environmental, and Geo- Engineering is something that I will cherish for the rest of my life.

Finally, I would not have been able to navigate through the tumultuous journey of pursuing a PhD without the sacrifice and contribution of my mother. Thank you for believing in me Amma!

सुखमापतितं सेव्यं दुःखमापतितं तथा।
चक्रवत् परिवर्त्तन्ते दुःखानि च सुखानि च॥

Accept Pains (Sorrow) as you would Pleasures (Happiness), for Pleasures and Pains have their revolutions like a wheel!

Abstract

Periodic structures have received conspicuous attention in recent years due to their inherent dynamic (phononic) characteristics that impart them the capability to function as mechanical filters or waveguides. In this regard, nonlinear periodic structures feature tunable phononic characteristics, and the ability to support unique features seldom observed in their linear counterparts. Therefore, the characteristics of propagating wave packets in nonlinear periodic structures are studied with the motive of leveraging the unique features associated with nonlinearity to achieve adaptive and tunable spatial wave manipulation. Specifically, the interplay of dispersion and nonlinearity is characterized for weakly nonlinear systems capable of supporting a wide variety of deformation patterns and crystal responses. To this end, multiple scale analysis of a simple nonlinear periodic structure is carried out under the assumption of small, but non-negligible nonlinear terms to establish the foundation for numerical exploration of a number of complex crystal configurations. It is observed that the primary effect of the interplay between nonlinearity and dispersion manifests as a modulation of the envelope of propagating wave packets. In the case of nonlinearity being represented by an equivalent quadratic nonlinear term, the envelope modulation is observed to result in the generation of a non-harmonic component in the response. This non-harmonic component can be quantitatively characterized as a function of the nonlinearity, and excitation parameters, thereby providing an alternate route to inversely measure nonlinear material properties from numerical or experimental data. This is demonstrated numerically by considering granular chains interacting through generic power law relations, and obtaining the imposed power law through the inverse problem set up for the corresponding periodic structure. The other important effect of nonlinearity is the generation of harmonics. The interplay of dispersion and nonlinearity in the generation

of harmonics gives rise to secondary wave packets with multiple characteristics. Particularly, one of the nonlinearly generated harmonic features characteristics that conform to the dispersive properties of the corresponding linear periodic structure. This provides an opportunity to engineer wave characteristics through the geometric and topological design of the unit cell, and results in the ability to activate complementary functionalities at low frequencies of excitation - effects seldom observed in linear periodic structures. The ability to design adaptive and tunable phononic switches are demonstrated using a number of periodic structure configurations which cover the entire gamut of nonlinear mechanisms realizable in elastic solids. Finally, an experimental characterization of harmonic generation is presented for the case of a nonlinear lattice by employing 3D Scanning Laser Doppler Vibrometry.

Contents

List of Tables

List of Figures

Chapter 1

Introduction

The motive of this dissertation is to understand the characteristics of finite-amplitude elastic wave propagation in periodic structures, and potentially leverage the unique features associated with nonlinearity to design tunable and adaptive spatial wave manipulators. The underlying assumption in this entire work is that the magnitude of wave propagation is small with respect to the length scale of the structure under consideration, albeit, large enough to incorporate the effects of finite deformation in these structures. The intention of this introductory chapter is to provide a brief insight into linear periodic structures and their unique dynamic (phononic) characteristics, which have been exploited by researchers to design systems that can serve as vibration filters and waveguides. Then, a concise history of nonlinear wave propagation in periodic structures is documented, with an emphasis on the technological applications conceived in recent years. Finally, the motivation for the current research and the organization of the rest of the dissertation is presented.

1.1 Periodic Structures

Periodic Structures are defined as structures constituted of discrete elements exhibiting a repetitive pattern. The repetitive pattern can be a manifestation of variation of geometric or material parameters of the structure, or a by-product of the boundary conditions imposed on the structure (as exhibited by the different examples in fig. 1.1). While the fundamental building block of natural or man-made materials (atoms and

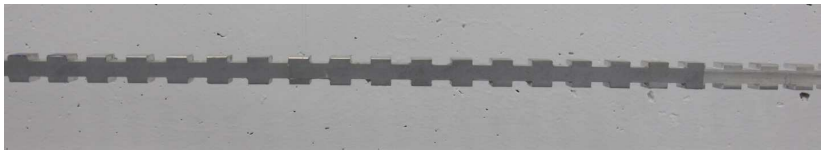

(a)

(b)

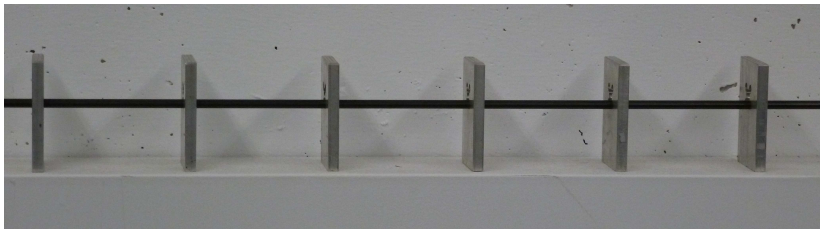

(c)

Figure 1.1: Examples of laboratory scale structures displaying periodicity - a) An Aluminum rod with periodically varying cross-section [36], b) A granular chain of Steel and PTFE spheres interacting through elastic contact, c) A periodically supported beam.

molecules) are essentially discrete entities, the length scale of this discreteness is much smaller when compared to the macroscopic dimensions of interest, typically allowing for a treatment of the macroscopic entity as a continuum. On the contrary, the length scale of the repetitive element in periodic structures is assumed to be comparable to the length scale of the structure, resulting in properties significantly different from that of the corresponding homogenized continuum. Such discrete structures are commonly found in a wide variety of natural and man-made structures. For example, Honeybees are known to build their nests with a hexagonal structure as shown in fig. 1.2a. Among man-made constructions, one of the most iconic structures, the Eiffel tower consists of a quasi-periodic repetition of truss elements with varying cross-sections[1], which imparts

[1]Technically, the Eiffel tower is called a hierarchical lattice, as it depicts lattice structures at different length scales - shown in the inset in fig. 1.2b.

the structure a very high stiffness to weight ratio. Another interesting periodic structure is the sculpture by Eusebio Sempere, displayed at the Juan March foundation in Madrid, which features interesting sound attenuation capabilities.

(a)

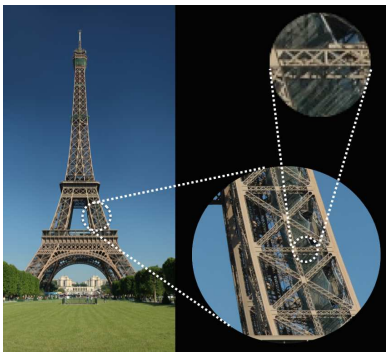

(b)

(c)

Figure 1.2: Examples of natural and man-made periodic structures - (a) Honeycomb structure[2], (b) Eiffel tower[3], (c) Kinematic Sculpture by Eusebio Sempere [87].

The notion of periodicity is often incorporated in the design of cellular solids (lattice structures with voids or multi-phase materials) that can exhibit very high stiffness-to-weight ratio when compared to their solid counterparts [2]. This design methodology follows the paradigm of mimicking the structure of atomistic scale of materials such as graphene, which consists of a single layer of carbon atoms arranged in a hexagonal packing, imparting it a strength of about 200 times that of steel [74].

In addition to the improved static properties, periodic structures also feature unique

[2] Photo by Giuliagi/Wikimedia.
[3] http://www.wired.com/2015/03/empzeal-eiffel-tower

dynamic characteristics, which will be covered in detail in the next two subsections.

1.1.1 Spectral Characteristics of Linear Periodic Structures

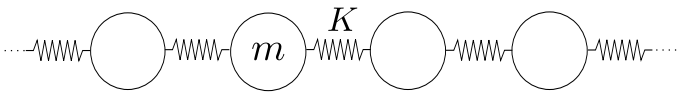

Figure 1.3: $1D$ monoatomic spring-mass chain

One of the first insights on dynamics of periodic structures is credited to Sir Isaac Newton, who used a $1D$ periodic spring-mass system to derive the velocity of sound in air. The same structure was later used by Lord Kelvin to establish the relationship between the spatial and temporal frequencies of wave propagation, commonly referred to as the *dispersion relation* of the structure [12]. For example, the dispersion relation of a $1D$ monoatomic spring-mass system shown in fig. 1.3 can be derived as

$$\omega = \sqrt{\frac{K}{m}}\sqrt{2 - 2\cos(k)}. \tag{1.1}$$

Eqn. (1.1) depicts a nonlinear relationship between the spatial (k) and temporal (ω) frequencies of wave propagation - a characteristic associated with dispersive systems. The interesting feature of eqn. (1.1) is that, beyond a particular frequency $\omega_c \left(= 2\sqrt{\frac{K}{m}}\right)$, the waves lose their spatial harmonicity, thereby leading to an attenuating characteristic (the amplitude decreases exponentially as the wave propagates through the structure). Therefore, this kind of a structure can be employed as a *low-pass filter*, in which, wave propagation with frequencies greater than the cut-off frequency is prohibited. By increasing the geometric or material distribution complexity of the periodic structure, it is possible to obtain band gaps in the dispersion relation (bounded frequency intervals within which waves are attenuated - fig. 1.4) in addition to the low-pass filter characteristics. Such a structure was realized using beams, springs, and masses in 1885 to depict one of the first mechanical filters designed using periodic structures [12].

The fundamental assumption in determining dispersion relations for periodic structures is that the response of the infinite structure can be completely captured by the

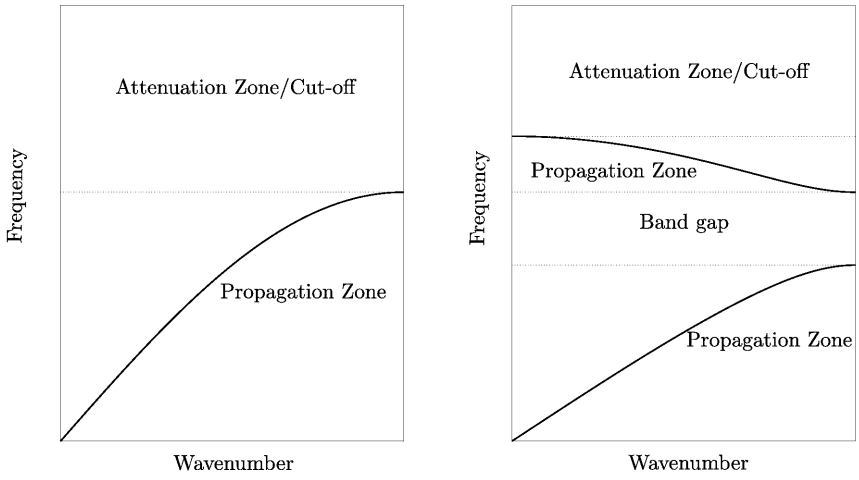

Figure 1.4: Band structure of a monoatomic and diatomic spring-mass chain.

response of a repetitive volume element (also referred to as the unit cell) up to a constant phase difference, i.e., the response of the repetitive volume element at two different locations in the structure can utmost differ by a constant phase. The ability to discern such solutions for $1D$ periodic structures was proved by Floquet in the context of $1D$ differential equations with periodic coefficients [49]. Separately, Bloch utilized the concept of crystallographic symmetries to establish the translational invariance in obtaining periodic solutions for $3D$ electronic waves in a solid state crystal [49]. Therefore, dispersion relations in periodic structures are commonly evaluated by application of the Floquet-Bloch theorem [71, 98].

In the case of multidimensional periodic structures, the frequency of propagation depends on all spatial components of the wave vector ($\mathbf{k}$), resulting in surfaces in the spectral domain referred to as phase constant surfaces, or simply, dispersion surfaces. However, the underlying symmetry of the periodic structure can be utilized to determine unique wavenumber combinations that characterize the complete spectral response of the system, referred to as the *Brillouin zone* [12]. Moreover, the symmetries of the unit cell geometry can be employed to further reduce the set of wavenumber combinations to the contour of the so called *irreducible Brillouin zone*, to elicit the complete spectral response of the periodic structure.

Since the location and width of the bandgaps depend on the material and geometric parameters of the repetitive volume element, significant research has been dedicated towards understanding the mechanisms of bandgap realization in a wide variety of materials and structures such as periodically supported $1D$ beams, perforated plates, $2D$ honeycomb, auxetic, re-entrant lattices, and $3D$ solid sphere inclusions [51, 57, 70, 71, 87, 98, 115, 117]. Excellent reviews documenting the entire gamut of research on the spectral characteristics of periodic structures has also been carried out by various authors [62, 89, 116].

The phenomenon of complex interference patterns experienced by propagating waves at the heterogeneous interface between unit cells in a periodic structure is referred to as Bragg-scattering, which in extreme scenarios gives rise to the introduction of bandgaps in the dispersion curves/surfaces. Another route to realize bandgaps in the dispersion relation of periodic structures is by the inclusion of locally resonant elements [55, 80]. A recent example of locally resonant bandgaps realized in LEGO® based metamaterials carried out by Celli and Gonella [20] is illustrated in fig. 1.5. In such structures, the formation of the bandgap is attributed to the localization of energy in the form of oscillatory motion of the resonant elements, thereby resulting in net subtraction of energy from the periodic medium. As a result, these structures can be employed for energy harvesting if suitable mechanisms can be embedded in the resonant element to harvest their vibrational energy. One such idea was proposed by Gonella et al. [52], who considered honeycomb structures featuring periodically distributed stiff cantilever beams provided with piezoelectric electrodes to convert the resonant energy of the beams to electrical energy.

1.1.2 Spatial Characteristics of Linear Periodic Structures

Being dispersive systems, periodic structures are also characterized by frequency dependent phase velocities (velocity of the wave $c = \omega(k)/k$), which gives rise to interesting phenomena in the spatiotemporal domain. For example, in a $1D$ periodic structure, the equation of a propagating wave packet consisting of two neighboring frequency components (k, ω and $k + \Delta k, \omega + \Delta\omega$) can be expressed as [54]

$$u \approx A \sin\left(\frac{\Delta k}{2}x - \frac{\Delta\omega}{2}t\right) \sin\left(kx - \omega t\right). \tag{1.2}$$

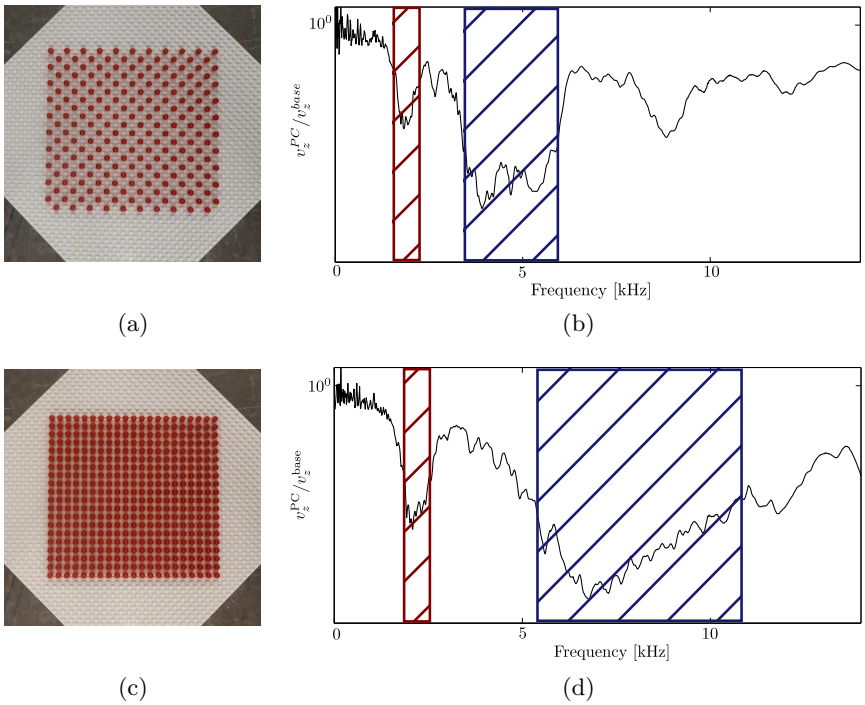

Figure 1.5: Band gap realization using locally resonant elements - (a) and (c) depict a LEGO® plate with periodically inserted cylindrical bricks (with different spacing), while (b) and (d) show the corresponding frequency response function. Two bandgaps are observed in these structures - one corresponding to the periodicity of the inclusion, whose location depends on the unit cell dimension, while the other corresponding to the resonance motion of the brick remains constant in both the cases [20].

Since $\Delta k, \Delta\omega$ are assumed to be small quantities, the effect of dispersion can be characterized as an amplitude modulation of a propagating wave packet with carrier frequency k, ω. In the limit of Δk, $\Delta\omega \to 0$, the amplitude modulation travels with a speed referred to as the group velocity of the wave packet ($c_g = d\omega/dk$). This phenomenon is also referred to as beating, and has important practical consideration since traveling excitations seldom consist of monofrequency content. The compact nature of any wave packet implies that the frequency spectrum typically consists of a number of frequencies centered around a carrier frequency, whose amplitudes can be controlled by choosing an appropriate form of narrow-band pulse. Such pulses are typically assumed to be traveling waves translating at the group velocity of the wave packet [54].

When wave propagation in multidimensional periodic structures is considered, the

velocity of propagating waves are also dependent on the direction of propagation of the incident waves (dictated by the orientation of the wave vector $\mathbf{k}$). Therefore, the spatial characteristics of propagating waves are determined by monitoring the directional dependence of the phase and group velocity characteristics of the wave packet [106]. The phase velocities are determined from the isofrequency contours (the possible combinations of the spatial frequency $\mathbf{k}$ for any temporal frequency ω such that the dispersion relation $f(\mathbf{k}, \omega) = \mathbf{0}$ is satisfied), which in turn provides information on the spatial characteristics of the propagating wave packet [51]. The gradient of the dispersion surfaces sampled at the isofrequency contours of interest depict the group velocity contours, which typically signify the preferential directions for energy flow in the structure. Furthermore, for specific geometries of the unit cell, it is possible to obtain cusps in the group velocity contours, commonly referred to as caustics, which imply significant focusing of the energy along the preferential direction [72, 120]. An example of such frequency-dependent spatial directivity is illustrated for a monoatomic $2D$ spring-mass triangular lattice in fig. 1.6.

Unfortunately, the underlying symmetry of the unit cell implies that the preferential directions of wave propagation also feature the same symmetry. This can be overcome by introducing additional microstructure [18] in the unit cell to obtain wave focusing along a single direction which can then be employed for potential applications such as acoustic radars [103]. Alternately, spatial directivity (wave guiding) can also be obtained in phononic crystals operating in the attenuating regime by considering locally resonant periodic structures interspersed with strategically introduced defects along the required wave-path [66].

Despite the unique spectro-spatial characteristics observed in linear periodic structures, the possible applications of such structures are limited due to their passivity, i.e., for a given geometry, material, and/or boundary conditions, the bandgaps and spatial directivity patterns are fixed. Therefore, researchers have explored a multitude of avenues to achieve tunability of the spectro-spatial characteristics of periodic structures. One particular avenue is to incorporate finite-deformation elastic effects, and such structures will be referred to as nonlinear periodic structures in this dissertation. The unique aspect of pursuing nonlinear periodic structures is that they also feature the ability to support phenomena seldom observed in linear periodic structures, thereby leading to

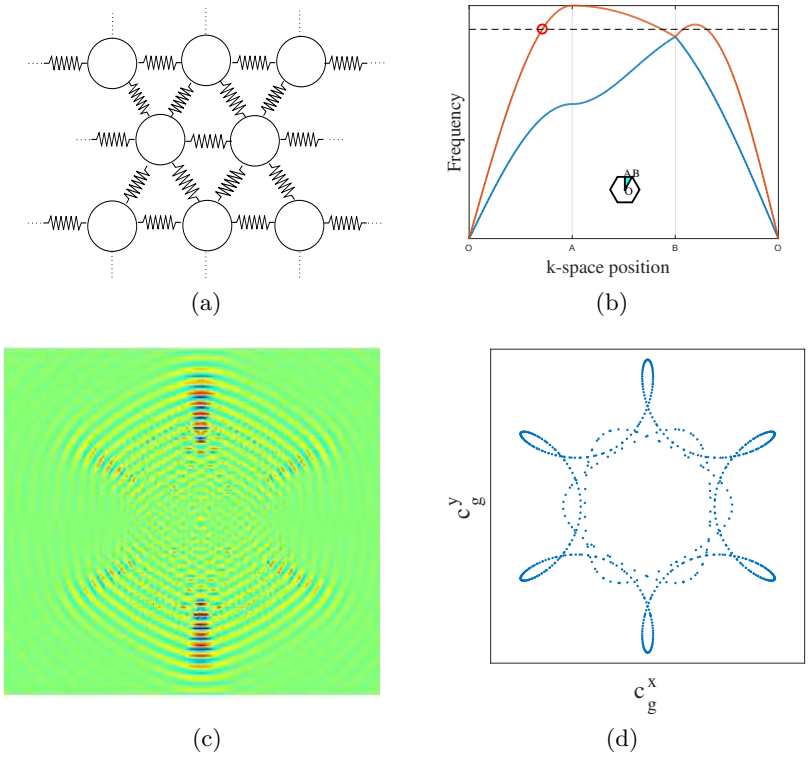

Figure 1.6: Spatial directivity in a $2D$ periodic structure - (a) A monoatomic triangular spring-mass lattice, (b) Band diagram calculated along the contour of the irreducible Brillouin zone, (c) Radial component of spatial wavefield, which shows preferential directions for wave propagation, (d) Group velocity contours at the chosen excitation frequency.

interesting applications, which will be discussed in detail in the next section.

1.2 Nonlinear Periodic Structures

The simplest case of a nonlinear periodic structure is a $1D$ chain of masses connected by springs with a nonlinear constitutive relation. A full study of such nonlinear systems were first carried out by Fermi et al. [41] to study the thermal ergodicity of the system, i.e., the equipartition of thermal energy among the normal modes of the system due to nonlinear self-interaction. Interestingly, it was found that the initial energy imparted to the system did not lead to equipartition, and actually returned to the initial mode of excitation. Zabusky and Kruskal [133] investigated this phenomenon by employing

a continuum approximation for the anharmonic chain (also referred to as FPU chains), which led to the Korteweg-de Vries (KdV) equation[4]. They observed that the solitary wave solutions for the KdV equation possessed the unique property of preserving their shape and speed after collision with one another, which supported the recurrence effect observed numerically by Fermi et al. [41].

A continuum approximation is typically utilized to analyze discrete nonlinear systems (periodic structures) as most systems do not posses an exact solution - commonly referred to as non-integrable lattices [104, 129]. However, there do exist few integrable lattices, the most prominent example being the Toda Chain [125], which is governed by an exponential interaction potential. While the continuum approximation in terms of a generalized-KdV equation is the most common form of analysis for discrete systems, the Boussinesq equation can also be employed by eliminating the assumption of unidirectional waves [78].

The drawback of using continuum approximations is that they can only model long-wavelength excitations. Zabusky and Deem [134] studied the short-wavelength regime by utilizing the phase difference of two consecutive masses to separate the odd and even masses, and employed a continuum approximation independently for these two sets of masses. It has been observed that nonlinear lattices feature solutions with solitonic characteristics even outside the long-wavelength regime. For a $1D$ monoatomic chain, a rough classification of solitary waves can be made among *kink, breather, envelope and dark solitons*, all of which have been numerically observed in monoatomic chains with anharmonic potentials [43]. Various researchers have also proved the mathematical existence of such solitary waves in lattices using variational calculus and classified the different families of solitary waves in these lattices [37–40, 44].

While solitons have been observed in a wide variety of mechanical systems, one of the most studied example are granular chains. In the simplest form, a granular chain is a $1D$ chain of particles interacting through elastic contact. Under the assumption that the elastic contact does not cause significant deformation of the materials at locations far from the contact itself, the system can be modeled as a spring-mass system with the force-displacement relationship derived from Hertzian theory [65]. For two elastic

[4]Originally, the Korteweg-de Vries equation was derived to model unidirectional propagation of shallow-water waves [101].

spheres in contact, the force-displacement relationship of the equivalent spring can be expressed as $F \propto \delta^{1.5}$. In addition to the intrinsically nonlinear response, granular systems also feature asymmetrical response, i.e, they can support only compressional waves as forces cease to exist when particles are no longer in contact. A systematic study of such systems was first carried out by Nesterenko [94], who obtained an analytical expression for the solution in the long-wavelength limit. This solution showed features similar to that of a solitary wave and was verified experimentally, first by Lazaridi and Nesterenko [73], and later by Coste et al. [25]. The seminal work of Nesterenko [94] has led to an explosion of interest in granular chains, particularly towards the analysis of solitary wave solutions in a wide variety of systems composed of different materials and/or geometries, and multiple dimensions [15, 17, 22, 26–28, 63, 64, 75, 83, 100, 108, 111, 121]. These unique properties can be leveraged to employ granular crystals in applications such as stress-wave mitigation [76], non-destructive evaluation [132], acoustic lensing [35, 119] etc.

Another interesting property of nonlinear lattices known as *Intrinsic Localized modes* or *Discrete Breathers* was discovered by Sievers and Takeno [114]. Discrete Breathers are time-periodic localized solutions that are supported by anharmonic lattices. These can also be viewed as the counterpart of localized modes observed in harmonic lattices with defects [114]. The existence of discrete breather solutions have been theoretically studied in FPU lattices [6, 42], and experimentally observed in precompressed diatomic granular chains [7]. Furthermore, such localized excitations typically display instability with respect to a perturbation of the amplitude, a feature which is denoted as *Modulational Instability* [67, 101]. Discrete breathers and modulational instability lead to energy localization, which can also be viewed as a manifestation of the interplay between nonlinearity and discreteness [16, 29, 97].

1.2.1 Adaptive Nonlinear Periodic Structures

Nonlinear periodic structures also exhibit significant differences in their phononic characteristics with respect to their linear counterparts. The nonlinearity in the system imparts an amplitude-dependent characteristic to the dispersion relation. This amplitude-dependence typically corresponds to a modification of the propagation and attenuation zones of the structure. The most common approach to determine the dispersion relation

is based on the application of the *Lindstedt − Poincaré* perturbation technique under the assumption that the contribution of the nonlinear terms to the response are much smaller in magnitude with respect to the contribution of the linear terms [3, 21, 81, 92]. The dispersion relation can be obtained by applying the perturbation theory for either the wavenumber or the frequency. Askar [3] obtained the dispersion relation for a monoatomic lattice with cubic and quartic nonlinear potentials while Narisetti et al. [92] obtained the dispersion relation for a quartic potential (cubic nonlinearity) by applying the perturbation expansion for the displacement and the frequency. Chakraborty and Mallik [21] obtained a dispersion relation by expanding the wavenumber instead of the frequency. In all cases, the change in cutoff frequency was observed to depend on the magnitude of nonlinearity as well as on the amplitude of the initial excitation.

The *Lindstedt − Poincaré* technique can also be applied to multi-degree of freedom systems and this has been carried out by Narisetti et al. [91], who showed that the spatial characteristics of the structure, depicted by the phase and group velocity contours also feature amplitude-dependent behavior. This was later generalized for any periodic structure modeled using finite elements by Manktelow et al. [85]. The assumption employed in the *Lindstedt − Poincaré* method is that the excitation is monochromatic. However, if the excitation consists of multiple harmonics, then the interaction of the harmonics affects the dispersion relations, which can be determined by employing a multiple scales technique [84, 86]. While most of the research in literature is focussed on the weakly nonlinear regime, some studies have also considered strongly nonlinear systems. Abedinnasab and Hussein [1] derived exact dispersion relations for nonlinear wave propagation in rods and beams, while Narisetti et al. [93] obtained dispersion relations for strongly nonlinear periodic structures by employing the Harmonic Balance method.

The amplitude-dependent phononic characteristics of nonlinear periodic structures can be exploited to design adaptive or actively-tunable vibration filters[5], i.e., systems that can autonomously modulate the characteristics of propagating waves depending upon the operating conditions. For example, the cut-off frequency of a monoatomic

[5]These structures are generically referred to as tunable systems in published literature, however, the prefix "active" is added to denote the closed loop or feedback oriented nature of tunability. This contrast is necessary to distinguish another form of tunability (passive) covered later in this chapter.

spring-mass chain with softening cubic nonlinearity decreases with increasing amplitude (shown in fig. 1.7). Therefore, if such a system is employed in applications where the operating frequency is close to the cut-off frequency of the structure, then the amplitude of the excitation will determine if the excitation has propagating or attenuating characteristics. Narisetti et al. [92] have demonstrated that, by altering the complexity of the nonlinear structure, the amplitude-dependency of the dispersion relation can be employed in a wide variety of vibration isolation applications.

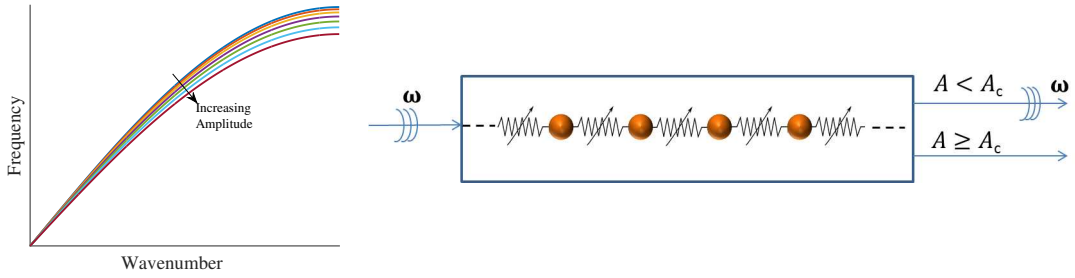

(a) (b)

Figure 1.7: (a) Dispersion curve of nonlinear spring-mass chain with softening nonlinearity which shows a decrease in cutoff frequency with increasing amplitude. (b) Example of an adaptive filter employing this chain, where the amplitude of wave packet will determine its spectro-spatial characteristics [92]

In linear periodic structures, the primary effect of dispersion is to modulate the envelope of propagating wave packets, which propagate at the group velocity of the wave packet. Additionally, when wave propagation over large distances are considered, the difference in phase velocities of the different harmonics constituting the wave packet also leads to a spatial distortion of the wave packet, which can be modeled using a multiple scale expansion. The amplitude modulation for a linear dispersive system in such long time scales is governed by the Linear Schrödinger equation [101]. In contrast, the amplitude modulation in the presence of nonlinear terms is modeled by the Nonlinear Schrödinger equation. The Nonlinear Schrödinger equation was first derived for a $1D$ nonlinear lattice by Taniuti and Yajima [123]. Expressing the amplitude modulation with the Nonlinear Schrödinger equation is advantageous as the equation can be solved exactly by the inverse scattering transform method. This was carried out by Shabat and Zakharov [112], who showed that the equation possessed a solitary wave solution. Therefore, the amplitude modulation of propagating excitations in nonlinear lattices are

commonly referred to as *envelope solitons*. The technique of multiple scales introduced by Taniuti and Yajima [123] has been used ubiquitously to address a wide range of problems such as determination of envelope modulation in electrodynamic nonlinear periodic structures [31] and nonlinear spring-mass lattices [45, 58, 124, 127, 128], to determine interaction characteristics of nonlinear modulated waves in Klein-Gordon systems [96], to determine gap solitons and intrinsic localized modes [59, 60] etc. The validity of the Nonlinear Schrödinger equation as a good approximation to describe the dynamics of propagating wave packets has also been theoretically established for a number of periodic structures [13, 23, 24, 109, 110]. However, to the best of the author's knowledge, a multiple scales treatment for spatial characteristics of wave propagation in nonlinear periodic structures has not percolated to the phononic crystals community.

Another effect of nonlinearity is the generation of super- and sub-harmonics in the response due to the self-interaction of the applied excitation. Zarembo and Krasil'Nikov [135] used perturbation analysis to show that finite-amplitude wave propagation in elastic solids is accompanied by the generation of harmonics. Furthermore, they showed that the nonlinearly generated second-harmonic was dependent on the higher order nonlinear parameters and grew in proportion to the propagation distance, which was experimentally observed in annealed or neutron irradiated copper single crystals by Breazeale and Ford [11]. These two studies considered only longitudinal wave motion in the solid; the effects of finite-amplitude shear wave motion and the interaction of longitudinal and shear wave motion have also been studied and are documented in [95]. It is important to note that all these studies consider nondispersive wave motion.

In dispersive systems, the ability to propagate higher-harmonics is governed by the availability of dispersion branches in the frequency range of the activated harmonics. This was demonstrated for nonlinear lamb wave propagation in isotropic plates by Deng [32] and de Lima and Hamilton [30]. In general, the generated higher-harmonics display oscillatory, bounded characteristics corresponding to the dispersion relation of the structure under consideration. However, the higher-harmonics become unbounded when resonance conditions are satisfied, i.e., when the fundamental- and the second-harmonic have the same phase velocity. This cumulative generation of second-harmonic has been observed experimentally in isotropic elastic plates [34, 88], thereby providing a route to experimentally measure nonlinear parameters using guided wave testing [4, 33].

Bradley [10] studied the generation of higher-harmonics in a nonlinear periodic waveguide by modeling the nonlinear fluid using the modified Westervelt equation and demonstrated experimentally the generation of spatially beating (bounded oscillation) second harmonic in an air-filled waveguide. The analysis of the Westervelt equation as a means to understand the dynamics of interaction of dispersion and nonlinearity in fluid systems has been extensively studied by various authors and an excellent review is available in [56]. For acoustic wave propagation in strongly precompressed monoatomic granular chains, Sánchez-Morcillo et al. [107] obtained an expression for the amplitude of the second-harmonic generated due to nonlinearity. The generation of higher-harmonics in a diatomic chain has also been studied theoretically and experimentally by Cabaret et al. [14]. In all these cases, the generated second-harmonic was considered to be non-resonant with the fundamental-harmonic. The case of resonances needs to be treated separately using the condition of three-wave-interaction and this has been analyzed for generic dispersive hyperbolic differential equations [109] and periodic lattices [50, 68]. In addition, nonlinearity also gives rise to sub-harmonics, which has been determined in precompressed monoatomic granular chains by Tournat et al. [126].

Nonlinearity in conjunction with phononic structures has been pursued as a potential avenue to break the spatial reversal symmetry of wave propagation - a feature that can be described as the elastic equivalent of an electric diode. However, nonlinearity is decoupled from the phononic characteristics of the structure, i.e., the effects of nonlinearity and periodicity act as independent entities. An example of this device was proposed by Liang et al. [79], who considered a $1D$ structure consisting of a nonlinear medium coupled to a superlattice (shown in fig. 1.8a). If the end of the structure with the nonlinear medium is excited with a frequency in the band gap of the lattice structure, only the nonlinear harmonics generated due to self-interaction propagate through the superlattice and reach the other end. However, if this end of the structure is excited at the same frequency, the superlattice prohibits the propagation of the driving frequency through the structure, thereby imparting the equivalent effect of rectification. Similarly, Boechler et al. [8] consider a finite strongly-precompressed monoatomic granular chain with a single defect located at one end (shown in fig. 1.8b). While driving the system at the non-defect end with a frequency in the attenuation region of the chain, no transmission of the excitation is observed. However, when the system is deployed

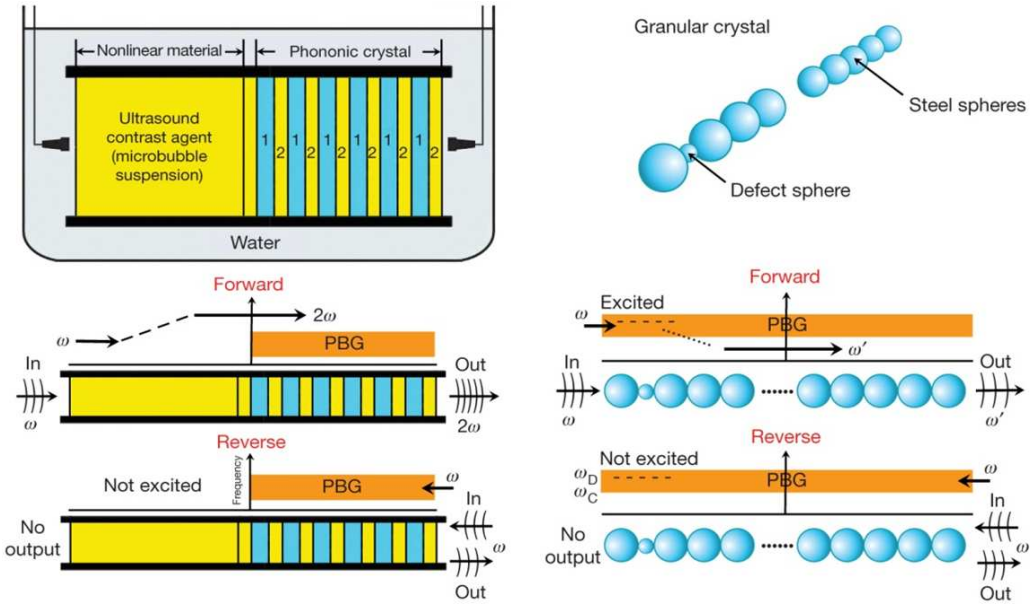

(a) Acoustic Diode [79] (b) Acoustic Rectifier [8]

Figure 1.8: Schematic describing structures realized to break spatial reversal symmetry of wave propagation [82].

in the reverse configuration, with the excitation applied to the end with the defect, localized modes featuring amplitude-dependent characteristics are observed due to the defect. Therefore, such a structure also functions as an acoustic rectifier.

In contrast, Li et al. [77] used the intrinsic nonlinearity of a periodic structure to design logic switches. They consider a monoatomic granular crystal being driven at a frequency (f_0) in the bandgap of the chain. However, if an additional control frequency (f_c) can be imparted along with the driving frequency, then linear combinations of the driving frequency and the control frequency ($mf_0 \pm nf_c$) can propagate through the structure. Furthermore, if the amplitude of the driving frequency is large enough, higher order harmonic generation will lead to the driving frequency propagating through the structure. Therefore, by controlling the state of the control frequency (on/off), it is possible to alter the propagation of energy through the structure.

1.2.2 Tunable Nonlinear Periodic Structures

In solids capable of supporting finite deformations, the characteristics of small amplitude wave propagation superimposed on static finite-deformations are significantly affected by the magnitude of the finite-deformation effects. In isotropic solids, this is typically captured as a stress-dependence of the velocity of propagating waves and is referred to as *acoustoelasticity*. Hughes and Kelly [61] used this stress dependence of the longitudinal and shear wave velocities in a solid subjected to hydrostatic pressure and uniaxial compression to determine experimentally the second order elastic constants of a number of materials. Daraio et al. [27] observed a similar effect with respect to the dependence of the speed and shape of solitary waves on the precompression force applied on a confined monoatomic granular chain. It is well known that granular chains can be modeled as FPU lattices in the limit of strong precompression (displacements much smaller than the static precompression applied to the structure). In this limit, the cutoff frequency of the corresponding chain is dependent on the magnitude of the applied precompression force. Therefore, by controlling the applied precompression force, the cutoff frequency of the chain can be tuned, which has been demonstrated experimentally in a $1D$ diatomic granular crystal by Boechler et al. [9].

(a) Adaptive or Actively-Tunable (b) Passively-Tunable

Figure 1.9: Schematic of structural logic for active and passive tuning of spectro-spatial characteristics of nonlinear periodic structures.

Along these lines, Bertoldi and Boyce [5] considered an elastomeric periodic structure featuring a square array of circular holes, and studied the propagation characteristics of small-amplitude waves superimposed on large static precompressions. They observed that the system showed instabilities under the application of large static forces, which produced pattern transformation of the structure characterized by a different irreducible unit cell. As a result of these pattern transformations, new bandgaps were introduced in the dispersion diagram of the structure. This type of reversible pattern transformation

has also been exploited to design structures with tunable band gaps and directionality features [5, 113, 130].

The mechanisms considered above do not affect the excitation directly, rather they provide an avenue to change certain features of the structure such that the output for a given excitation can feature a wide spectrum of characteristics. Therefore, such effects can be classified as passive tunability of the periodic structure (fig. 1.9). In addition to elastic tunability, researchers have also employed a multitude of alternate routes such as electricity [19, 131], magnetism [102] and thermal shape transformation [105] to achieve passive tunability of the properties of the periodic structure.

1.3 Motivation and Outline of the dissertation

In the literature on phononic crystals, the emphasis on nonlinearity has been typically towards achieving passive tunability, i.e., the ability to alter the state of the system in situ to modify the characteristics of propagating excitations, or, to exploit the unique features of nonlinearity such as solitary waves and discrete breathers. Recently, effort has also been directed towards realizing adaptive structures which can autonomously modify the spectral characteristics (propagating/attenuating) of wave propagation. However, in this regard, the effect of nonlinearity on altering the *spatial* characteristics of propagating excitations has been only marginally explored. While most studies have looked at the theoretical understanding of waves in nonlinear structures, the interplay of nonlinearity and dispersion in the spatiotemporal regime has not been fully decoded. Therefore, the motivation of this work is to elucidate the spatial characteristics of propagating wave packets in weakly nonlinear periodic structures, in the entire region of propagation (First Brillouin Zone). Specifically, the goal is to unravel the unique effects of nonlinearity on spatial wave manipulation, which can potentially be employed for engineering applications.

In the first part of this work, a multiple scale analysis of the equations of motion of a simple nonlinear spring-mass chain with quadratic and cubic nonlinearity is considered to facilitate the theoretical analysis of the fundamental effect of nonlinearity on wave propagation. Then, the same system is studied using full-scale numerical simulations and the evolution of signals with plane-wave features are monitored. Signal

processing techniques such as wavenumber filtering are applied to highlight the features of wave propagation, and topological wave packet descriptors are determined from the spatiotemporal evolution of the input excitation. The numerical features are compared with the analytical results available in published literature, and the quantitative effect of nonlinearity is determined in terms of wave packet descriptors, which can be viewed as estimators of nonlinear parameters. The versatility of utilizing a numerical approach is then demonstrated by considering different granular crystals and employing the wave packet descriptors to inversely determine the power law characterizing the contact interaction in granular crystals.

In the second part of this work, the multiple scale analysis is extended to a $1D$ diatomic spring-mass chain to elucidate the higher order effects of nonlinearity on wave propagation. Then, a strategy for spatial and modal wave manipulation in nonlinear periodic structures is developed, which revolves around the concept of modal mixing, whereby, the generation of higher harmonics in crystals with complex modal structures are utilized to induce jumps in the response across the available propagation modes. As a result, the system experiences a blend of modes and the simultaneous activation of complementary functionalities. This approach based on modal mixing features the ability to yield a wide variety of functional configurations without changes in the shape, size or topology of the nonlinear phononic crystal. To demonstrate the versatility of this approach, a family of granular crystal configurations and nonlinear lattice structures featuring a variety of wave control functionalities are studied.

The outline of the rest of the dissertation is as follows

- Chapter 2 introduces the multiple-scale formalism for weakly nonlinear spring-mass chains, and numerical results of these chains are elaborated to determine the invariants of nonlinearity. The numerical results of this chapter are partly derived from "**R. Ganesh and S. Gonella. Spectro-spatial wave features as detectors and classifiers of nonlinearity in periodic chains. *Wave Motion*, 50(4):821–835, June 2013**"

- Chapter 3 utilizes the invariants of nonlinearity to inversely determine the power

law interaction governing contact mechanisms in monoatomic and diatomic granular chains. This chapter is adapted from "**R. Ganesh and S. Gonella. Invariants of nonlinearity in the phononic characteristics of granular chains. *Phys. Rev. E*, 90:023205, Aug 2014**"

- In Chapter 4, the multiple scale formalism is extended to the diatomic chain to showcase the unique phenomena associated with nonlinear periodic structures featuring complex dispersion characteristics. Then a preliminary spring-mass example is elucidated to showcase the concept of adaptive modal switching.

- Chapter 5 demonstrates mode hopping and modal mixing phenomena in granular phononic crystals and nonlinear lattice structures. In the case of nonlinear lattice structures, experimental validation of a simple nonlinear lattice using $3D$ Scanning Laser Vibrometry is also presented. The details on granular phononic crystals are adapted from "**R Ganesh and S Gonella. From modal mixing to tunable functional switches in nonlinear phononic crystals. *Physical review letters*, 114(5):054302, 2015**".

- Chapter 6 summarizes the observations made in this dissertation.

Chapter 2

Wave Propagation in Weakly Nonlinear Periodic Structures

The primary objective of this dissertation is to delineate the characteristics of propagating wave packets in weakly nonlinear periodic structures. To this end, a $1D$ traveling wave in a linear dispersive system can be represented as

$$u(x,t) = Ae^{i(kx-\omega(k)t)}.$$

However, the compact nature of the wave packet implies that the spectral signature is spread over a band of frequencies rather than being monochromatic. Therefore, the equation of a traveling wave packet can be written as

$$u(x,t) = \int_{-\infty}^{\infty} F(k)e^{i(kx-\omega(k)t)}dk = \int_{k_0-\Delta k_0}^{k_0+\Delta k_0} F(k)e^{i(kx-\omega(k)t)}dk\,, \tag{2.1}$$

where $F(k)$ is the Fourier amplitude corresponding to a specified wavenumber k. $F(k)$ is assumed to be non-zero only in a limited band of spatial frequencies $[k_0 - \Delta k, k_0 + \Delta k]$, and ω (for every k) can be determined from the dispersion relation $\omega = f(k)$. Traveling waves with this frequency signature can be obtained by employing probe excitations consisting of a carrier frequency (ω_0/k_0) modulated by a long-wavelength envelope such that the spectral signature is limited to a small band ($\Delta\omega/\Delta k$ - shown in fig. 2.1). Within this frequency band, the equation of the wave packet can be simplified

by employing a Taylor series expansion for the frequency (ω) in the neighborhood of the carrier frequency ($\omega_0 = \omega(k_0)$) as

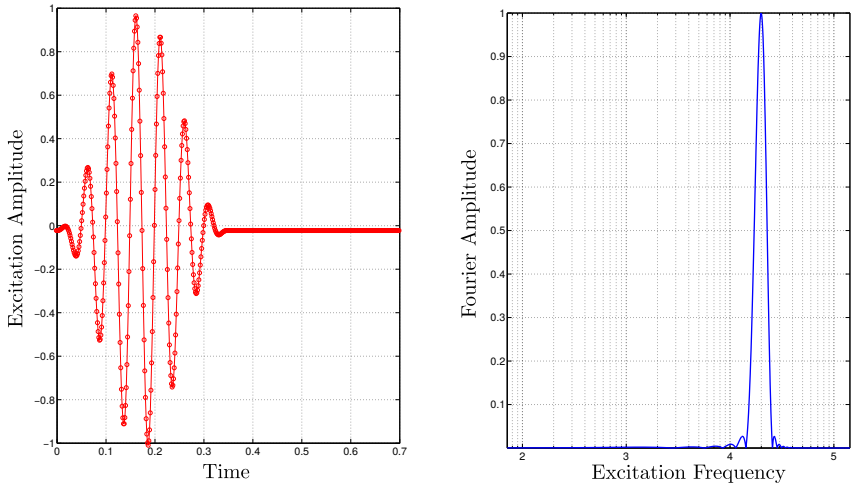

Figure 2.1: Spatial and spectral representation of tone burst.

$$\omega(k) = \omega(k_0 + \chi) = \omega_0 + \left.\frac{d\omega}{dk}\right|_{k_0} \chi + \left.\frac{d^2\omega}{dk^2}\right|_{k_0} \chi^2 + \cdots . \tag{2.2}$$

Substituting eqn. (2.2) in eqn. (2.1),

$$\begin{aligned} u(x,t) &\approx e^{i(k_0 x - \omega_0 t)} \int_{-\Delta k_0}^{\Delta k_0} F(k_0 + \chi) e^{i(\chi x - \omega'(k_0)\chi t - \omega''(k_0)\chi^2 t)} d\chi \\ &= A(\chi(x - \omega'(k_0)t), \chi^2 \omega''(k_0)t) e^{i(k_0 x - \omega_0 t)}, \end{aligned} \tag{2.3}$$

where $\omega' = d\omega/dk$ and $\omega'' = d^2\omega/dk^2$. Since χ corresponds to a perturbation of the carrier frequency, the variable $\chi(x - \omega' t)$ can be considered as a spatiotemporal variable of $\mathcal{O}(\varepsilon)$, where $\varepsilon << 1$. Therefore, the fast oscillations ($e^{i(k_0 x - \omega_0 t)}$) in eqn. (2.3) are invariant in the spatiotemporal space $x - c_p t$, where $c_p = \omega_0/k_0$ corresponds to the phase velocity of the propagating wave packet. The slow spatiotemporal scale $\varepsilon(x - \omega' t)$ corresponds to a frame of reference translating at a speed given by the group velocity ($c_g = d\omega/dk$), evaluated at the carrier frequency of the wave packet. This variable captures the group velocity dependence of the amplitude envelope of the wave packet. In addition, the envelope of the propagating wave packet also depends on the variable

$\varepsilon^2 t$, which corresponds to a slow time scale. Thus, the envelope of the wave packet can be assumed to be a traveling wave that varies on a very slow time scale of $\mathcal{O}(\varepsilon^2)$. This description of the wave packet is consistent with the property of dispersive systems ($c_g \neq c_p$), where different spectral components of the wave travel at different speeds, thereby leading to a distortion/broadening of the propagating waveform in a slower temporal scale [101].

In weakly nonlinear systems, the contribution of the nonlinear terms to the response are assumed to be $\mathcal{O}(\varepsilon)$. This weakness could be a result of the material property of the system, or due to the magnitude of the propagating waves, which in turn determines the strength of the nonlinear contribution. As a result of weak nonlinearity, eqn. (2.3) could possibly be employed to express propagating wave packets in such systems. Therefore, in this chapter, the equation for a propagating wave packet in weakly nonlinear periodic structures will be derived using a multiple scale expansion of the equations of motion, and, these results will be analyzed quantitatively using numerical simulations to characterize the effect of weak nonlinearity on wave propagation.

2.1 Weakly Nonlinear Spring-Mass Chains

Consider a spring-mass system as shown in fig. 2.2. The potential energy of the spring is assumed to be nonlinearly dependent on the change in length of the spring. However, under the assumption of small displacements with respect to the equilibrium position of the masses ($\delta \approx \mathcal{O}(\varepsilon)$), the restoring force in the spring can be expressed using a Taylor series expansion as

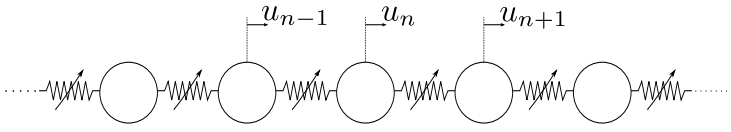

Figure 2.2: $1D$ Nonlinear monoatomic spring-mass chain

$$f_r(\delta) \;=\; K_2\,\delta \;+ K_3\,\delta^2 + K_4\,\delta^3 + \mathcal{O}(\varepsilon^4), \tag{2.4}$$

where f_r is the restoring force in the spring for a change in length of the spring δ. K_2, K_3, K_4 are the equivalent linear, quadratic, and cubic spring constants determined

from the Taylor series expansion. The number of terms that need to be retained in the Taylor series expansion depend on the magnitude of the displacements established in the springs. Using this constitutive relation, the governing equation for free vibration of the n^{th} mass can be derived as

$$\begin{aligned} m\,\ddot{u}_n \;+\; K_2\,(2\,u_n - u_{n-1} - u_{n+1}) \;+\; \varepsilon\,K_3\,[(u_n - u_{n-1})^2 - (u_{n+1} - u_n)^2] \\ +\; \varepsilon^2\,K_4\,[(u_n - u_{n-1})^3 - (u_{n+1} - u_n)^3] \;=\; 0, \end{aligned} \tag{2.5}$$

where u_i corresponds to the displacement of the i^{th} mass, and the approximation $u \approx \mathcal{O}(\varepsilon)$ has been incorporated to establish the relative orders of the terms in the equation. Due to the weak nature of the nonlinear terms, the solution to eqn. (2.5) can be written using a perturbative expansion as the sum of progressively smaller traveling wave packets. Under the assumption that the traveling wave at each order of expansion can be expressed in the form of eqn. (2.3), the axial displacement of the n^{th} mass can be written as

$$u_n(t) \;=\; \sum_{i=0}^{\infty} \varepsilon^i u^i(\theta_n, \xi_n, \tau), \tag{2.6}$$

where $\theta_n = kn - \omega(k)t$, $\xi_n = \varepsilon(n - c_g t)$, and $\tau = \varepsilon^2 t$. In order to find a solution for $u(n,t)$, it is necessary to convert the discrete partial differential equations (eqn. (2.5)) to a set of ordinary differential equations. The slowly-varying spatiotemporal variable ξ_n leads to the introduction of new variables in the multiple scale expansion ($\theta_{n\pm1}$, $\xi_{n\pm1}$). However, the long-wavelength nature of the slow spatiotemporal variable ξ_n can be exploited to perform a truncated Taylor series expansion of the displacement in terms of ξ_n as

$$u_{n\pm1}(\theta_{n\pm1}, \xi_{n\pm1}, \tau) = u_{n\pm1}(\theta_{n\pm1}, \xi_n, \tau) \pm \varepsilon \frac{du_{n\pm1}}{d\xi_n}(\theta_{n\pm1}, \xi_n, \tau) + \frac{1}{2}\varepsilon^2 \frac{d^2 u_{n\pm1}}{d\xi_n^2}(\theta_{n\pm1}, \xi_n, \tau). \tag{2.7}$$

At the fast spatiotemporal scale (θ_n), Bloch-Floquet conditions can be used to simplify the dependence of the neighboring displacements ($u_{n\pm1}$) in terms of u_n as,

$$u_{n\pm1} = e^{\pm ik} u_n.$$

Now, the total derivative with respect to t can be expressed using the assumption of independence of the multiple scale variables as

$$\begin{aligned}\frac{d()}{dt} &= \frac{\partial()}{\partial\theta_n}\frac{d\theta_n}{dt} + \frac{\partial()}{\partial\xi_n}\frac{d\xi_n}{dt} + \frac{\partial()}{\partial\tau}\frac{d\tau}{dt} \\ &= -\omega\frac{\partial()}{\partial\theta_n} - \varepsilon c_g\frac{\partial()}{\partial\xi_n} + \varepsilon^2\frac{\partial()}{\partial\tau}. \end{aligned} \tag{2.8}$$

The higher order derivatives with respect to t can be evaluated by the chain rule of differentiation. Assuming that a second order expansion of the displacements and the time-scales (up to ε^2) are sufficient to describe the nonlinear characteristics of wave motion, the equations at each order of expansion can be written as

$$\varepsilon^0 \quad : \quad m\,\omega^2\,\frac{\partial u_n^0}{\partial\theta_n^2} \;+\; K_2\,(2u_n^0 - u_{n-1}^0 - u_{n+1}^0) = 0 \tag{2.9}$$

$$\varepsilon^1 \quad : \quad m\,\omega^2\,\frac{\partial u_n^1}{\partial\theta_n^2} \;+\; K_2\,(2u_n^1 - u_{n-1}^1 - u_{n+1}^1) = F^1 \tag{2.10}$$

$$\varepsilon^2 \quad : \quad m\,\omega^2\,\frac{\partial u_n^2}{\partial\theta_n^2} \;+\; K_2\,(2u_n^2 - u_{n-1}^2 - u_{n+1}^2) = F^2, \tag{2.11}$$

where, F^1 and F^2 are given as

$$F^1 = -2m\omega c_g\frac{\partial^2 u_n^0}{\partial\xi_n\partial\theta_n} + K_2\left(\frac{\partial u_{n+1}^0}{\partial\xi_n} - \frac{\partial u_{n-1}^0}{\partial\xi_n}\right) + K_3\left[(u_{n+1}^0 - u_n^0)^2 - (u_n^0 - u_{n-1}^0)^2\right], \tag{2.12}$$

$$\begin{aligned} F^2 = {} & 2m\omega\frac{\partial^2 u_n^0}{\partial\tau\partial\theta_n} - mc_g^2\frac{\partial^2 u_n^0}{\partial\xi_n^2} - 2m\omega c_g\frac{\partial^2 u_n^1}{\partial\xi_n\partial\theta_n} + K_4\left[(u_{n+1}^0 - u_n^0)^3 - (u_n^0 - u_{n-1}^0)^3\right] \\ & + K_3\left[\left(u_{n+1}^1 + \frac{\partial u_{n+1}^0}{\partial\xi_n} - u_{n-1}^1 + \frac{\partial u_{n-1}^0}{\partial\xi_n}\right)(u_{n+1}^0 + u_{n-1}^0 - 2u_n^0)\right] \\ & + K_3\left[(u_{n+1}^0 - u_{n-1}^0)\left(u_{n+1}^1 + u_{n-1}^1 - 2u_n^1 + \frac{\partial u_{n+1}^0}{\partial\xi_n} - \frac{\partial u_{n-1}^0}{\partial\xi_n}\right)\right] \\ & + K_2\left(\frac{\partial u_{n+1}^1}{\partial\xi_n} - \frac{\partial u_{n-1}^1}{\partial\xi_n}\right) + \frac{K_2}{2}\left(\frac{\partial^2 u_{n+1}^0}{\partial\xi_n^2} + \frac{\partial^2 u_{n-1}^0}{\partial\xi_n^2}\right). \end{aligned} \tag{2.13}$$

By introducing the multiple scale expansion, the governing equation for the weakly nonlinear spring-mass chain has been converted to a set of cascading linear differential

equations at each order of expansion, with $\mathcal{O}(\varepsilon)$ and higher being heterogeneous equations with the forcing function determined from the solutions obtained at all the lower orders of expansion. Therefore, the solution at each order of expansion can be determined by solving the corresponding linear differential equation. Considering eqn. (2.9), the solution can be written as

$$u_n^0 = A_0(\xi_n,\tau) + A(\xi_n,\tau)\, e^{i\theta_n} + A^*(\xi_n,\tau)\, e^{-i\theta_n} \tag{2.14}$$

$$u_{n+1}^0 = A_0(\xi_n,\tau) + A(\xi_n,\tau)\, e^{ik}\, e^{i\theta_n} + A^*(\xi_n,\tau)\, e^{-ik}\, e^{-i\theta_n} \tag{2.15}$$

$$u_{n-1}^0 = A_0(\xi_n,\tau) + A(\xi_n,\tau)\, e^{-ik}\, e^{i\theta_n} + A^*(\xi_n,\tau)\, e^{ik}\, e^{-i\theta_n}, \tag{2.16}$$

where A_0 and A are constants only dependent on the slower scale variables, and A^* is the complex conjugate of A. Substituting eqns. (2.14-2.16) in eqn. (2.9), and enforcing the non-triviality of the constant A, the linear dispersion relation for the system can be obtained as

$$\omega = \sqrt{K_2/m}\sqrt{2-2\cos(k)}, \tag{2.17}$$

where the wavenumber is assumed to be a real quantity ($k \in \mathbb{R}$). In order to determine the functional dependence of A_0 and A on the slow scale variables, the higher order equations (eqns. 2.10-2.11) need to be solved. The forcing function at $\mathcal{O}(\varepsilon)$, obtained by substituting eqns. (2.14-2.16) in eqn. (2.12) is

$$F^1 = -i2mc_g\omega\frac{\partial A}{\partial \xi_n}e^{i\theta_n} + i2K_2\sin k\frac{\partial A}{\partial \xi_n}e^{i\theta_n} - i8K_3\sin k\sin^2\frac{k}{2}A^2e^{i2\theta_n} + c.c, \tag{2.18}$$

where $c.c$ refers to the complex conjugate of the terms listed. Using the fact that

$$c_g = \frac{d\omega}{dk} = \frac{K_2\sin k}{m\omega},$$

F^1 can be simplified as

$$F^1 = -i8K_3\sin k\sin^2\left(\frac{k}{2}\right)A^2e^{i2\theta_n} + c.c. \tag{2.19}$$

If the terms containing $e^{i\theta_n}$ were present in the expression for F^1, then the solution to eqn. (2.10) would contain terms of the form $\theta_n e^{i\theta_n}$, thereby depicting a solution

linearly increasing with time t, which would in turn violate the assumption of perturbation expansion. Such terms in the forcing function are referred to as secular terms. Therefore, it is customary to assume the velocity of the slow spatiotemporal scale ξ_n as undetermined, and choose an appropriate value such that the secular terms vanish in eqn. (2.12). In this case, the choice of the velocity to be the group velocity of the linear wave automatically nullifies the secular terms in the expansion.

Considering the expression for F^1, the solution at $\mathcal{O}(\varepsilon)$ can be written as

$$u_n^1 = B(\xi_n, \tau)\, e^{i2\theta_n} + c.c. \tag{2.20}$$

$$u_{n+1}^1 = B(\xi_n, \tau)\, e^{i2\theta_{n+1}} + c.c. \tag{2.21}$$

$$u_{n-1}^1 = B(\xi_n, \tau)\, e^{i2\theta_{n-1}} + c.c. \tag{2.22}$$

Substituting eqns. (2.19-2.22) in eqn. (2.10), the constant B can be determined as

$$\begin{aligned}(-4m\omega^2 + K_2(2 - 2\cos(2k)))(B(\xi_n, \tau)\, e^{i2\theta_n} \quad &+ \quad c.c) = -i8K_3 \sin k \sin^2 \frac{k}{2} A^2 e^{i2\theta_n} + c.c \\ \Rightarrow B(\xi_n, \tau) \quad &= \quad i\frac{K_3}{K_2} \cot\left(\frac{k}{2}\right) A^2(\xi_n, \tau).\end{aligned}$$

Note that only the particular solution to eqn. (2.10) has been considered. The nature of the homogeneous solution will depend on the initial conditions and the conditions of non-secularity imposed at the higher orders of the perturbation expansion. For the time being, this is neglected as the solution at the zeroth order (A_0 and A) have not yet been determined.

At $\mathcal{O}(\varepsilon^2)$, the forcing function F^2 can be obtained by substituting eqns. (2.14-2.16),

and eqns. (2.20-2.22) in eqn. (2.13) as

$$\begin{aligned}
F^2 =& K_2\frac{\partial^2 A_0}{\partial \xi_n^2} + K_2\cos k\frac{\partial^2 A}{\partial \xi_n^2}e^{i\theta_n} - mc_g^2\frac{\partial^2 A_0}{\partial \xi_n^2} - mc_g^2\frac{\partial^2 A}{\partial \xi_n^2}e^{i\theta_n} + i2m\omega\frac{\partial A}{\partial \tau}e^{i\theta_n} \\
&- K_3\left[8\sin^2\left(\frac{k}{2}\right)\cos k\left(\frac{\partial A}{\partial \xi_n}A^* + \frac{\partial A^*}{\partial \xi_n}A\right) - 4\sin^2 k\left(\frac{\partial A}{\partial \xi_n}A^* + \frac{\partial A^*}{\partial \xi_n}A\right)\right] \\
&- K_3\left[8i\sin^2\left(\frac{k}{2}\right)\sin 2kBA^*e^{i\theta_n} - 8i\sin^3 kA^*Be^{i\theta_n}\right] - K_3\left[8\sin^2\left(\frac{k}{2}\right)\frac{\partial A_0}{\partial \xi_n}Ae^{i\theta_n}\right] \\
&+ K_4[48|A|^2A\sin^4\left(\frac{k}{2}\right)e^{i\theta_n}] + c.c + higher\ harmonics \\
=& G^0 + G^1e^{i\theta_n} + c.c + higher\ harmonics, \qquad (2.23)
\end{aligned}$$

where

$$\begin{aligned}
G^0 =& \frac{m\omega^2}{4}\frac{\partial^2 A_0}{\partial \xi_n^2} + \frac{2K_3m\omega^2}{K_2}\frac{\partial |A|^2}{\partial \xi_n} \\
G^1 =& i2m\omega\frac{\partial A}{\partial \tau} - \frac{m\omega^2}{4}\frac{\partial^2 A}{\partial \xi_n^2} - \frac{2K_3m\omega^2}{K_2}\frac{\partial A_0}{\partial \xi_n}A - \left(\frac{2K_3^2m\omega^2(4K_2 - m\omega^2)}{K_2^3}\right)|A|^2A \\
&+ \frac{3K_4m^2\omega^4}{K_2^2}|A|^2A.
\end{aligned}$$

At $\mathcal{O}(\varepsilon^2)$, not all the secular terms vanish. Particularly, eqn. (2.23) contains two types of secular terms - one is the constant, which leads to a solution of the form θ_n, and the other is the fundamental harmonic $e^{i\theta_n}$, which leads to a solution of the form $\theta_n^2e^{i\theta_n}$. In order to obtain a valid solution at $\mathcal{O}(\varepsilon^2)$, these secular terms must vanish, which leads to the following conditions that need to be satisfied

$$\frac{\partial^2 A_0}{\partial \xi_n^2} + \frac{8K_3}{K_2}\frac{\partial |A|^2}{\partial \xi_n} = 0 \qquad (2.24)$$

$$i\frac{\partial A}{\partial \tau} - \frac{\omega}{8}\frac{\partial^2 A}{\partial \xi_n^2} - \frac{K_3\omega}{K_2}\frac{\partial A_0}{\partial \xi_n}A - \left(\frac{K_3^2\omega(4K_2 - m\omega^2)}{K_2^3} + \frac{3K_4m\omega^3}{2K_2^2}\right)|A|^2A = 0. \qquad (2.25)$$

Eqns. (2.24) and (2.25) can be simplified to obtain two independent expressions for A_0 and A as

$$i\frac{\partial A}{\partial \tau} - \frac{\omega}{8}\frac{\partial^2 A}{\partial \xi_n^2} + \left(\frac{K_3^2\omega}{K_2^3}(4K_2 + m\omega^2) - \frac{3K_4m\omega^3}{2K_2^2}\right)|A|^2A = 0 \qquad (2.26)$$

$$\frac{\partial A_0}{\partial \xi_n} = -8\frac{K_3}{K_2}|A|^2. \qquad (2.27)$$

Eqn. (2.26) is the well known Nonlinear Schrödinger equation, which is an integrable equation and its solution can be obtained using the inverse scattering transform. In eqn. (2.27), the constant of integration is neglected under the assumption that the initial excitation is purely harmonic. Now, the solution at the lowest order can be written as

$$u_n^0(t) = A_0(\varepsilon(n - c_g t), \varepsilon^2 t) + A(\varepsilon(n - c_g t), \varepsilon^2 t)\, e^{i(kn-\omega t)} + A^*(\varepsilon(n - c_g t), \varepsilon^2 t)\, e^{-i(kn-\omega t)}, \tag{2.28}$$

where A_0 and A are determined by solving eqns. (2.26-2.27). If the masses are connected by linear springs ($K_3 = K_4 = 0$), then the zeroth order term completely characterizes the propagating wave packet. Furthermore, the distortion of the initial wave packet due to dispersion is described by the Linear Schrödinger equation ($A_0 = 0$) as

$$i\frac{\partial A}{\partial \tau} - \frac{\omega}{8}\frac{\partial^2 A}{\partial \xi_n^2} = 0.$$

From eqn. (2.27), it can be concluded that the effect of weak nonlinearity is to introduce a non-harmonic envelope modulation of the wave packet, which is completely attributed to the equivalent quadratic nonlinearity in the system. In addition, the modulation of the harmonic component typically gives rise to a modification of the dispersion relation, i.e., the traveling wave takes the form

$$f(kn - (\omega_0(k) + \varepsilon\omega_1(k) + \varepsilon^2\omega_2(k))t,$$

where ω_0 is the fundamental frequency given by the linear dispersion relation, and ω_1, ω_2 are the higher order corrections to the frequency due to the nonlinear terms in the constitutive relation.

While the modification of the dispersion relation can be obtained from the solution of the Nonlinear Schrödinger equation, it is customary to assume a monochromatic wave to derive the modified dispersion relation. Then, a perturbative expansion such as the $Lindstedt - Poincaré$ technique or the Multiple scales expansion (given in Appendix A) can be employed, and the dispersion relation for the above system is obtained as

$$\omega(k) = \omega_0(k) + \varepsilon^2\omega_2(k), \tag{2.29}$$

where

$$\omega_0 = \sqrt{K/m}\sqrt{2 - 2\cos(k)} \tag{2.30}$$

$$\omega_2 = \left(\frac{K_3^2}{K_2^3}(4K_2 - m\omega_0^2) - \frac{3K_4}{2K_2^2}m\omega_0^2\right)\omega_0 r^2 \tag{2.31}$$

Eqn. (2.29) shows that the change in the dispersion relation due to nonlinearity is $\mathcal{O}(\varepsilon^2)$, thereby leading to a very small correction of the linear dispersion relation. Therefore, at $\mathcal{O}(1)$, the effect of nonlinearity is predominantly observed in the modification of the wave packet envelope.

The higher order perturbation solutions consist of homogeneous and non-homogeneous terms. The non-homogeneous terms give rise to higher harmonic components, whose spectral signature depend on the initial condition, and the order of expansion considered. The homogeneous terms corresponding to the fundamental harmonic can be neglected by assuming that the zeroth order solution completely satisfies the initial condition. However, the homogeneous terms corresponding to the nonlinearly-generated harmonics cannot be neglected, and the characteristics of these terms will be studied in the later part of this dissertation.

By solving the Nonlinear Schrödinger equation [60, 101], the expression for the non-harmonic component of the envelope can be determined, and this can be used to quantitatively characterize the dependence of this non-harmonic component on the magnitude of nonlinearity and the amplitude and frequency of excitation. While similar equations can be derived for multiatomic or multidimensional spring-mass chains, the equations are cumbersome to handle and seldom carried out. Therefore, in this chapter, a numerical analysis of wave motion will be performed to quantitatively characterize the effect of weak nonlinearity on wave propagation.

2.2 Numerical Analysis

The characteristics of wave propagation in nonlinear chains are studied by numerical integration of the state-space model of eqn. (2.5) using the Verlet Algorithm [122]. The input signal is a Hann-modulated seven-cycle sine burst, where the modulation ensures the excitation of a minimal band of frequencies centered at a prescribed carrier

frequency. This input signal is prescribed at the first mass in a semi-infinite chain to ensure a complete evolution of the burst without contamination due to reflections from the boundary. Furthermore, the mass and the linear spring coefficient are assumed to be unity ($m = K_2 = 1$), and the cubic nonlinearity (K_4) is assumed to be zero. The coefficient of quadratic nonlinearity (K_3), and the amplitude (u_0) and frequency of excitation (ω) are varied to quantitatively describe the characteristics of the wave packet.

In fig. 2.3, the spectral contours ($2D$ DFT of the spatiotemporal wave field $u(n,t)$) are plotted for the linear chain ($K_3 = K_4 = 0$) and a quadratic chain ($K_4 = 0$) in various regions of the Brillouin zone ($\omega \in [0,2]$). In the case of the linear chain, the spectral contours (fig. 2.3a) in the long-wavelength (low frequency) regime have a linear profile which implies that dispersion does not play a significant role. As the wavelength decreases (increasing frequency), the spectral contours have a nonlinear profile which conforms to the global nature of the dispersion curve (figs. 2.3b, 2.3c). On the contrary, the major spectral content in the nonlinear chain is observed to be present in the very low wavenumber region ($k, \omega \approx 0$), even in regimes where the effect of dispersion is negligible (figs. 2.3d, 2.3g). The spectral contours observed in the spectral band of the incident wave conform to the global nature of the dispersion curve, however, the corresponding amplitude decreases with increasing nonlinearity.

The spectral characteristics of the propagating wave packet observed in fig. 2.3 are consistent with the zeroth order solution given by eqn. (2.28), i.e., the packet consists of two spectral features - a non-harmonic and a harmonic component. In order to delineate these features, the spatiotemporal evolution of the wave packet is monitored. Fig. 2.4 shows snapshots of the wave profile at the end of simulation for various amplitudes of excitation and different values of frequencies in the Brillouin zone. For very small frequencies, the wave packet in the linear chain is unaffected by dispersion and travels through the system without any distortion. However, even for small amplitudes of excitation in the nonlinear chain, macroscopic differences with respect to the linear chain are observed. All the masses behind the head of the wave packet have a non-zero displacement associated with them, i.e., once the wave packet travels through a certain particle, the particle remains displaced from its equilibrium position. This evolution is markedly different from the linear chain, where at any time instant, only a part of the

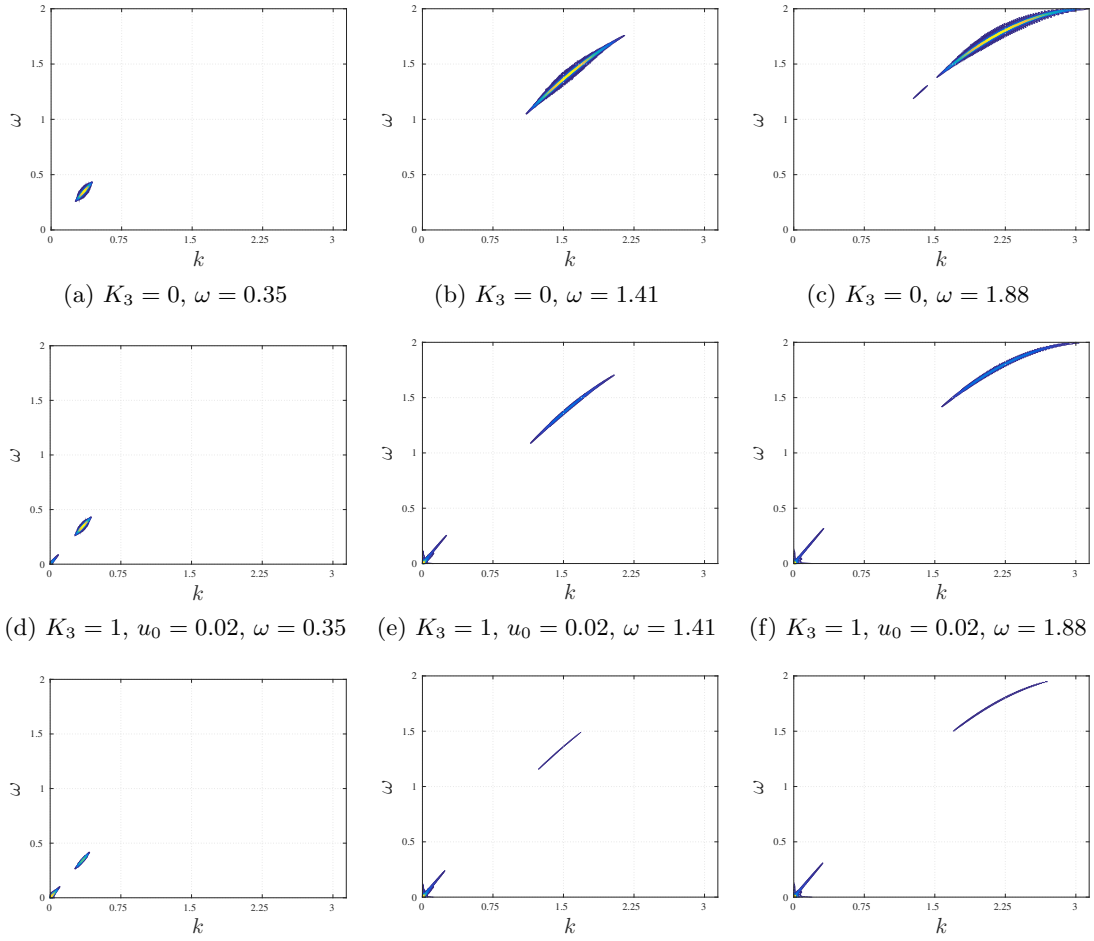

(a) $K_3 = 0$, $\omega = 0.35$ (b) $K_3 = 0$, $\omega = 1.41$ (c) $K_3 = 0$, $\omega = 1.88$

(d) $K_3 = 1$, $u_0 = 0.02$, $\omega = 0.35$ (e) $K_3 = 1$, $u_0 = 0.02$, $\omega = 1.41$ (f) $K_3 = 1$, $u_0 = 0.02$, $\omega = 1.88$

(g) $K_3 = 1$, $u_0 = 0.09$, $\omega = 0.35$ (h) $K_3 = 1$, $u_0 = 0.09$, $\omega = 1.41$ (i) $K_3 = 1$, $u_0 = 0.09$, $\omega = 1.88$

Figure 2.3: $2D$ Spectral contours of the wave packet for different regions of the Brillouin zone. k is the wavenumber and ω is the frequency. The excitation amplitude increases across rows and the frequency increases across columns.

chain is displaced from its equilibrium position.

As the wavenumber is increased, dispersion-associated distortion in the form of stretching of the wave packet and reduction of amplitude is observed in the linear chain. In the nonlinear chain, the stretching of the wave packet is observed in conjunction with the non-harmonic displacement. While the two components of the wave packet are indeed observed in the spatiotemporal domain, these features cannot be delineated by mere visual inspection. Therefore, the two distinct spectral contributions in fig. 2.3 are

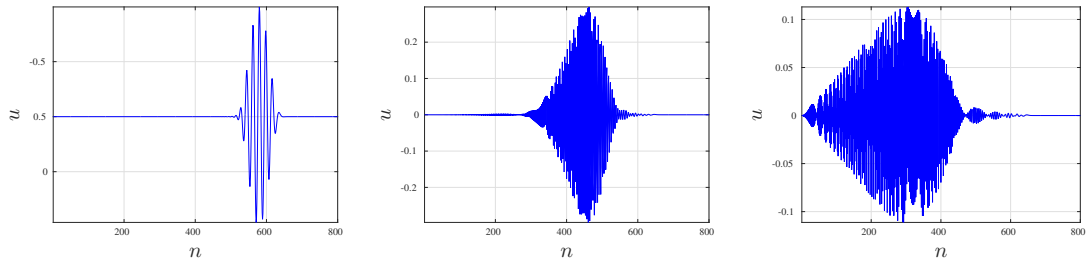

(a) $K_3 = 0$, $\omega = 0.35$ (b) $K_3 = 0$, $\omega = 1.41$ (c) $K_3 = 0$, $\omega = 1.88$

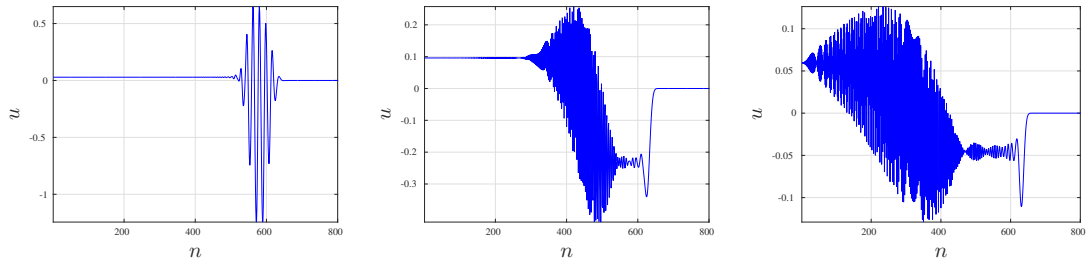

(d) $K_3 = 1$, $u_0 = 0.02$, $\omega = 0.35$ (e) $K_3 = 1$, $u_0 = 0.02$, $\omega = 1.41$ (f) $K_3 = 1$, $u_0 = 0.02$, $\omega = 1.88$

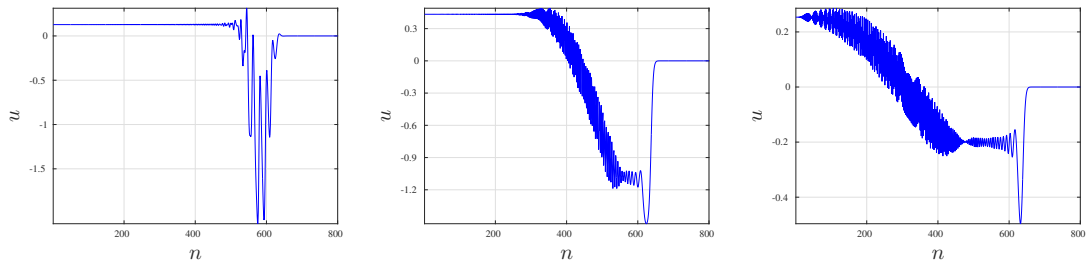

(g) $K_3 = 1$, $u_0 = 0.09$, $\omega = 0.35$ (h) $K_3 = 1$, $u_0 = 0.09$, $\omega = 1.41$ (i) $K_3 = 1$, $u_0 = 0.09$, $\omega = 1.88$

Figure 2.4: Spatial profile of the wave packet at the end of simulation. n indicates the position in the x-domain in terms of chains links, u is the displacement history at the end of simulation. The excitation amplitude increases across rows and the frequency increases across the columns.

analyzed independently by filtering the wave packet into a long-wavelength component, and a component in the spectral band of the incident wave. In order to delineate the characteristics of the harmonic component, the final wave packet at the end of simulation for the corresponding linear chain is also plotted. Figs. 2.5b and 2.5d shows that the spatial component corresponding to the harmonic component is identical to the wave packet obtained from the simulation of a linear chain. This observation implies that the nonlinear terms in eqn. (2.26) describing the modulation of the harmonic component

are negligible, and the linear Schrödinger equation sufficiently captures the modulation of the harmonic component in the wave packet. Furthermore, this observation is also consistent with the modified dispersion relation for the nonlinear chain, where the nonlinear effects are only observed at $\mathcal{O}(\varepsilon^2)$. From fig. 2.5c, the long-wavelength component is observed to be very similar to a sigmoidal curve, where the transition from the higher asymptote to the lower asymptote occurs within the support of the linear wave profile. Thus, the solution to the non-harmonic component in eqn. (2.27), is given by the sigmoidal component [1].

From eqn. (2.28) and fig. 2.5, it can be concluded that the effect of quadratic nonlinearity is completely captured by the presence of a non-harmonic component in the wave packet. It is therefore sufficient to monitor the non-harmonic component to determine the quantitative effects of nonlinearity, i.e., the dependence of the spatial wave features upon the magnitude of nonlinearity (K_3) and the excitation parameters (u_0, ω). Moreover, the non-harmonic or sigmoidal component also exhibits a constant amplitude, which can be easily inferred from simulated or measured data. A general sigmoidal curve can be represented as

$$y(x) = P + \frac{Q - P}{1 + e^{-(x-R)/S}} \tag{2.32}$$

where P, Q are the higher and lower asymptotes, respectively, R is the inflexion point, and S is the width of the transition region from the higher to the lower asymptote.

A nonlinear fit of eqn. (2.32) to the filtered long-wavelength component of the wave packet is carried out, and by performing the curve fit for multiple values of k in the Brillouin zone and different values of K_3 and A_0, the functional dependence of parameters P, Q, R and S on the nonlinear parameter K_3 in terms of the amplitude u_0 and the frequency ω can be obtained. While any one of these constants can be used to elucidate the effects of nonlinearity on wave propagation; from figs. 2.3d an 2.3f, the tail amplitude of the sigmoidal (asymptote P in eqn. (2.32)) presents itself as the most tractable characteristic for parameterization. This feature can in fact be easily extracted from simulated or experimental results even in the early stages of propagation, without requiring the complete evolution of the sigmoidal component or advanced signal

[1] The sigmoidal component can be represented in the form of hyperbolic tangent function which is the solution derived in [60] for the monoatomic spring-mass chain

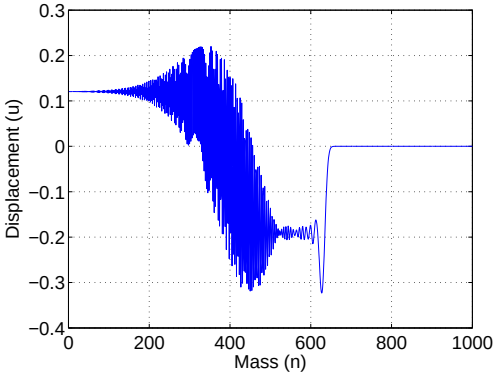

(a) Complete wave packet

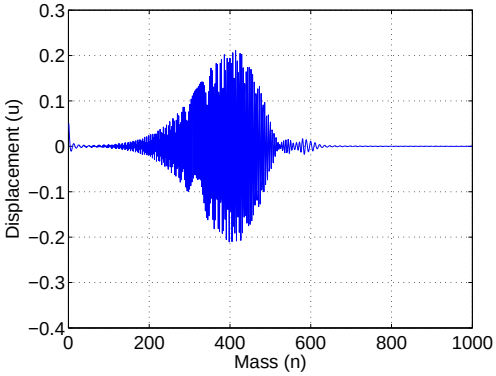

(b) Filtered harmonic component of wave packet

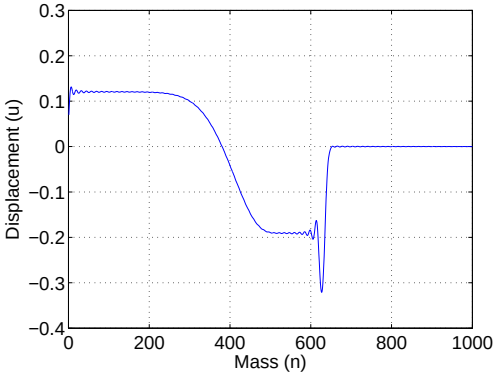

(c) Filtered long-wavelength component of wave packet

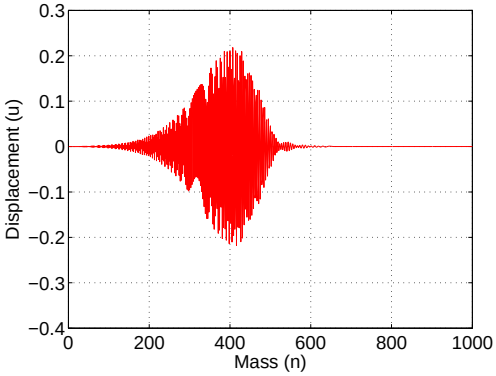

(d) Complete wave packet in the linear chain

Figure 2.5: Wave Packet at the end of simulation and separation of the long- and short-wavelength spectral components. The wave packet at the end of simulation in the corresponding linear system is also shown.

processing techniques.

Fig. 2.7a shows a cubic variation of the tail amplitude (upper asymptote P) with respect to the frequency (ω). Furthermore, the different curves for P are observed to be sorted in increasing order of a combination of the magnitude of nonlinearity and the amplitude of excitation given by $K_3u_0^2$. This is verified in fig. 2.7b, where the tail amplitude normalized with respect to ($K_3u_0^2$) is plotted. Hence, the expression for the tail amplitude P can be written as

$$P = K_3u_0^2(a\omega^3 + b\omega^2 + c\omega + d), \tag{2.33}$$

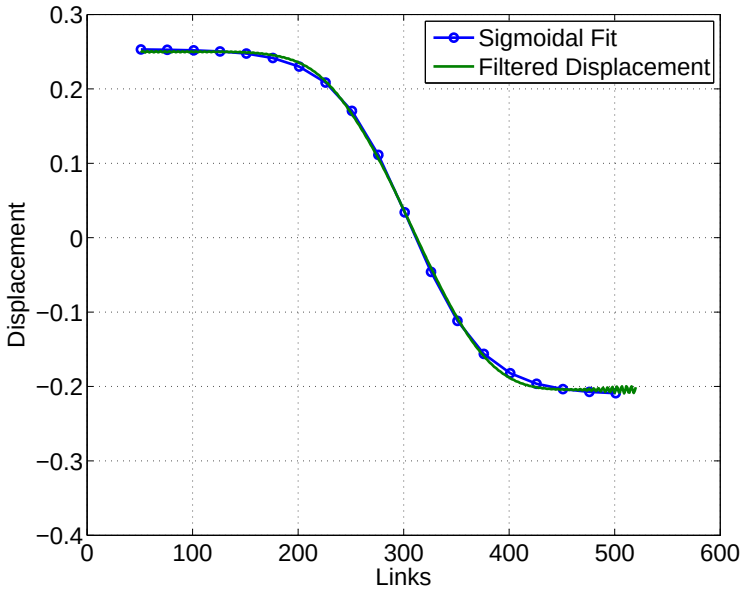

Figure 2.6: Long-wavelength component fit to a sigmoidal curve

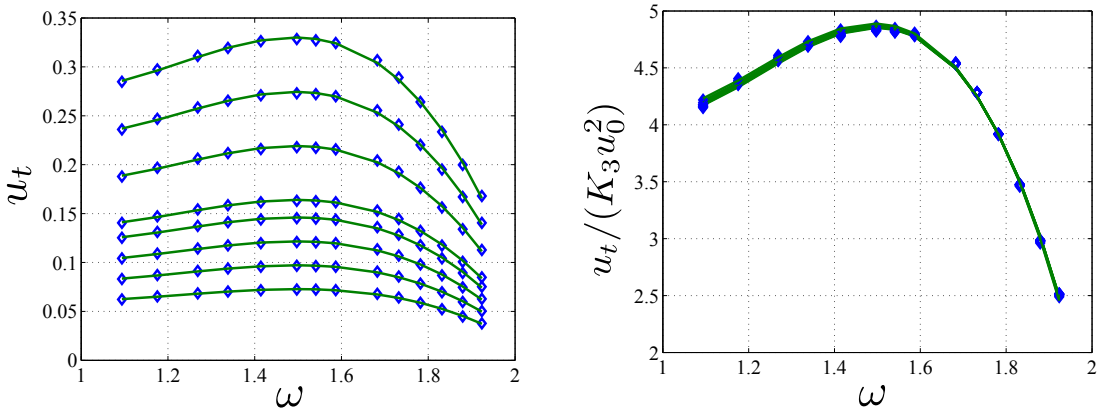

(a) (b)

Figure 2.7: Variation of tail amplitude of the wave packet with respect to the excitation frequency in a spring-mass chain with quadratic nonlinearity - (a) Variation of the tail amplitude (u_t), (b) Variation of the normalized tail amplitude ($u_t/(K_3u_0^2)$).

where the constants a, b, c, d can be classified as the invariants of quadratic nonlinearity in monoatomic spring-mass chains, as they are universally valid for all monoatomic chains exhibiting a quadratic nonlinear behavior. The dependence of the tail amplitude on the parameter $K_3u_0^2$ is also recovered from eqn. (2.27), which further ratifies the

observations made from the numerical simulations. Therefore, eqn. (2.33) can be easily applied to simulated or experimental data obtained from generic $1D$ monoatomic nonlinear periodic structures to setup an inverse problem to determine/verify the equivalent quadratic nonlinear parameter of the periodic system. Furthermore, this numerical technique can be easily extended to multiatomic, multidimensional systems with complex unit cell architecture such as lattices, while the analytical formulation would have to be carried out independently for each periodic system.

2.3 Conclusion

The characteristics of propagating wave packets in periodic structures with weak quadratic and cubic nonlinearity has been analyzed theoretically and numerically, and it has been shown that the primary effect of weak nonlinearity manifests as a modulation of the amplitude envelope of the wave packet. This amplitude modulation results in the generation of a non-harmonic or sigmoidal component even when the initial excitation is purely harmonic, and can be modeled by the Nonlinear Schrödinger equation. Topological wave packet descriptors that describe the non-harmonic component can be quantitatively characterized as a function of the nonlinearity and excitation parameters, which in turn can be used to determine or validate nonlinear constitutive relations. In the next chapter, this form of parametric inversion will be applied to data obtained from numerical simulation of wave propagation in granular chains to showcase the advantage of the numerical technique.

Chapter 3

Invariants of Nonlinearity in the Phononic Characteristics of Granular Chains

3.1 Monoatomic Granular Chains

Consider a $1D$ chain of homogeneous spheres interacting through nonlinear contact forces, as shown in fig. 3.1. The system of equations governing wave motion are

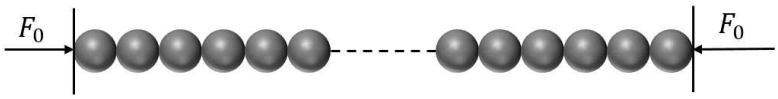

Figure 3.1: $1D$ Monoatomic chain of spheres

$$m\,\ddot{u}_n \;-\; A\left[\delta_0 + u_{n-1} - u_n\right]_+^p \;+\; A\left[\delta_0 + u_n - u_{n+1}\right]_+^p = 0, \tag{3.1}$$

where u_n is the displacement of the n^{th} sphere; $p = 3/2$ and $A = \frac{E\sqrt{2R}}{3(1-\nu^2)}$ are the power law and the equivalent stiffness governing the contact interaction, derived from Hertzian theory [65]; m and R are the mass and radius of the sphere, while E and ν are the Young's modulus and Poisson's ratio of the material, respectively; δ_0 is the precompression displacement between two consecutive spheres due to the application of

the static force F_0 at the ends of the chain ($\delta_0 = (F_0/A)^{2/3}$). Granular chains transmit forces only when there is effective compression between two consecutive masses, i.e., forces exist only for positive values of the quantity in brackets: $[u]_+ = max(0, u)$.
A semi-infinite chain made of 1350 steel spheres ($R = 4.76$ mm, $E = 210$ GPa, $\nu = 0.3$) is excited at the left end by a seven-cycle Hann-modulated sine burst ($u_1(t) = u_0\, H(t)\, \sin(7\Omega t)$, $H(t)$ is the Hann window function) with the amplitude of excitation set to be less than 20% of the precompression displacement applied to the system ($u_0 < 0.2\delta_0$). Since the granular chain is a periodic system, the non-dimensional excitation frequency $\omega(= \Omega/\sqrt{K/m} \in [0, 2])$ is varied only in the first irreducible Brillouin zone, and the wave profile at the end of simulation for two different excitation frequencies is shown in fig. 3.2. The wave packet in the granular chain bears striking similarities to the

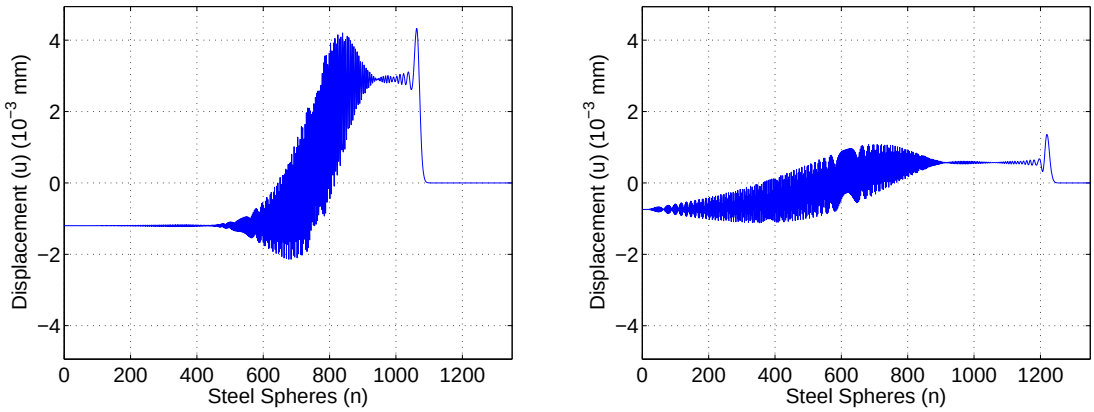

Figure 3.2: Displacement profile in the monoatomic granular chain at one time instant of simulation for two different excitation frequencies, which lie in the dispersive region of the Brillouin zone.

wave packet observed in the nonlinear spring-mass chains in chapter 2. This similarity is obtained due to the fact that the power law terms in eqn. (3.1) can be simplified using a Taylor series expansion under the assumption of small amplitudes of displacement with respect to the initial precompression applied to the system ($\|u_{n\pm1} - u_n\| \ll \delta_0$) to yield

$$\begin{aligned} m\ddot{u}_n + K_2(2u_n - u_{n-1} - u_{n+1}) + K_3((u_n - u_{n-1})^2 - (u_{n+1} - u_n)^2) \\ + K_4((u_n - u_{n-1})^3 - (u_{n+1} - u_n)^3) = 0, \end{aligned} \tag{3.2}$$

where $K_2 = \frac{3}{2}A\delta_0^{1/2}$, $K_3 = -\frac{3}{8}A\delta_0^{-1/2}$ and $K_4 = -\frac{3}{48}A\delta_0^{-3/2}$. Eqn. (3.2) is identical to eqn. (2.6) except for the fact that the equivalent coefficient of quadratic and cubic nonlinearity are negative. Therefore, eqn. (2.33) can be effectively used to determine the equivalent quadratic nonlinear contribution in the case of granular chains with interactions governed by arbitrary power laws.

3.1.1 Reconstruction of nonlinearity in granular chains

Exploiting the qualitative similarity of the long-wavelength component in figs. (3.2) and (2.5a), the variation of tail amplitude is determined as a function of the non-dimensional excitation frequency (ω) for different values of power law (p), initial pre-compression (δ_0) and excitation amplitude (u_0). Across all cases, the tail amplitude is found to have a cubic dependence on ω (fig. 3.3).

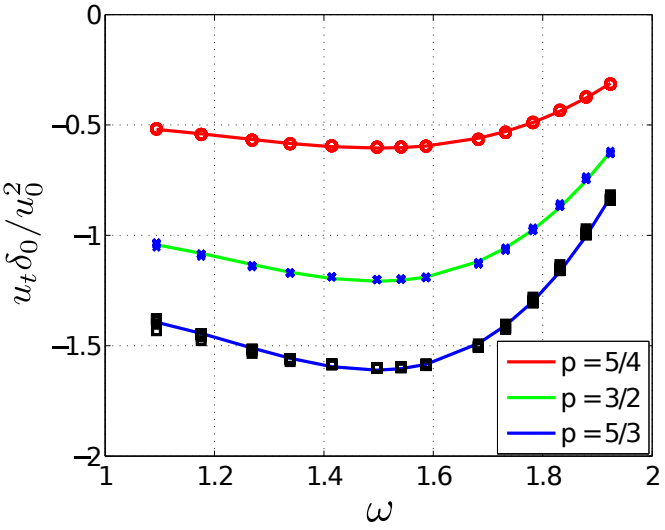

Figure 3.3: Variation of tail amplitude with non-dimensional excitation frequency in monoatomic granular chains for different power law interactions.

$$u_t^* = \overline{a}\omega^3 + \overline{b}\omega^2 + \overline{c}\omega + \overline{d} \tag{3.3}$$

Eqn. (2.33) was derived under the assumption of unit mass and linear spring coefficient. This condition can be obtained in eqn. (3.2) as

$$\frac{1}{\omega_n^2}\ddot{u}_n + (2u_n - u_{n-1} - u_{n+1}) + G_2((u_n - u_{n-1})^2 - (u_{n+1} - u_n)^2) + G_3((u_n - u_{n-1})^3 - (u_{n+1} - u_n)^3) = 0, \tag{3.4}$$

where $\omega_n = \sqrt{K/m}$. For any arbitrary power p, it can be easily shown that

$$G_2 = -\frac{(p-1)}{2\delta_0} \tag{3.5}$$

Under the assumption that eqns. (2.33) and (3.3) describe the same feature of the non-harmonic component, the ratio of any one of the constants ($\overline{a}/a$, $\overline{b}/b$, $\overline{c}/c$, $\overline{d}/d$) can be utilized to provide an expression for the scaling due to nonlinearity and excitation amplitude. Hence, a closed form expression for the interaction power law p can be obtained as

$$p = 1 - \frac{2\delta_0}{u_0^2}\frac{\overline{a}}{a}, \tag{3.6}$$

where the scaling ratio $\overline{a}/a$ has been used. The parameter $\overline{a}$ is determined from the numerical simulation of the granular chain (eqn. 3.1) by sweeping ω in the irreducible Brillouin zone, while a corresponds to the invariant parameter obtained from the monoatomic spring-mass chain with quadratic nonlinearity. The other two quantities (δ_0 and u_0) are extrinsic parameters, i.e., they can be controlled externally. The values of p obtained by substituting the numerically determined constant ($\overline{a}$) in eqn. (3.6) for granular chains governed by different power laws are given in table 3.1.

Table 3.1: Power law reconstructed from eqn. (3.6) using numerical simulations.

Imposed power law	Reconstructed from curve	Error %
1.25	1.2473	0.22
1.5	1.4948	0.34
1.667	1.6613	0.33

In table 3.1, remarkable agreement is observed between the imposed and the reconstructed power law, proving that the invariants of quadratic nonlinearity in monoatomic spring-mass systems can indeed be used to estimate nonlinearity in generic monoatomic

granular chains.

Even though the granular chains considered here are obtained by assembling spheres, other geometries can also be considered, as a change in the inertial parameters does not affect the inverse problem paradigm. Therefore, the inverse problem can be used as a technique to verify/estimate contact power laws for monoatomic chains with different geometries.

The monoatomic granular chain verifies the numerical problem established in chapter 2. However, the efficiency of the technique lies in the ease of transferability to periodic structures with additional complexity. Therefore, the case of a diatomic granular chain will also be analyzed to showcase the versatility of the numerical inverse problem.

3.2 Diatomic Granular Chains

Consider the diatomic granular chain shown in fig. 3.4. The equations of motion for this system are

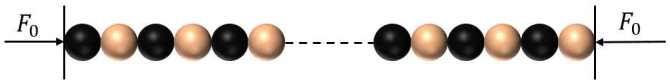

Figure 3.4: Diatomic chain of spheres.

$$M\ddot{u}_n - A[\delta_0 + v_{n-1} - u_n]_+^p + A[\delta_0 + u_n - v_n]_+^p = 0$$
$$m\ddot{v}_n - A[\delta_0 + u_n - v_n]_+^p + A[\delta_0 + v_n - u_{n+1}]_+^p = 0$$

where u_n and v_n are the displacements of the two masses M and m in the n^{th} unit cell. The equivalent stiffness is given by $A = \frac{2\sqrt{2R}}{3}\left(\frac{1-\nu_M^2}{E_M} + \frac{1-\nu_m^2}{E_m}\right)^{-1}$, where the subscript denotes the Young's Modulus and Poisson's ratio of the corresponding material respectively. The first mass M is assumed to be the heavier mass ($\alpha = m/M < 1$) for convenience.

The presence of two particles in the unit cell gives rise to two propagation modes - the acoustic mode and the optical mode. The mass contrast also significantly affects the dispersion relation, even in the case of a linear diatomic spring-mass chain; unlike the monoatomic chain, where the inertial properties only act as a scaling parameter.

Therefore, the quantitative characteristics of nonlinear wave propagation will also be affected by the mass contrast (α), and the acoustic mode of excitation will be considered in this example to delineate the effects of the inertial mismatch.

As before, numerical simulations of the equations of motion are considered for different diatomic chains obtained by permuting the choice of bead material among Steel, Aluminum ($E = 69$ GPa, $\nu = 0.3$) and PTFE ($E = 1.46$ GPa, $\nu = 0.46$). The wave profile in the heavier mass of three different chain configurations for a given non-dimensional excitation frequency is shown in fig. 3.5.

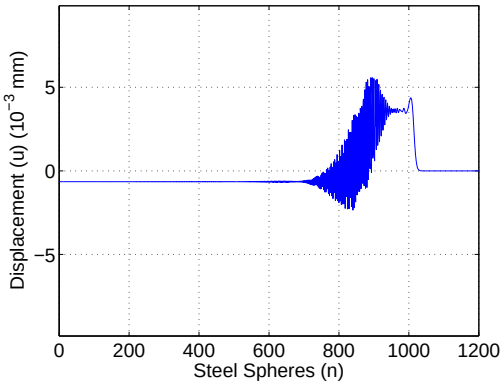

(a) Steel-Aluminum Diatomic Chain

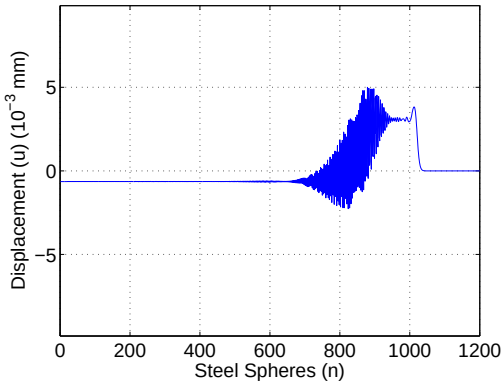

(b) Steel-PTFE Diatomic Chain

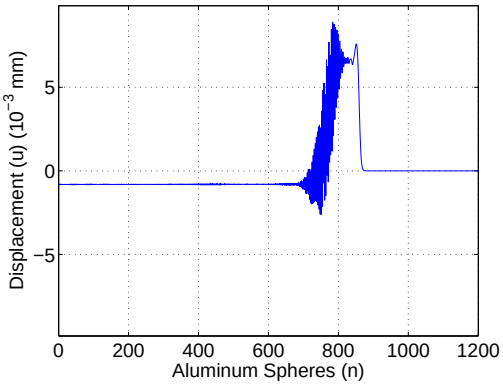

(c) Aluminum-PTFE Diatomic Chain

Figure 3.5: Displacement profile at one time instant of simulation for three different diatomic granular chains. The displacement of the heavier mass is shown in the figure and the non-dimensional excitation frequency is the same for all three diatomic chains.

The non-harmonic feature is observed in all the chains in fig. 3.5. The wave profiles

are again found to exhibit bi-spectral content (long- and short-wavelength) - analogous to the observations made for the monoatomic chain. Hence, it is sufficient to monitor the long-wavelength component to determine the dependence of the spatial wave characteristics upon nonlinearity and excitation parameters. In this regard, it is noted that the modulated envelope of the wave is significantly different between the Al-PTFE chain and either the Steel-Aluminum or the Steel-PTFE chain; this is attributed to the difference in inertial contrast of the different chains ($\alpha = 0.84$ for Al-PTFE, $\alpha = 0.3$ for Steel-Al and $\alpha = 0.25$ for Steel-PTFE). In order to facilitate the analysis of the effect of the inertial parameter, it is necessary to the study the equivalent diatomic spring-mass chain.

3.2.1 Quadratic diatomic spring-mass chains

Consider a diatomic spring-mass chain with quadratic nonlinearity (G_2) and mass ratio (α) whose equations of motion are described by eqn. 3.8. Wave propagation in this chain is monitored to determine the tail amplitude of the long-wavelength envelope feature. The quantitative dependence on nonlinearity and excitation parameters is first obtained by fixing the mass ratio. From fig. 3.6a, the tail amplitude in a given diatomic chain is found to have the same scaling with respect to the nonlinearity (G_2) and excitation amplitude (u_0) as that exhibited by the monoatomic chain. The dependence on the frequency (ω) is also found to be cubic.

$$\ddot{u}_n + (2u_n - v_{n-1} - v_n) + G_2((u_n - v_{n-1})^2 - (v_n - u_n)^2) = 0 \tag{3.7}$$

$$\alpha\ddot{v}_n + (2v_n - u_n - u_{n+1}) + G_2((v_n - u_n)^2 - (u_{n+1} - v_n)^2) = 0 \tag{3.8}$$

However, some numerical inconsistencies are observed in the scaling of the tail amplitude for a given frequency, i.e., for all the diatomic chains studied, some frequencies do not conform to the scaling parameters. This is illustrated in fig. 3.6b for the case of $\alpha = 0.6$, and is attributed to reflections at the interface between heterogeneous beads. Thus, the points which have a large variance after normalization by the parameter $G_2u_0^2$ are neglected from the data considered to perform the curve fit.

The variation of the normalized tail amplitude as a function of frequency for different values of the mass ratio is shown in fig. 3.6c. When the constants of the cubic curve are

monitored as a function of α, no global scaling parameter (a function of α common to all curves) is obtained. Hence, a generic expression for the tail amplitude in a diatomic spring-mass chain with quadratic nonlinearity is written as

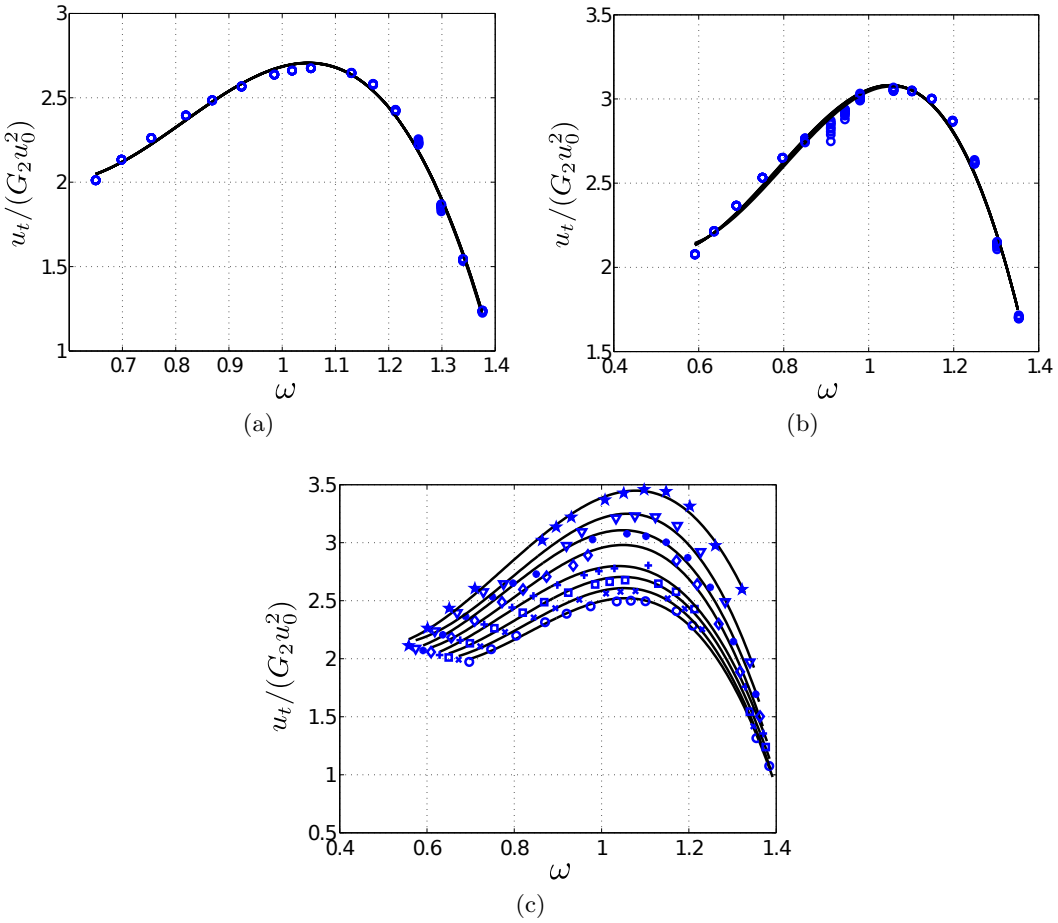

Figure 3.6: Parameterization of tail amplitude of the heavier mass in a nonlinear diatomic spring-mass chain - (a) for $\alpha = 0.3$, (b) for $\alpha = 0.6$, (c) as a function of mass ratio (α).

$$u_t = G_2 u_0^2 (a(\alpha)\omega^3 + b(\alpha)\omega^2 + c(\alpha)\omega + d(\alpha)) \tag{3.9}$$

Eqn. (3.9) is similar to eqn. (2.33), except that the coefficients of the cubic expression are now a function of the mass ratio. Thus, these coefficients cannot be classified as invariants of nonlinearity, as they are not universally valid for all diatomic chains.

The lack of a scaling parameter leads us towards a few other instructive observations. Visual inspection of the curves in fig. 3.6c suggests that the maximum tail amplitude occurs at the same non-dimensional frequency for all diatomic chains. This value can be determined from the location of the stationary point of the cubic curves, which is given by the expression

$$\omega|_{u_t^m} = \frac{-b(\alpha) + \sqrt{b(\alpha)^2 - 3a(\alpha)c(\alpha)}}{3a(\alpha)}, \tag{3.10}$$

where u_t^m is the maximum tail amplitude. The values of the non-dimensional frequencies determined from eqn. (3.10) for α ranging from 0.1 to 0.8 are shown in table 3.2, and these values indeed confirm the initial visual observations.

α	0.1	0.15	0.2	0.25	0.3	0.35	0.4	0.45
ω_m	1.054	1.051	1.049	1.047	1.049	1.048	1.056	1.062

α	0.5	0.55	0.6	0.65	0.7	0.75	0.8
ω_m	1.053	1.051	1.058	1.064	1.068	1.073	1.083

Table 3.2: Value of non-dimensional frequency corresponding to the maximum tail amplitude in a nonlinear diatomic spring-mass chain for different values of mass ratio (α).

Substituting eqn. (3.10) in eqn. (3.9), a function for u_t^m in terms of quadratic nonlinearity (G_2), excitation (u_0) and inertial (α) parameters can be obtained. Since the non-dimensional frequency corresponding to u_t^m is the same for all chains, u_t^m becomes an instructive parameter to quantify the characteristics of nonlinear wave motion. The variation of the normalized maximum tail amplitude ($u_t^m/(G_2u_0^2)$) as a function of α is plotted in fig. 3.7. The dependence on α is determined to be cubic and therefore, u_t^m can be expressed as

$$u_t^m = G_2u_0^2(e\alpha^3 + f\alpha^2 + g\alpha + h) \tag{3.11}$$

From eqn. (3.11), the constants e, f, g and h universally apply to all diatomic chains, thereby allowing a classification of these constants as invariants of nonlinearity for all $1D$ diatomic systems.

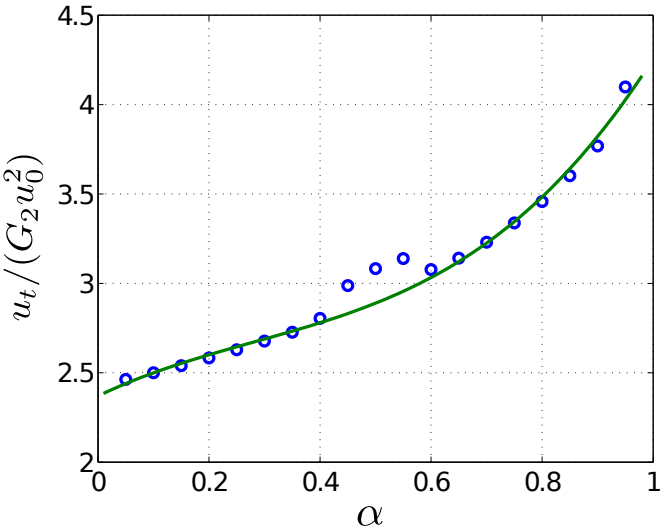

Figure 3.7: Variation of normalized maximum tail amplitude in the nonlinear diatomic spring-mass chain as a function of mass ratio (α).

3.2.2 Reconstruction of nonlinearity in diatomic granular chains

The variation of tail amplitude with respect to the non-dimensional excitation frequency (ω) is obtained from numerical simulations of diatomic granular chains for different values of the power law exponent (p), initial precompression (δ_0) and excitation amplitude (u_0). The nonlinear coefficient obtained from the Taylor series expansion does not change and can still be expressed by eqn. (3.5), which allows the use of the normalization parameter (δ_0/u_0^2). The normalized tail amplitude is plotted as a function of ω for different power laws (p) in fig. 3.8, and the cubic dependence on frequency is recovered. Furthermore, the softening behavior of the granular chain reflects in the change from maximum to minimum tail amplitude, which is also obtained at the same ω for all cases, thereby reiterating the equivalence between generic granular chains and spring-mass systems with quadratic nonlinearity.

In the case of diatomic granular chains, it is important to note that it is not necessary to obtain the variation of the tail amplitude as a function of frequency. It is sufficient to extract the minimum (or maximum) tail amplitude directly from numerical simulations (or experiments), and compare this value with the corresponding equivalent quadratic nonlinear contribution described by eqn. (3.11). Thus, an explicit expression for p can

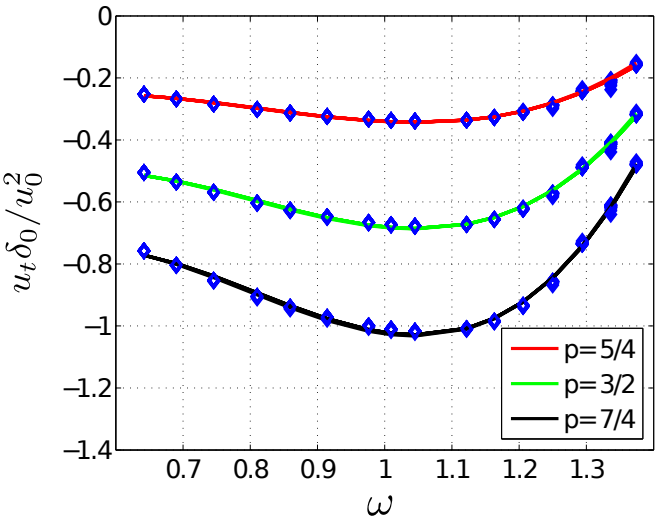

Figure 3.8: Variation of normalized tail amplitude as a function of non-dimensional excitation frequency in the Steel-Al diatomic granular chain for different power law interactions.

be obtained as

$$p = 1 - \frac{2\delta_0}{u_0^2}\frac{u_t^m}{F(\alpha_0)} \tag{3.12}$$

where $F(\alpha_0) = e\alpha_0^3 + f\alpha_0^2 + g\alpha_0 + h$. The constants e, f, g, and h are the invariants of nonlinearity estimated in the spring-mass diatomic system; α_0 is the specific mass ratio for the system under investigation, while δ_0 and u_0 are again extrinsic parameters that are prescribed.

The values of p reconstructed from numerical simulations of the three different diatomic chains for different hypothetical power laws are shown in table 3.3. Irrespective of the granular chain considered, the estimated values show remarkable agreement with the imposed power law.

Table 3.3: Power law reconstructed from eqn. (3.12) using numerical simulations

Imposed power law	Reconstructed from Steel-Al chain	Reconstructed from Steel-PTFE chain	Reconstructed from Al-PTFE chain
$p = 5/4 = 1.25$	1.2493	1.2482	1.2473
$p = 3/2 = 1.5$	1.4984	1.4967	1.4948
$p = 7/4 = 1.75$	1.7478	1.7454	1.7426

Even though we have so far assumed the two masses to have identical geometry and different material parameters, an equivalent mass ratio of a diatomic chain can also be obtained by considering masses made of the same material and featuring different geometry. Thus, the inverse problem constructed for the diatomic chain can be used to determine (or verify) the interaction power law for different contact geometries, such as sphere-cylinder, sphere-cuboid, etc.

3.3 Summary

In conclusion, the understanding of weakly nonlinear wave manipulation, which manifests as wave packet modulation, provides a method to inversely determine nonlinear system parameters from numerical or simulated data. Therefore, packet modulation can be used to determine nonlinearity in generic structures/materials by incorporating a notion of discreteness or periodicity to invoke the effects of interplay between dispersion and nonlinearity, and provide an alternate route to determine material parameters.

Chapter 4

Mode Hopping in Weakly Nonlinear Periodic Structures

Until now, the effect of nonlinearity on the solution of the zeroth order perturbation expansion ($\mathcal{O}(1)$) of the equations of motion has been studied. The solution at the higher orders of perturbation expansion, especially ($\mathcal{O}(\varepsilon)$) can also have a significant contribution to the spatial and spectral characteristics of wave motion, as the magnitude of the forcing function is dependent on the relative strength of nonlinearity and the amplitude of excitation established in the system. Therefore, in this chapter, solutions of the form

$$u = u^0(kn - \omega t, \varepsilon(n - c_g t), \varepsilon^2 t) + \varepsilon^1 u^1(kn - \omega t, \varepsilon(n - c_g t), \varepsilon^2 t),$$

will be considered to enunciate the characteristics of the solution at $\mathcal{O}(\varepsilon)$. Since the effect of nonlinearity at $\mathcal{O}(\varepsilon)$ is expected to lead to the generation of higher-harmonics [135], periodic structures with unit cells characterized by multiple degrees of freedom will be considered to delineate the interplay of dispersion and nonlinearity in the presence of modal complexity. The multiplicity of the degrees of freedom could be due to multidimensional wave propagation, or due to the ability of the unit cell to feature multiple modes of deformation to support unidimensional wave propagation. First, a diatomic chain will be considered, as it is the simplest multi degree of freedom system that is amenable to both numerical and analytical techniques. After deconstructing the

solution of the diatomic chain, periodic systems featuring additional modal complexity will be employed to generalize the characteristics of the higher order solutions for generic weakly nonlinear periodic structures.

4.1 Diatomic Spring-Mass chain

Consider a diatomic periodic chain consisting of two masses m_1 and m_2 connected by a nonlinear spring as shown in fig. 4.1. The equations of motion for the n^{th} set of masses (m_1 and m_2) in this nonlinear chain are

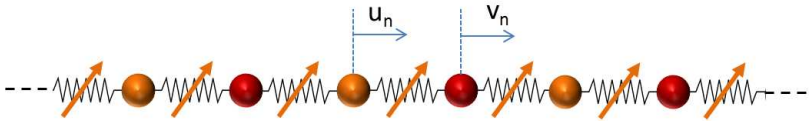

Figure 4.1: Diatomic spring-mass chain

$$\begin{bmatrix} m_1 & 0 \\ 0 & m_2 \end{bmatrix} \begin{Bmatrix} \ddot{u}_n \\ \ddot{v}_n \end{Bmatrix} + \begin{bmatrix} 2K_2 & -K_2 \\ -K_2 & 2K_2 \end{bmatrix} \begin{Bmatrix} u_n \\ v_n \end{Bmatrix} + \begin{bmatrix} 0 & -K_2 \\ 0 & 0 \end{bmatrix} \begin{Bmatrix} u_{n-1} \\ v_{n-1} \end{Bmatrix} + \begin{bmatrix} 0 & 0 \\ -K_2 & 0 \end{bmatrix} \begin{Bmatrix} u_{n+1} \\ v_{n+1} \end{Bmatrix} + \begin{Bmatrix} \varepsilon\, K_3 \left[(u_n - v_{n-1})^2 - (v_n - u_n)^2\right] \\ \varepsilon\, K_3 \left[(v_n - u_n)^2 - (u_{n+1} - v_n)^2\right] \end{Bmatrix} + \begin{Bmatrix} \varepsilon^2\, K_4 \left[(u_n - v_{n-1})^3 - (v_n - u_n)^3\right] \\ \varepsilon^2\, K_4 \left[(v_n - v_{n-1})^3 - (u_{n+1} - v_n)^3\right] \end{Bmatrix} = 0 \tag{4.1}$$

where u_n, v_n correspond to the displacement of the n^{th} set of masses m_1, m_2. K_2, K_3, and K_4 are the equivalent linear, quadratic, and cubic coefficients of the weakly nonlinear spring. Due to the weak nature of the nonlinear terms, the solution to eqn. (4.1) can once again be written using a perturbative expansion as

$$\mathbf{u}_n = \begin{Bmatrix} u_n(t) \\ v_n(t) \end{Bmatrix} = \begin{Bmatrix} \sum_{i=0}^{\infty} \varepsilon^i u^i(\theta_n, \xi_n, \tau) \\ \sum_{i=0}^{\infty} \varepsilon^i v^i(\theta_n, \xi_n, \tau) \end{Bmatrix}, \tag{4.2}$$

where $\theta_n = kn - \omega(k)t$, $\xi_n = \varepsilon(n - c_g t)$, and $\tau = \varepsilon^2 t$. Using this expression, the equations at each order of the perturbation expansion can be simplified as

$$\mathcal{O}(\varepsilon^p): \quad \omega^2 \mathbf{M} \frac{\partial^2 \mathbf{u}_n^p}{\partial \theta_n^2} + \sum_{i=n-1}^{n+1} \mathbf{K}_i \mathbf{u}_i^p = \mathbf{f}^p, \tag{4.3}$$

where

$$\mathbf{M} = \begin{bmatrix} m_1 & 0 \\ 0 & m_2 \end{bmatrix}; \ \mathbf{K}_n = \begin{bmatrix} 2K_2 & -K_2 \\ -K_2 & 2K_2 \end{bmatrix}; \ \mathbf{K}_{n-1} = \begin{bmatrix} 0 & -K_2 \\ 0 & 0 \end{bmatrix}; \ \mathbf{K}_{n+1} = \begin{bmatrix} 0 & 0 \\ -K_2 & 0 \end{bmatrix}.$$

The forcing function at the first two orders of expansion are[1]

$$\begin{aligned} \mathbf{f}^0 &= 0, \\ \mathbf{f}^1 &= \begin{Bmatrix} -2m_1\omega c_g \frac{\partial^2 u_n^0}{\partial \xi_n \partial \theta_n} - K_2 \frac{\partial v_{n-1}^0}{\partial \xi_n} + K_3 \left[(v_n^0 - u_n^0)^2 - (u_n^0 - v_{n-1}^0)^2 \right] \\ -2m_2\omega c_g \frac{\partial^2 v_n^0}{\partial \xi_n \partial \theta_n} + K_2 \frac{\partial u_{n+1}^0}{\partial \xi_n} + K_3 \left[(u_{n+1}^0 - v_n^0)^2 - (v_n^0 - u_n^0)^2 \right] \end{Bmatrix}. \end{aligned} \tag{4.4}$$

At $\mathcal{O}(1)$, the homogeneous solution can be expressed as

$$\mathbf{u}_n^0 = A_0(\xi_n, \tau) + A(\xi_n, \tau)\, \boldsymbol{\phi}\, e^{i\theta_n} + A^*(\xi_n, \tau)\, \boldsymbol{\phi}^*\, e^{-i\theta_n}, \tag{4.5}$$

where ω, k, and $\boldsymbol{\phi}$ satisfy the eigenvalue problem

$$\left(-\omega^2 \begin{bmatrix} m_1 & 0 \\ 0 & m_2 \end{bmatrix} + \begin{bmatrix} 2K_2 & -K_2(1 + e^{-ik}) \\ -K_2(1 + e^{ik}) & 2K_2 \end{bmatrix} \right) \boldsymbol{\phi} = 0. \tag{4.6}$$

The solution to the eigenvalue problem can be written as

$$\begin{aligned} \omega_{ac/op} &= \sqrt{\frac{K_2}{m_1 m_2}(m_1 + m_2) \mp \frac{K_2}{m_1 m_2}\sqrt{m_1^2 + m_2^2 + 2m_1 m_2 \cos k}}, \\ \boldsymbol{\phi}_{ac/op} &= \begin{Bmatrix} \frac{-(1+e^{-ik})m_2}{m1 - m2 \mp \sqrt{m_1^2 + m_2^2 + 2m_1 m_2 \cos k}} \\ 1 \end{Bmatrix}. \end{aligned}$$

[1] The slow spatiotemporal variable $\xi_{n\pm1}$ is expressed in terms of ξ_n using a Taylor series expansion as in chapter 2.

For any wavenumber k, there exist two possible frequencies of wave propagation, one corresponding to the acoustic mode (ω_{ac}, ϕ_{ac}), and the other corresponding to the optical mode (ω_{op}, ϕ_{op}). In this work, the input excitation will be assumed to belong to the acoustic mode of wave propagation (referred to as ω, ϕ henceforth).

In order to determine the slowly varying envelopes at $\mathcal{O}(1)$, the secular terms in the forcing functions at $\mathcal{O}(\varepsilon)$ and $\mathcal{O}(\varepsilon^2)$ need to be determined. At $\mathcal{O}(\varepsilon)$, the forcing function depends on the zeroth order solution, and can be written as

$$\mathbf{f}^1 = \begin{Bmatrix} -K_2 \frac{\partial A_0}{\partial \xi_n} \\ K_2 \frac{\partial A_0}{\partial \xi_n} \end{Bmatrix} + \frac{\partial A}{\partial \xi_n} e^{i\theta_n} \begin{Bmatrix} -2im_1\omega c_g \phi_u - K_2 \phi_v e^{-ik} \\ -2im_2\omega c_g \phi_v + K_2 \phi_u e^{ik} \end{Bmatrix} \tag{4.7}$$

$$+ K_3 A^2 e^{i2\theta_n} \begin{Bmatrix} (1 - e^{-i2k})\phi_v^2 - 2(1 - e^{-ik})\phi_v \phi_u \\ (e^{i2k} - 1)\phi_u^2 - 2(e^{ik} - 1)\phi_v \phi_u \end{Bmatrix} + c.c, \tag{4.8}$$

where $\boldsymbol{\phi} = \left\{ \phi_u,\ \phi_v \right\}^T$. The first two terms in $\mathbf{f}^1$ will lead to secular solutions if they resonate with the corresponding eigen solutions for eqn. (4.6), which are

$$[\omega, k] = [0, 0],\ \left[\sqrt{\frac{K_2}{m_1 m_2}(m_1 + m_2) - \frac{K_2}{m_1 m_2}\sqrt{m_1^2 + m_2^2 + 2m_1 m_2 \cos k}},\ k \right],$$

$$\phi = \begin{Bmatrix} C \\ C \end{Bmatrix}, \begin{Bmatrix} \frac{-(1+e^{-ik})m_2}{m1 - m2 - \sqrt{m_1^2 + m_2^2 + 2m_1 m_2 \cos k}} \\ 1 \end{Bmatrix},$$

where C is a constant. Secular solutions can be eliminated if the forcing function for a given eigenfrequency (ω, k) is orthogonal to the corresponding eigenvector $\boldsymbol{\phi}$. This orthogonality condition is trivially satisfied for the eigenfrequency pair $(0, 0)$, and after some algebraic manipulation, it can be shown that[2]

$$\phi_u^*(i2m_1\omega c_g \phi_u + K_2 e^{-ik}\phi_v) + \phi_v^*(i2m_2\omega c_g \phi_v - K_2 e^{ik}\phi_u) = 0, \tag{4.9}$$

which implies that the forcing function corresponding to $e^{i\theta_n}$ is also orthogonal to the corresponding eigenvector. As seen in the case of monoatomic chains, assuming the velocity of slow spatiotemporal space to be the group velocity of the wave packet automatically nullifies the presence of secular terms in the perturbation expansion. Therefore,

[2] A symbolic computing language (Mathematica) was employed to simplify the expression.

the solution at $\mathcal{O}(\varepsilon)$ can be written as

$$\mathbf{u}_n^1 = B(\xi_n, \tau)\, \mathbf{\Phi}\, e^{i2\theta_n} + B^*(\xi_n, \tau)\, \mathbf{\Phi^*}\, e^{-i2\theta_n}, \tag{4.10}$$

where $B = K_3 A^2$, and

$$\mathbf{\Phi} = \begin{bmatrix} -4\omega^2 m_1 + 2K_2 & -K_2(1+e^{-i2k}) \\ -K_2(1+e^{i2k}) & -4\omega^2 m_2 + 2K_2 \end{bmatrix}^{-1} \begin{Bmatrix} (1-e^{-i2k})\phi_v^2 - 2(1-e^{-ik})\phi_v\phi_u \\ (e^{i2k}-1)\phi_u^2 - 2(e^{ik}-1)\phi_v\phi_u \end{Bmatrix} \tag{4.11}$$

It is important to note that the above equation has a solution iff

$$\omega(2k) \neq 2\omega(k). \tag{4.12}$$

The negation of the above condition is referred to as phase matching or resonance of the second-harmonic. In single degree of freedom monoatomic chains, the non-resonance condition for the second-harmonic is trivially satisfied due to the dispersive nature of the system. In multi degree of freedom systems, this phase matching or resonance can occur between two different dispersion curves or surfaces. Therefore, if the second-harmonic is resonant with the corresponding homogeneous solution, additional conditions need to be incorporated in the solution (similar to the group velocity constraint imposed for the fundamental-harmonic). Typically, a three-wave-interaction model is assumed to study resonant second-harmonic generation [50, 69], which will not be considered in this dissertation.

In order to determine the exact form of A_0 and A, it is necessary to consider the set of equations at $\mathcal{O}(\varepsilon^2)$. From the numerical simulations of the diatomic chain in chapter 3, it is observed that the slow spatiotemporal envelope can be represented by a Nonlinear Schrödinger equation, which is consistent with the equations determined in published literature [59, 99]. Since the focus of this chapter is to delineate the qualitative characteristics of the solution at $\mathcal{O}(\varepsilon)$, the exact solution for A_0 and A will not be reproduced here.

Eqn. (4.10) only describes the particular solution at $\mathcal{O}(\varepsilon)$. The homogeneous solution at $\mathcal{O}(\varepsilon)$ has to be chosen such that the initial conditions specified for the diatomic chain are satisfied. For a semi-infinite chain excited at one end with the harmonic excitation,

the initial condition at $\mathcal{O}(\varepsilon)$ corresponds to the absence of second-harmonic features at the first mass. Therefore, under the assumption that the solution at $\mathcal{O}(1)$ completely describes the fundamental-harmonic features, the complete solution at $\mathcal{O}(\varepsilon^1)$ can be written as

$$\mathbf{u}_n^1 = D(\xi_n, \tau)\, \boldsymbol{\chi}\, e^{i\psi_n} + B(\xi_n, \tau)\, \boldsymbol{\Phi}\, e^{i2\theta_n} + c.c, \tag{4.13}$$

where $\psi_n = k(2\omega)n - 2\omega t$ is the fast spatiotemporal variable that satisfies the linear eigenvalue problem. $\boldsymbol{\chi}$ is the eigenvector corresponding to the eigenfrequency $[2\omega, k(2\omega)]$ and D is determined from the condition $u_0^1 = 0$. The solution to eqn. (4.1), truncated at $\mathcal{O}(\varepsilon)$ is

$$\mathbf{u}_n = A_0(\xi_n, \tau) + A(\xi_n, \tau)\, \boldsymbol{\phi}\, e^{i\theta_n} + \varepsilon D(\xi_n, \tau)\, \boldsymbol{\chi}\, e^{i\psi_n} + \varepsilon B(\xi_n, \tau)\, \boldsymbol{\Phi}\, e^{i2\theta_n} + c.c. \tag{4.14}$$

As expected, the higher order effects of nonlinearity lead to the generation of higher-harmonics, which is captured in eqn. (4.14). However, the interesting feature associated with periodic structures is that the generated second-harmonic has multiple spatiotemporal characteristics, one corresponding to the forcing term $(2k(\omega)n - 2\omega t)$, and the other corresponding to the homogeneous solution $(k(2\omega)n - 2\omega t)$. In monoatomic periodic structures, the two components can be viewed as a single second-harmonic feature modulated by a spatially beating amplitude ($B \propto e^{i(2k - k(2\omega))n}$) [10, 107]. However, in periodic structures featuring multiple modes of wave propagation, the two second-harmonic features have different modal distributions (contribution to each mass), thereby, not necessarily giving rise to a spatial beating.

From eqn. (4.14), it can be seen that the homogeneous part of the nonlinearly generated higher-harmonics conforms to the linear dispersion relation of the structure, which implies that the characteristics of this component can be determined from a simple eigen analysis of the corresponding linear structure. In order to elaborate this statement, numerical analysis of a semi-infinite diatomic spring mass chain (with $m_1 = 1, m_2 = \alpha$)[3] with unit linear and nonlinear spring coefficient ($K2 = K_3 = 1$, $K_4 = 0$) is considered for a burst excitation applied to the first mass. The carrier frequency of the excitation is chosen to belong to the acoustic mode of wave propagation. The spatial wave profile in this system for a given excitation frequency (at a particular time

[3]The heavier mass is assumed to be m_1 for convenience ($\alpha < 1$).

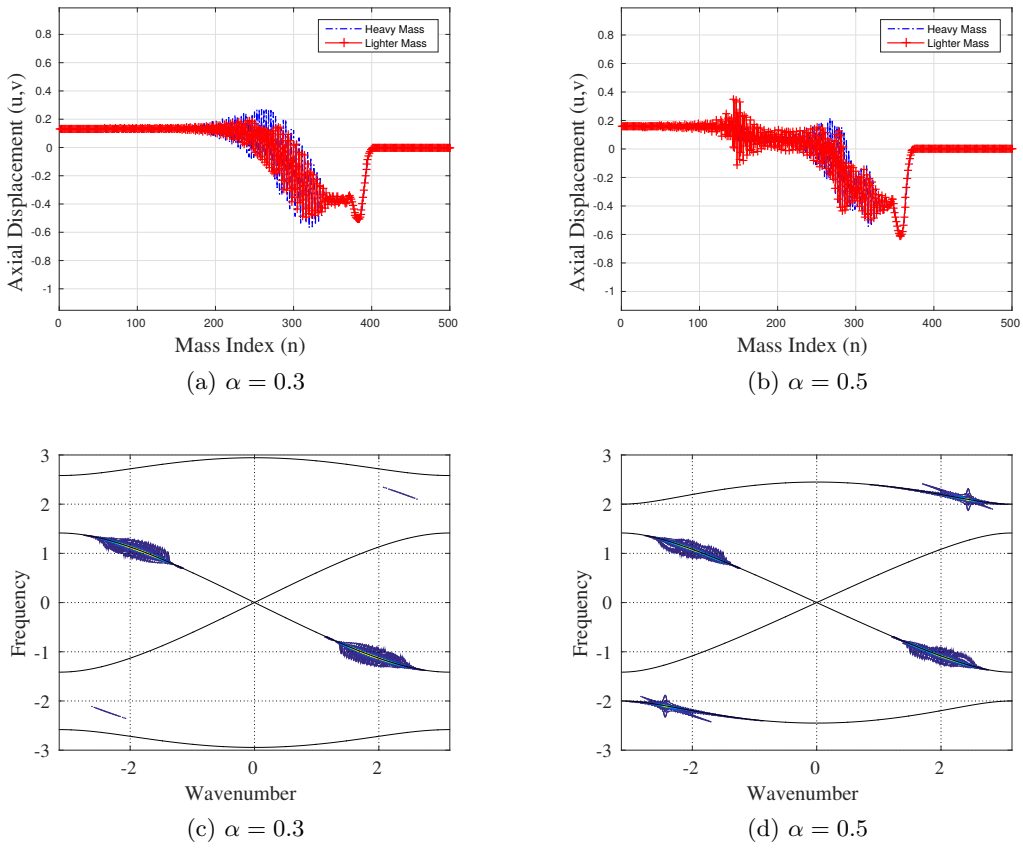

(a) $\alpha = 0.3$ (b) $\alpha = 0.5$

(c) $\alpha = 0.3$ (d) $\alpha = 0.5$

Figure 4.2: Spatial and spectral wave profile in two diatomic chains characterized by different mass ratio for the same input excitation (a-b) Spatial wave profile in the heavy and light masses, (c-d) $2-D$ DFT of spatial wave profile in lighter mass for both the cases.

instant) is plotted for two different choices of the mass ratio ($\alpha = 0.3, 0.5$) in figs. 4.2(a-b). It is seen that, for the same excitation parameters, the spatial profile is significantly affected by the change in mass ratio. In order to understand the differences between the two spatial profiles, the spectral contours of the lighter mass corresponding to the two cases are also plotted in figs. 4.2(c-d)[4]. It is important to note that the spectral contours are plotted in the entire region of wave propagation ($\pm k, \pm\omega$) as the acoustic and optical mode for the diatomic chain have complementary wave characteristics, i.e.,

[4]The long-wavelength envelope which dominates the spectral response has been filtered out to emphasize the harmonic components of the spatiotemporal profile.

the group velocity of the acoustic and the optical wave packets have opposite signs, which implies that they occupy different quadrants in the spectral domain. In figs. 4.2(c-d), the corresponding linear dispersion relations have also been superimposed on to the spectral contours, which provides the explanation for the significant difference in the spatiotemporal profiles plotted in figs. 4.2(a-b). For the case of smaller mass ratio ($\alpha = 0.3$), the second-harmonic (2ω) lies in the bandgap of the structure, i.e., the value of k satisfying the dispersion relation at 2ω is imaginary. Therefore, the homogeneous component has an attenuating characteristic and only the second-harmonic component corresponding to the forcing function ($2kn-2\omega t$) propagates through the structure. The spectral component corresponding to $2kn - 2\omega t$ appears in the optical mode of wave propagation due to the fact that the resolution of the wavenumber is only achieved within the fundamental period ($k \in [-\pi\, \pi]$) [69]. On the contrary, for the larger mass ratio ($\alpha = 0.5$), the second-harmonic lies in the optical mode of wave propagation, which gives rise to a propagating characteristic for the homogeneous component of the nonlinearly-generated second-harmonic. Therefore, the amplitude of the second-harmonic (2ω) is much larger in this system when compared to that of the system with the smaller mass ratio.

When the choice of fundamental-harmonic is such that the generated second-harmonic lies in the bandgap of the periodic structure, the structure effectively acts as an adaptive filter, converting a part of the energy from the initial wave packet into a non-propagating mode. Alternately, a suitable choice of the fundamental-harmonic such that the second-harmonic lies in the domain of the optical mode of wave propagation leads to the phenomenon of *mode hopping*, whereby, a part of the energy injected into the system hops from the acoustic to the optical mode. Therefore, this component of the energy propagates through the system with fundamentally different modal characteristics when compared to the initial excitation.

In fig. 4.2, the modal characteristics of the forced harmonic are also different from that of the fundamental-harmonic. However, the modal contribution of the forced second-harmonic are determined from the modal characteristics of the fundamental-harmonic and the nature of nonlinearity in the system (eqn. 4.11), which implies that these characteristics are fixed for a given fundamental mode of wave propagation. In contrast, the homogeneous component can be engineered to feature complementary modal

characteristics by simply altering the parameters of the linearized structure, thereby providing an opportunity for adaptive spatial wave manipulation. The advantage of pursuing mode hopping in periodic systems featuring modal complexity will be illustrated in the next subsection by considering a structure featuring additional degrees of freedom.

4.2 $1D$ Spring-Mass Truss

Consider the nonlinear spring-mass system shown in fig. 4.3, which consists of a pair of monoatomic spring-mass chains connected to each other via cross springs. All the masses are assumed to be constrained to move only axially, and the potential energy of the springs is assumed to have a nonlinear (cubic in this case) dependence upon the change in length.

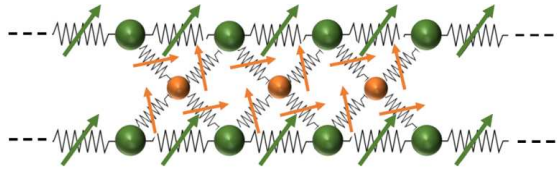

Figure 4.3: Schematic of $1D$ nonlinear crystal waveguide with cross links.

Let x_i, y_i and x_j, y_j denote the positions of two masses i and j connected by a spring. If the displacement of the i^{th} mass is denoted as u_i, then the relative displacement between masses i and j can be written as

$$\Delta_{ij} = \sqrt{(\tilde{x}_j - \tilde{x}_i)^2 + (y_j - y_i)^2} - \sqrt{(x_j - x_i)^2 + (y_j - y_i)^2},$$

where $\tilde{x}_i = x_i + u_i$. From geometric considerations, we can write $x_j = x_i + d_1$; $y_j = y_i + d_2$, where d_1 and d_2 are the horizontal and vertical distance between the masses in the equilibrium configuration. The displacements of the masses, which determine the change in length of the spring, are assumed to be small with respect to the initial unstretched length of the springs, thereby allowing a linearization of the geometric

nonlinearity. Therefore, the net displacement Δ_{ij} can be simplified as

$$\Delta_{ij} = -\frac{d_1(u_j^x - u_i^x)}{\sqrt{d_1^2 + d_2^2}}. \tag{4.15}$$

The force-displacement relationship for the spring is now written as

$$F = K_2\Delta_{ij} + K_3\Delta_{ij}^2.$$

Therefore, the equations of motion can be written as

$$\mathbf{M}\ddot{\mathbf{u}}_n + \sum_{i=n-1}^{n+1} \mathbf{K}_i\mathbf{u}_i + \varepsilon\mathbf{f}_{NL} = 0, \tag{4.16}$$

where $\mathbf{u}_n$ is a vector of displacements of the n^{th} set of masses, $\mathbf{M}$ and $\mathbf{K}$ are the mass and linear stiffness matrices, respectively, and $\mathbf{f}_{nl}$ is a force vector which has a nonlinear dependence on the displacements. The weakness of the nonlinear term follows from the assumption of small displacements of the masses with respect to the length-scale of the system ($u/L \approx \mathcal{O}(\varepsilon)$). The angle of the cross links is assumed to be 45° and, for simplicity, all the parameters of the system (masses, initial lengths of springs and linear and nonlinear spring coefficients) are taken to be unity. The dispersion relation for the linearized system obtained by employing the Floquet-Bloch condition is plotted in fig. 4.4.

From the dispersion curve, it is possible to choose a working frequency that lies in the domain of the acoustic mode of wave propagation such that, the corresponding second-harmonic lies in the domain of the optical mode (fig. 4.5a). In addition, the eigenmodes of the linear system show that the top and the bottom layers move in-phase with respect to each other in the acoustic mode, while they move out-of-phase with respect to each other in the optical mode (figs. 4.5(b-c)). This implies that the acoustic mode of wave propagation activates longitudinal deformation in the waveguide while the optical mode results in the activation of shear horizontal deformation. Therefore, an excitation in the acoustic mode of wave propagation can be imparted optical mode characteristics by appealing to the concept of mode hopping.

A numerical simulation of the nonlinear system is carried out for a burst excitation

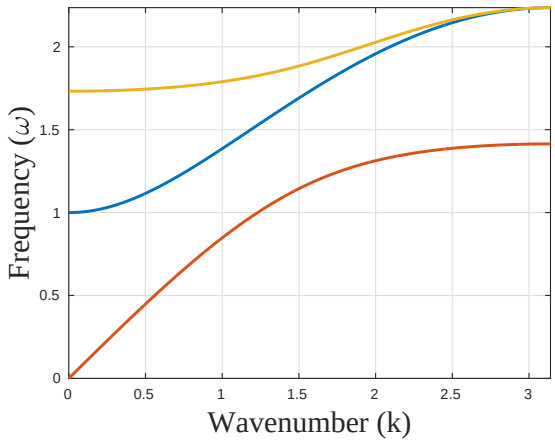

Figure 4.4: Linearized dispersion relation of nonlinear spring-mass waveguide.

applied at the first mass of the bottom layer. The spatial wave profile established in the bottom and top layers is plotted in figs. 4.6(a-b) for two different amplitudes of excitation. For sufficiently small amplitudes, the effect of the nonlinearity is observed only in the modulation of the amplitude, which results in the establishment of a non-harmonic component. Furthermore, the harmonic component in the bottom and the top layer have the same amplitude and move in-phase as predicted by the mode shapes determined from the dispersion curves. As the amplitude is increased, the component of the response with frequency content corresponding to the second-harmonic *hops* from the acoustic to the optical mode. This is illustrated in fig. 4.6c, in which the spectral content of the wave is superimposed on the dispersion curves, and shows the spectral signature of the second-harmonic to coincide with the optical mode. The heterogeneous component of the second-harmonic $(2k, 2\omega)$ is observed only when the fundamental-harmonic is isolated (shown in fig. 4.6d), which implies that the strength of this component is much smaller when compared to the homogeneous component.

The spatial wave profile in the truss (fig. 4.7) for the case of high amplitude features two distinct oscillatory components (both modulated by the asymmetric envelope): a faster, dominant feature and a slower, secondary contribution, whose difference in speed corresponds to the slight gap in group velocity between the two dispersion branches at the hopping point. Furthermore, it is observed that while the faster component exhibits in-phase dynamics between the top and bottom layers, the slower harmonic exhibits

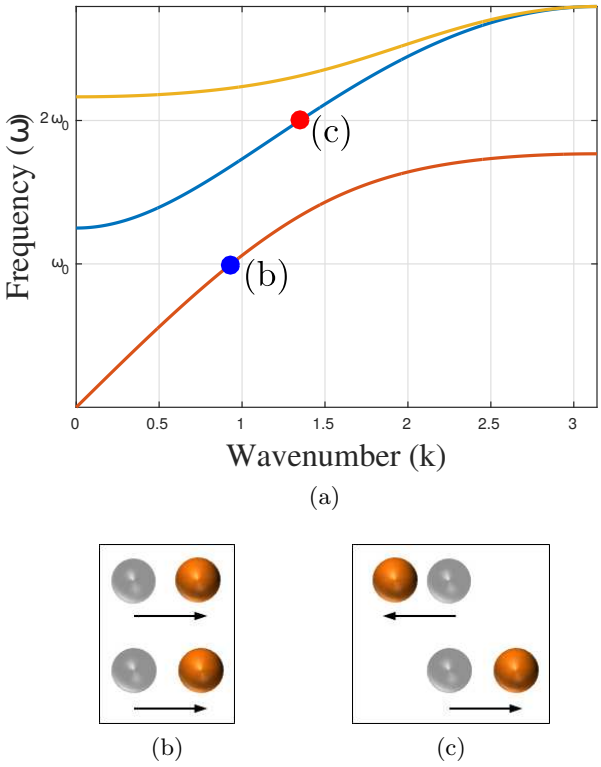

Figure 4.5: (a) Concept of Mode Hopping illustrated for one particular choice of fundamental excitation (b-c) Modal structure of the bottom and top layers in the acoustic and optical mode at the fundamental- and second-harmonic respectively.

out-of-phase dynamics between the top and bottom layers, a characteristic consistent with the mode shapes of the linearized system. Therefore, the activation of the second-harmonic by mode hopping yields an output signal with a broader frequency spectrum that stretches over multiple branches and blends the deformation characteristics of multiple modes, a feature that will be referred to as *modal mixing* henceforth.

In summary, the waveguide behaves as an amplitude-controlled switch between two distinct operating modalities. For sufficiently weak excitations, the energy travels along the waveguide with high speed and primarily axial deformation, while larger amplitudes induce a partial energy migration to a slower mode that shears the structure horizontally. Therefore, by simply controlling the amplitude, we have access to deformation patterns and modal attributes that are typical of the optical mode, even while we excite the

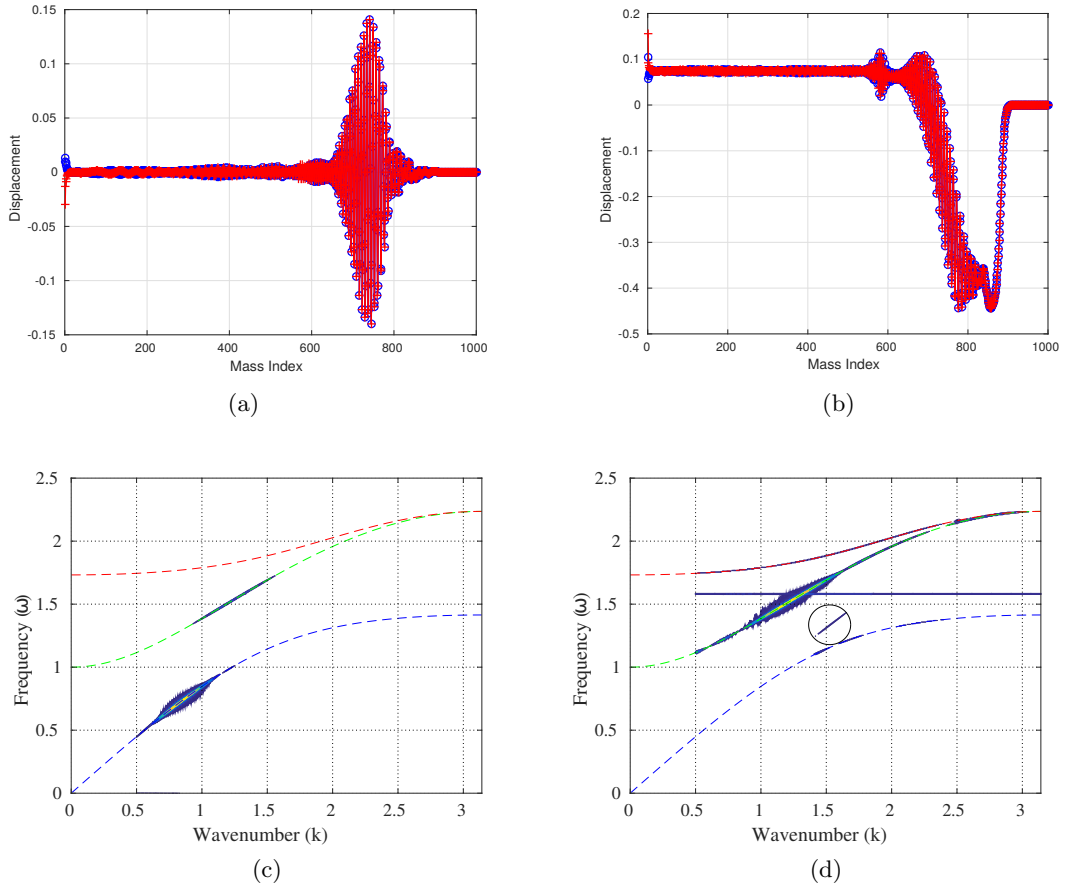

Figure 4.6: Proof of concept of mode hopping: (a-b) Spatial wave profile in top and bottom layers of $1D$ nonlinear crystal waveguide for two different amplitudes of excitation (c) Spectral contour of response for the high amplitude excitation displaying the hopping mechanism resulting in the activation of the optical mode for an excitation applied in the acoustic range (d) Filtered spectral contour of the high amplitude excitation displaying the spectral contours corresponding to the forced second-harmonic component.

system in the low-frequency regime.

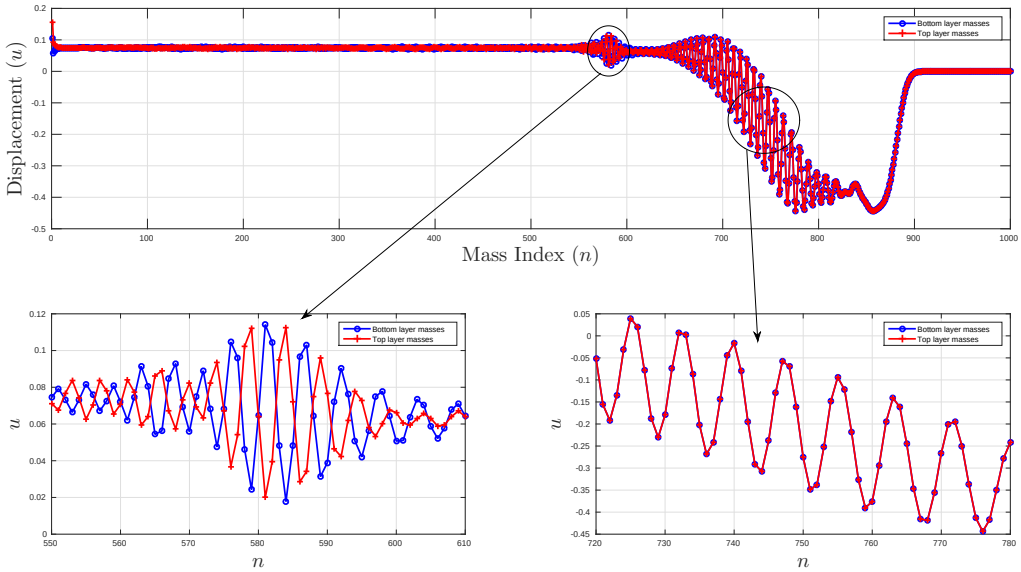

Figure 4.7: Proof of concept of modal mixing: Snapshot of a wave packet revealing co-existence of a faster acoustic mode (fundamental-harmonic) and a slower optical mode (second-harmonic). The second-harmonic response displays out-of-phase dynamics and shear deformation between top and bottom layers, while the fundamental-harmonic response displays in-phase dynamics and axial (longitudinal) deformation. The displacement is normalized by the maximum excitation amplitude.

4.3 Conclusion

The interplay of nonlinearity and dispersion in generating higher-harmonics in the response features certain unique characteristics seldom observed in nondispersive systems. Specifically, the presence of modal complexity in the structure leads to jumps in the response across the available propagation modes, thereby giving rise to a mixture of modes and the simultaneous activation of complementary functionalities. As a result, functionalities that are normally associated with high-frequency modes can be activated in the response even while applying low-frequency excitations. Ultimately, the topological complexity of the crystal and the nature of nonlinearity determine the available opportunities for mode hopping and modal mixing, along with the landscape of functionalities that can be activated, thereby enabling access to virtually endless opportunities to engineer materials with desired switchable functionalities.

Chapter 5

Adaptive and Tunable Phononic Switches

In this chapter, the concept of mode hopping and modal mixing will be demonstrated in granular phononic crystals and nonlinear lattice structures - systems that cover the entire gamut of nonlinear mechanisms realizable in elastic solids (geometric, material, and contact nonlinearity). In addition, preliminary experimental validation of mode hopping in nonlinear lattices using Scanning Laser Doppler Vibrometry (SLDV) will also be presented.

5.1 $1D$ Granular Waveguide

Consider a granular waveguide consisting of two monoatomic granular chains made of Aluminum spheres, cross-linked by an intermediate layer of stiffer Steel spheres. This system is the granular counterpart of the spring-mass truss studied in chapter 4. The diameter of the inner beads is chosen such that the angle of the cross springs is 45°, and the corresponding configuration is shown in fig. 5.1. This configuration can also be viewed as a rectangular lattice with interstitial inclusions featuring a single tiling in the vertical direction. The system is precompressed in the horizontal and vertical directions to ensure that the beads remain in contact, and the excitation is applied at the first bead of the lower layer. Wave motion is constrained along the horizontal direction, however, each mass is allowed to have two degrees of freedom (horizontal and vertical

displacement) to accommodate axial and flexural wave motion. The net compression between two spheres in contact can be derived as (similar to eqn. 4.15)

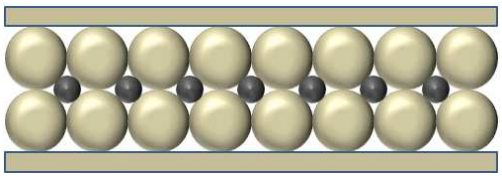

Figure 5.1: $1D$ Granular Waveguide

$$\Delta_{ij} = -\frac{d_1(\delta_{ij}^x + u_j^x - u_i^x) + d_2(\delta_{ij}^y + u_j^y - u_i^y)}{\sqrt{d_1^2 + d_2^2}},$$

where Δ_{ij} is the relative displacement of two spheres i and j, and u_i^x, u_i^y are the horizontal (x) and vertical (y) displacements of the i^{th} sphere. d_1 and d_2 are the distance between the spheres in the case of zero precompression, and, $\delta_{ij}^x, \delta_{ij}^y$ denote the net precompression in the horizontal and vertical direction between the i^{th} and j^{th} sphere. Using this definition, the contact force between the two particles can be expressed using Hertzian Theory as

$$F(\Delta_{ij}) = A\,[\Delta_{ij}]_+^{3/2},$$

where A is a constant dependent on the material properties of the two spheres, determined as

$$A = \frac{4E_iE_j\sqrt{\frac{R_iR_j}{R_j+R_i}}}{3E_j(1-\nu_i^2) + 3E_i(1-\nu_j^2)}.$$

R corresponds to the radius of the sphere, while E and ν are the Youngs modulus and poissons ratio of the material, respectively. As in chapter 3, granular chains transmit forces only when there is effective compression between two consecutive spheres, i.e., forces exist only for positive values of the quantity: $[\Delta_{ij}]_+ = max(0, \Delta_{ij})$.

The equations of motion for the periodic structure can be linearized under the assumption of small displacement to precompression ratio ($u << \delta$), which is used to determine the dispersion characteristics of the system. The unit cell consists of three masses and six degrees of freedom, which implies that the dispersion relation features six branches. The lowest four modes of the dispersion curves are plotted in fig. 5.2 for

one particular choice of precompression in the x and y direction.

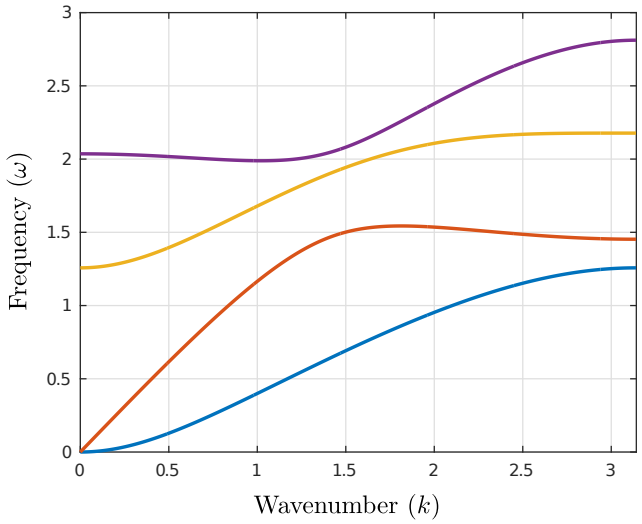

Figure 5.2: Linearized Dispersion Relation of $1D$ Granular Waveguide

In this system, the existence of two acoustic modes at low frequencies implies that even the fundamental harmonics propagate with multimodal characteristics featuring a mixture of axial and flexural deformation. The spatial and spectral contours (corresponding to the lateral degree of freedom) of linear wave propagation for a frequency in the acoustic mode is illustrated in fig. 5.3(a-b), where two harmonic contributions are indeed observed. As the amplitude is increased, the optical modes corresponding to the nonlinear generation of the second-harmonic are also activated. The effect of mode hopping is observed as an additional burst of lateral displacement in the propagating wave packet, which travels at an intermediate speed between those of the acoustic modes. This is shown in fig. 5.3c, where the lateral displacement profile corresponding to the nonlinear system features three distinct oscillatory contributions in the wave profile - two corresponding to the incident acoustic excitation and one corresponding to the nonlinearly-generated harmonic with optical mode characteristics. Furthermore, two contributions corresponding to the second-harmonic are observed in the corresponding spectral contour (fig. 5.3d) - one with the forced harmonic feature $(2k, 2\omega)$, and the other with the homogeneous spectral characteristic $(k(2\omega), 2\omega)$. In this system, the homogeneous component is again observed to be stronger than the forced component of

the second-harmonic.

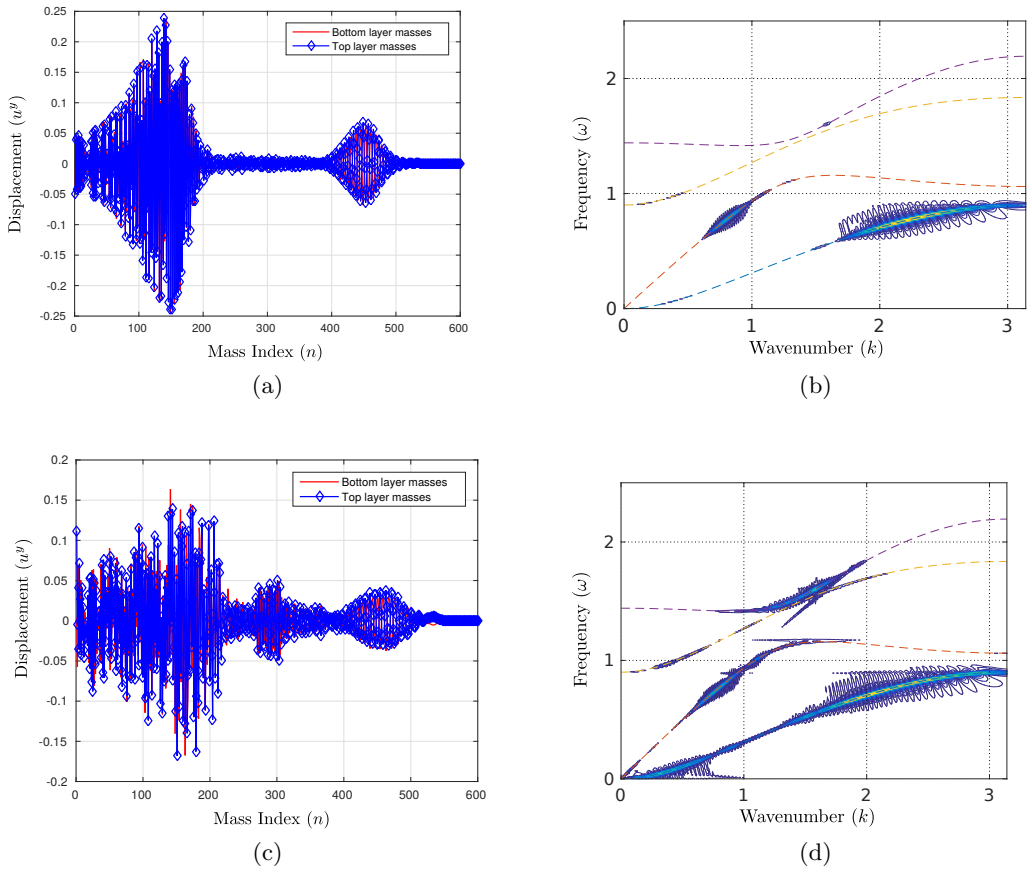

Figure 5.3: Mode hopping and modal mixing in a granular waveguide: (a-c) Lateral wave profile in the waveguide for two different amplitudes of excitation, (b-d) Spectra of the response superimposed on the linearized dispersion relation. The excitation frequency is normalized by the linearized resonance frequency.

From this example, it can be seen that the features of mode hopping and modal mixing can be extended to systems with multiple degrees of freedom seamlessly, and the homogeneous features of the nonlinearly-generated harmonic still conform to the linearized dispersion characteristics of the system. Since the lateral degrees of freedom predominantly display the effect of modal mixing, this system can be envisioned as the logical building block of an amplitude filter in which the energy of high-amplitude excitations is rerouted laterally away from the main waveguide direction.

5.2 $2D$ Granular Phononic crystals

In the case of $1D$ wave propagation in waveguides, the presence of modal complexity gives rise to the ability to engage complex intra-cell deformation mechanisms by the phenomenon of modal mixing, even while preserving the direction of wave propagation. On the contrary, if wave propagation in multidimensions is considered, each harmonic will have its own spatial directivity features, which could potentially be used to adaptively impart complementary spatial directivity to propagating excitations, thereby rerouting some energy away from the main wave direction. In order to study the use of nonlinearity as a means to control spatial directivity in two-dimensional periodic structures, the classical hexagonally packed $2D$ granular phononic crystal depicted in fig. 5.4 is considered, in which, for simplicity, all the beads are made of the same material and the confining loads are applied such that all the beads experience the same net precompression.

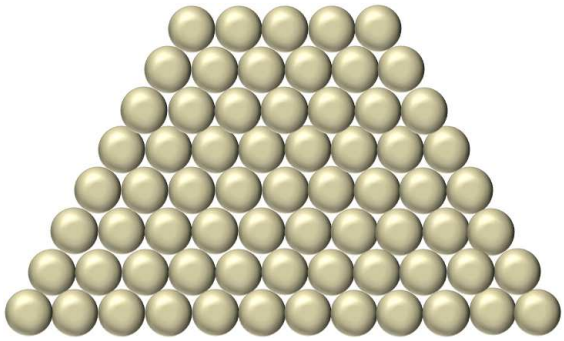

Figure 5.4: $2D$ Hexagonal Close Packed Granular Crystal

In the limit of small-amplitude displacements, the Hertzian contact can be linearized and the system can be represented equivalently by a triangular spring mass lattice as shown in fig. 5.5a. The band structure for this unit cell evaluated along the contour of the irreducible Brillouin zone is also shown in fig. 5.5b. Since the system under consideration is monoatomic, it displays low-pass filter characteristics, whereby excitations beyond a particular frequency cannot propagate through the system. However, in the propagation zone, there exist two modes of wave propagation, one corresponding to the longitudinal mode, and the other corresponding to the shear mode. At certain frequencies, wave propagation is possible only in the longitudinal mode as the shear mode has a lower

cutoff-frequency than the longitudinal mode. Therefore, in the nonlinear system, mode hopping could potentially be employed to change the modal mixture of the response in a way that globally favors longitudinal mechanisms. Therefore, a pair of frequencies are

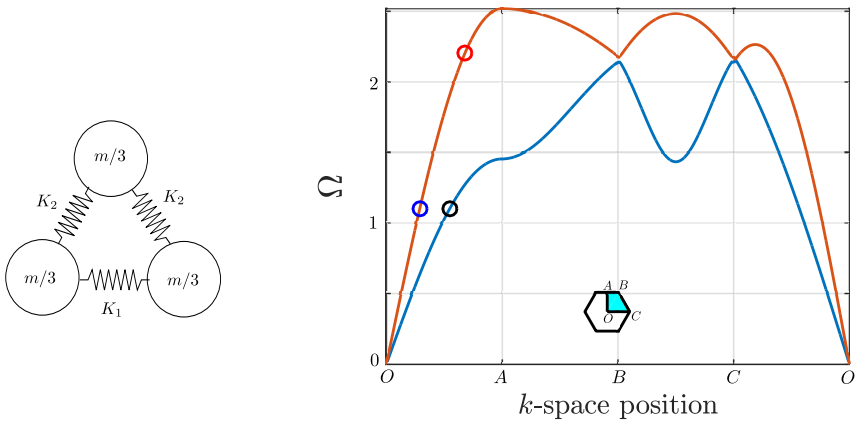

(a) (b)

Figure 5.5: (a) Linearized unit cell for the 2-D HCP granular crystal, (b) Band structure along the contour of the irreducible Brillouin Zone when all the beads are subjected to the same precompression in the X and Y direction.

considered from the linearized band structure such that the higher frequency excitation results in activation of only the longitudinal mode of wave propagation ($\Omega = 1.1$ and $\Omega = 2.2$)[1]. For these two frequencies, the spatial directivity of the linearized lattice is obtained by monitoring the group velocity contours, which are shown in fig. 5.6. For the lower frequency excitation, the longitudinal and shear mode coexist in the response, and the shear mode displays preferential direction for wave propagation (fig. 5.6a), while the longitudinal mode is essentially isotropic. However, at the higher frequency, the longitudinal mode also displays preferential directions, which is complementary to the preferential directions of the shear mode excited at the lower frequency (fig. 5.6b).

To verify the preferential directions of wave propagation, the system is excited in the vertical direction by applying a narrow-band tone burst to the middle bead of the bottom layer. The component of the displacement corresponding to the longitudinal and shear mode of wave propagation at each bead is determined by evaluating the

[1]The frequencies are normalized with respect to the resonance frequency of the linearized spring-mass system.

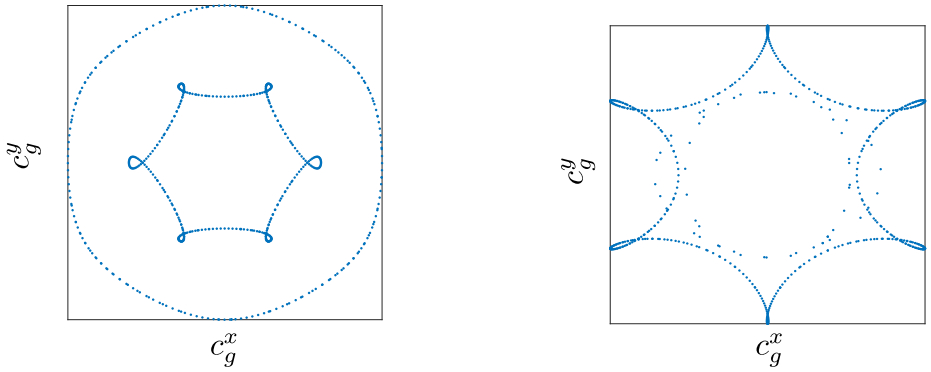

(a) $\Omega = 1.1$ (b) $\Omega = 2.2$

Figure 5.6: Group velocity contours of the $2D$ HCP granular crystal for two excitation frequencies.

radial and tangential components of the bead with respect to the point of excitation. The radial component of the displacement, which captures the features of longitudinal wave motion is plotted in fig. 5.7 for the two frequencies of wave propagation (the amplitude of excitation is set to be much smaller than the applied precompression to realize linear wave propagation characteristics). For the low-frequency excitation, the longitudinal and shear mode coexist in the response with complementary directions of wave propagation: the shear mode propagates along the boundary of the structure, while the longitudinal mode propagates in the direction of excitation (fig. 5.7a). At the higher frequency, the short-wavelength longitudinal mode is directional with the classical six-folded symmetry (fig. 5.7b), which is identical to the group velocity contours determined from Bloch analysis for this frequency in fig. 5.6b.

As the amplitude of excitation is increased, the second-harmonic is excited in the system. This is verified by monitoring the radial component of displacement (plotted in fig. 5.8a), where the additional contribution to the longitudinal deformation of the crystal (with shorter wavelength and lower group velocity than the one excited by the fundamental-harmonic) is observed. Since the lower frequency wave dominates the response, a high-pass filter is applied to the numerical data to isolate the second-harmonic features. The radial component of the filtered displacement is plotted in fig. 5.8b, where the six fold symmetry of the higher harmonic component is indeed observed.

Thus, by increasing the amplitude of excitation and triggering the second-harmonic,

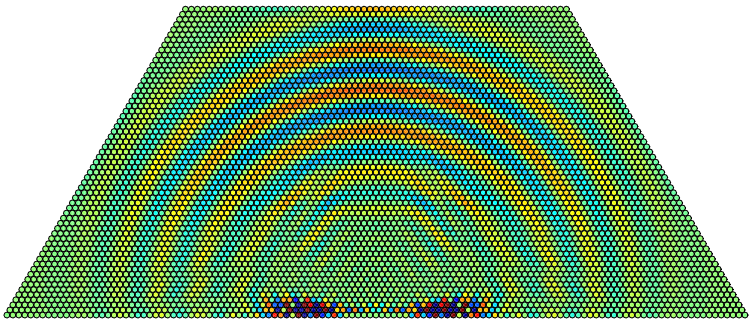

(a) $\Omega = 1.1$

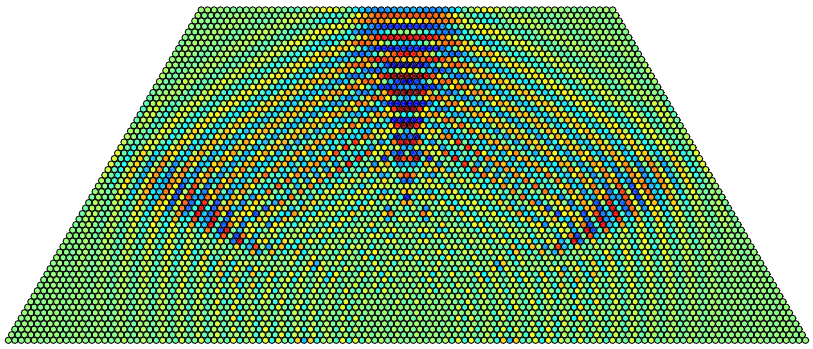

(b) $\Omega = 2.2$

Figure 5.7: Radial component of displacement at every bead obtained numerically for the pair of frequencies ($\Omega = 1.1$ and $\Omega = 2.2$). The lower frequency displays circular wave profile which implies that wave motion is isotropic, while the higher frequency is significantly focussed along specific directions.

the modal mixture of the response is altered in a way that globally favors longitudinal mechanisms and additional directivity characteristics which are normally experienced at higher frequencies of excitation are also activated at lower frequencies of excitation.

5.2.1 Tunable Granular Phononic Crystals

In granular crystals, the activation of mode hopping and modal mixing mechanisms are dependent on the relative strength of nonlinearity in the system, which in turn is dependent on the ratio of excitation amplitude to the initial precompression established

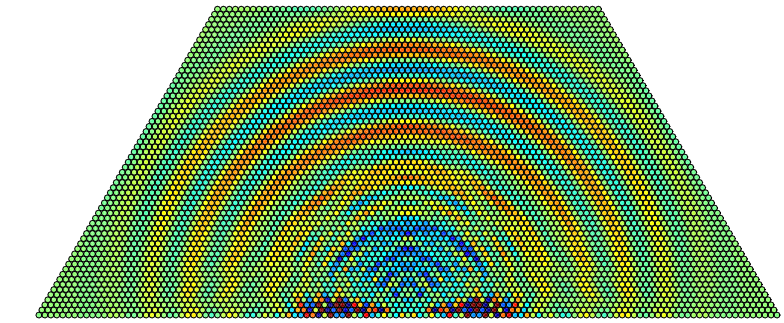

(a)

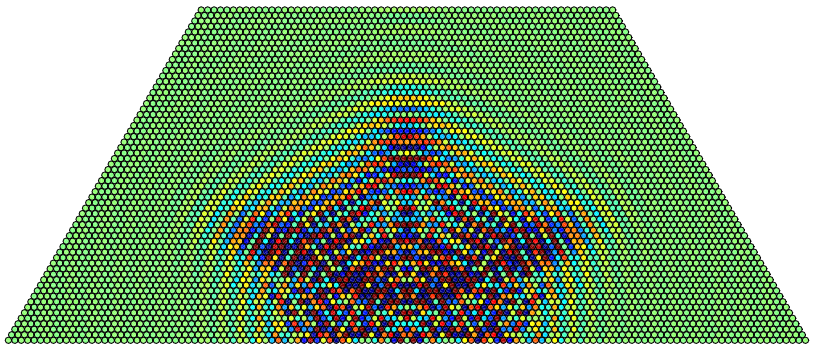

(b)

Figure 5.8: Proof of Modal Mixing in $2D$ Granular Crystal: (a) Radial component of displacement at every bead obtained for the high-amplitude low-frequency excitation ($\Omega = 1.1$). (b) The filtered radial component corresponding to the nonlinearly-generated second-harmonic.

in the system. Therefore, for a given excitation amplitude, the precompression applied on the structure can be varied to activate/de-activate mode hopping and modal mixing mechanisms. Thus, granular phononic crystals can function as *adaptive* and *tunable* switches, whereby the reversible activation and deactivation of mode hopping and modal mixing mechanisms can be obtained either as a spontaneous response to changes in the amplitude of excitation or via external parameter tuning.

In addition, tunability can also be utilized to alter the characteristics of the nonlinearly generated harmonics. In order to demonstrate the tunable characteristics of

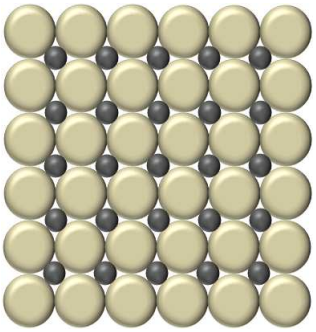

Figure 5.9: $2D$ Rectangular Close Packed Granular Crystal

granular crystals, consider the classical rectangular close-packed $2D$ dimer crystal depicted in fig. 5.9, in which the bigger beads are made of Aluminum while the interstitial beads are made of Steel. This configuration can also be seen as a $2D$ extension of the truss structure in fig. 5.1. The structure is subjected to a differential precompression in the horizontal and vertical directions, and the linearized dispersion relations for two different conditions of initial precompression ($F_x > F_y$ and $F_x < F_y$ keeping F_x fixed) are shown in fig. 5.10. It can be noticed that changing the precompression force results in profound modifications of the band diagram, namely a shift of the center and width of the bandgap. Now, under the assumption that both the systems are excited with a wave of frequency ω, the second-harmonic (2ω) will either have propagating or attenuating characteristics depending upon the ratio of the precompression forces established in the structure. Therefore, by merely changing the external forces, a portion of the energy injected in to the system can be diverted into an attenuating mode or imparted complementary spatial characteristics.

5.3 Nonlinear Lattice Structures

Until now, the concepts of mode hopping and modal mixing have been demonstrated theoretically in spring-mass lattices and numerically in granular phononic crystals, where the nonlinearity stems from the contact interaction between two beads. However, physical realization of a granular structure poses many challenges as a wide variety of effects such as disorder, plasticity, dissipation, and additional rotational degrees of freedom can affect the ideality of the system. Another route to realize nonlinear phononic crystals

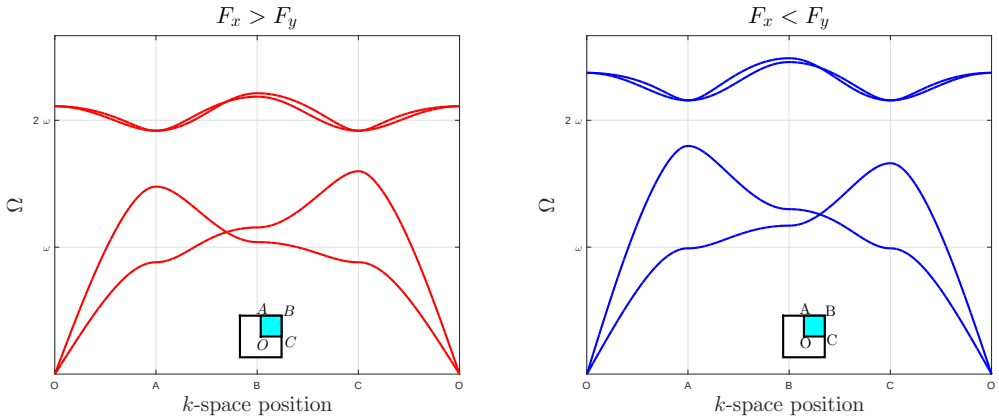

Figure 5.10: Linearized dispersion relation of the $2D$ RCP granular crystal along the irreducible Brillouin zone $OABCO$ for two different values of precompression in the horizontal and vertical direction. The force in the horizontal direction is kept constant while the force in the vertical direction is varied.

consists of employing lattice structures made of materials which can undergo large deformation. While the literature on lattice materials in the field of phononic crystals has been for the most part limited to the linear regime, recent interest in nonlinear periodic structures has grown in the soft materials community, particularly with regards to the objective of developing tunable lattice structures. Soft materials feature nonlinear stress-strain relationships, a feature often referred to as material nonlinearity, which is exploited to obtain finite-deformation effects. On the other hand, nonlinear strain-displacement relationships in materials exhibiting a linear stress-strain dependence can also be exploited to design lattice structures capable of supporting finite-deformation effects. For example, a curved beam exhibits an intrinsically nonlinear strain-displacement relationship even for small values of stress and strain, which can be utilized as the building block for lattice structures exhibiting finite-deformation effects. Therefore, in the following section, finite-deformation mechanics of elastic structures will be reviewed with the goal of establishing a framework to simulate and analyze wave propagation in nonlinear lattice structures, and a benchmark periodic structure will be analyzed within the framework to showcase the potential for the design of adaptive phononic switches.

5.3.1 Overview of Nonlinear Elasticity

The equation of motion governing wave propagation in elastic solids (in the absence of body forces) capable of supporting finite-amplitude deformations are obtained from the principle of conservation of momentum as

$$\nabla \cdot (\mathbf{FS}) = \rho_0 \ddot{\mathbf{u}} \tag{5.1}$$

where $\mathbf{u}$ are the displacements and $\ddot{\mathbf{u}}$ refers to the second derivative of the displacements with respect to time. $\mathbf{F}$ is the deformation gradient given by $\mathbf{F} = \mathbf{I} + \nabla\mathbf{u}$, and ρ_0 corresponds to the density of the solid in the undeformed coordinates $\mathbf{X}$. The second-Piola Kirchoff stress tensor $\mathbf{S}$ is assumed to be derived from a generic hyperelastic strain energy function W, given in terms of the Green strain $\mathbf{E}$ or the right Cauchy-Green stretch field $\mathbf{C}$ (given by $\mathbf{C} = \mathbf{F}^T\mathbf{F}$) as

$$\mathbf{S} = DW(\mathbf{E}) = 2D\tilde{W}(\mathbf{C})$$

In this work, the strain energy is assumed to be expressed as an expansion of the strains as [95]

$$\mathcal{W} = \frac{1}{2}C_{ijkl}E_{ij}E_{kl} + \frac{1}{6}C_{ijklmn}E_{ij}E_{kl}E_{mn} + \cdots,$$

where C_{ijkl} and C_{ijklmn} are the second- and third-order moduli respectively. The Green strain is given by $\mathbf{E} = \frac{1}{2}\left[(\nabla\mathbf{u}) + (\nabla\mathbf{u})^T + (\nabla\mathbf{u})^T(\nabla\mathbf{u})\right]$. For isotropic solids, the second- and third-order moduli can be completely described by two and three constants, respectively, as [90]

$$\mathcal{W} = \frac{\lambda + 2\mu}{2} I_1^2 - 2\mu\, I_2 + lI_1^3 + mI_1I_2 + nI_3, \tag{5.2}$$

where λ and μ are the second-order Lame parameters, and l, m, n are the third-order Murnaghan potential constants. I_1, I_2, and I_3 are the invariants of the Green strain tensor defined as

$$I_1 = tr(\mathbf{E}), \quad I_2 = \frac{1}{2}\left((tr(\mathbf{E}))^2 - tr(\mathbf{E}^2)\right), \quad I_3 = det(\mathbf{E}).$$

If the displacements $\mathbf{u}$ are constrained to be $\mathcal{O}(\varepsilon)$, the left hand side of eqn. (5.1) for a second-order potential ($l = m = n = 0$ in eqn. (5.2)) can be written in indicial notation

as

$$\begin{aligned}\frac{\partial \mathbf{P}_{ij}}{\partial X_j} =&\rho_0 \frac{\partial^2 \mathbf{u}_i}{\partial t^2} = \lambda \frac{\partial^2 u_k}{\partial X_k \partial X_i} + \mu \left(\frac{\partial^2 u_i}{\partial X_j \partial X_j} + \frac{\partial^2 u_j}{\partial X_j \partial X_i} \right) \\ &+ \varepsilon\lambda \frac{\partial^2 u_i}{\partial X_j \partial X_j} \frac{\partial u_k}{\partial X_k} + \varepsilon(\lambda+\mu) \left(\frac{\partial^2 u_p}{\partial X_i \partial X_k} \frac{\partial u_p}{\partial X_k} + \frac{\partial^2 u_k}{\partial X_j \partial X_k} \frac{\partial u_i}{\partial X_j} \right) \\ &+ \varepsilon\mu \left(2 \frac{\partial^2 u_i}{\partial X_j \partial X_k} \frac{\partial u_k}{\partial X_j} + \frac{\partial^2 u_k}{\partial X_j \partial X_j} \frac{\partial u_i}{\partial X_k} + \frac{\partial^2 u_k}{\partial X_j \partial X_j} \frac{\partial u_k}{\partial X_i} \right) + \mathcal{O}(\varepsilon^2), \end{aligned} \tag{5.3}$$

where $\mathbf{P}$ is the first Piola-Kirchoff stress tensor defined as $\mathbf{P} = \mathbf{FS}$. The scale ε is once again introduced to denote the relative strength of the nonlinear terms with respect to the linear terms. The nonlinearity in the system which is due to the incorporation of finite-deformations in the elastic solid (the component $(\nabla \mathbf{u})^T (\nabla \mathbf{u})$ in the strain tensor) can be classified as geometric nonlinearity. The inclusion of material nonlinearity (non-zero third-order potentials) only modifies the coefficients of the weakly nonlinear term as the potentials are expressed as a power series expansion of the strain tensor. Expressions for the governing equation in the case of non-zero third-order potentials are available in published literature [95] and will not be reported here.

In order to relate eqn. (5.3) to those studied in chapter 2, consider a one-dimensional system supporting longitudinal wave motion. The governing equations (eqn. 5.3) can be simplified using the assumptions: $\mathbf{u}_i = [u, 0, 0]$ and $X_i = X$ as

$$\rho_0 \frac{\partial^2 u}{\partial t^2} = (\lambda + 2\mu) \frac{\partial^2 u}{\partial X^2} \left(1 + \varepsilon 3 \frac{\partial u}{\partial X} \right).$$

If the nonlinearity is sufficiently small enough to be neglected, the system admits a traveling wave solution of the form

$$f(X,t) = e^{X-ct},$$

where $c = \sqrt{\frac{\lambda+2\mu}{\rho_0}}$ is the phase/group velocity of the longitudinal wave[2]. In the presence of nonlinear terms, a perturbative expansion $u = u^0 + \varepsilon u^1$ can be employed to simplify

[2]When the nonlinear terms are neglected, the system becomes nondispersive.

the equations to a set of cascading linear differential equations as

$$\rho_0 \frac{\partial^2 u^0}{\partial t^2} - (\lambda + 2\mu) \frac{\partial^2 u^0}{\partial X^2} = 0$$
$$\rho_0 \frac{\partial^2 u^1}{\partial t^2} - (\lambda + 2\mu) \frac{\partial^2 u^1}{\partial X^2} = 3(\lambda + 2\mu) \frac{\partial^2 u^0}{\partial X^2} \frac{\partial u^0}{\partial X}.$$

It is well known that the solution to the equation at $\mathcal{O}(\varepsilon)$ predicts the generation of a cumulative second-harmonic [135] which travels at the same velocity as that of the fundamental-harmonic.

While the structure of eqn. (5.3) is amenable to analysis using perturbative techniques as shown above, the important distinction is that it does not contain a dispersive term. Hence, if discreteness is introduced by considering a lattice structure, with the unit cell made of a material whose deformations are expressed by eqn. (5.3), the interplay of dispersion and nonlinearity in these systems can be studied using the multiple scale expansion techniques employed in the previous chapters.

However, a numerical analysis of wave motion offers a more versatile paradigm to investigate these effects in a wide range of structures and materials especially when geometric complexity forbids obtaining an analytical treatment. Therefore, the analysis of nonlinear lattice structures is carried out by performing transient finite element simulations of wave propagation in these systems.

5.3.2 Square Lattice Sheet: Dispersion Relations and Directivity

The structure under investigation is a periodically perforated, thin $3D$ sheet made of Aluminum (shown in fig. 5.11). The perforations are square holes of length 0.375 in, and the distance between the center of two holes in either direction is 0.5 in. The out-of-plane thickness of the sheet is 0.032 in. These particular dimensions of the sheet are chosen to match the specimen analyzed experimentally, the results of which will be presented later in this chapter.

The unit cell of the periodic structure is a square lattice. However, the tessellation is only in the X-Y plane and the structure does not display periodicity along the Z-direction (out-of-plane direction in fig. 5.11). In order to determine the linearized dispersion characteristics, the unit cell is discretized using 8-node isoparametric brick elements,

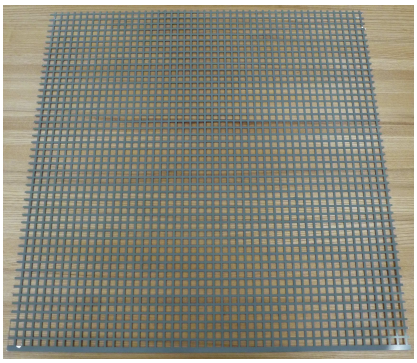

Figure 5.11: $3D$ Perforated Aluminum Sheet tessellated in the X-Y plane.

and Floquet-Bloch conditions are applied to the mass and stiffness matrices at each infinitesimal layer of the boundary of the unit cell, along all the three dimensions to yield a reduced eigenvalue problem. The dispersion surfaces ($\omega(k_x, k_y)$) are calculated by varying the wave vector, and the band structure obtained by sampling the wavevector along the contour of the irreducible Brillouin zone is shown in fig. 5.12.

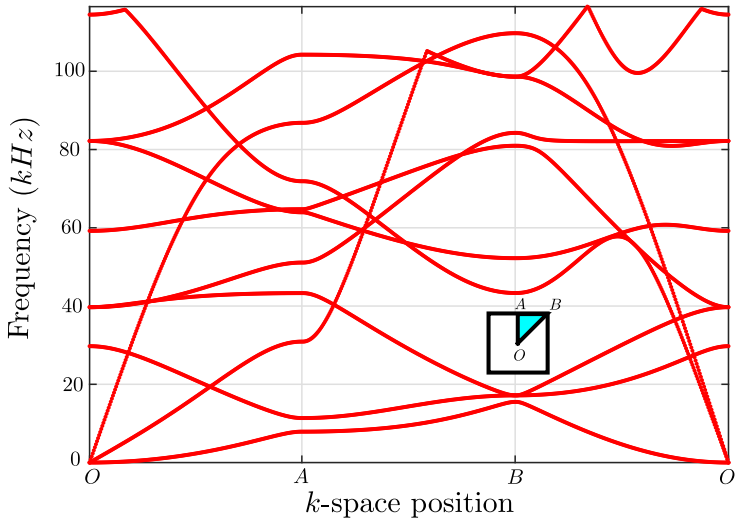

Figure 5.12: Linearized $3D$ band structure of Aluminum sheet along the contour of the irreducible Brillouin zone $OABO$. The First Brillouin zone for the unit cell is shown in the inset.

The band structure shown in fig. 5.12 consists of a mix of in-plane and out-of-plane wave modes. In order to distinguish these two different modes of wave propagation, a $2D$ model of the unit cell is considered to determine the band structure of the in-plane modes of wave propagation. By superimposing the results from the $2D$ and the $3D$ Bloch analysis, the dispersion curves corresponding to the out-of-plane modes can be inferred, and this is illustrated in fig. 5.13a. In order to verify the band structure of the $3D$ unit cell, the isofrequency contours (all k_x, k_y pairs corresponding to a given ω) are plotted in fig. 5.13(b-c) for the first two modes of wave propagation (determined from the $3D$ Bloch analysis). Since the second branch of wave propagation is a combination of the second out-of-plane mode and the in-plane shear mode (resulting from the solution of the Bloch eigenvalue problem), the corresponding isofrequency contour displays the additional longer-wavelength cross-pattern, a feature which is indeed associated with the in-plane shear mode of wave propagation in square lattices [98].

5.3.3 Potential for Mode Hopping and Modal Mixing

Since the thickness of the sheet is much smaller than the other dimensions, out-of-plane deformation displays a higher chance of exhibiting finite-deformation effects even for relatively small magnitudes of excitation. Therefore, flexural wave motion in the out-of-plane direction (with the components of the wave vector (k_x, k_y) varying in the plane of tessellation (X-Y plane)) is considered. Under this assumption, two particular frequencies ($\omega = 9\,kHz$ and $\omega = 18\,kHz$) lying on the first two out-of-plane modes are considered as they appear to be amenable to study the possible modal mixing opportunities (fig. 5.14). The choice of these frequencies are motivated by the fact that the corresponding isofrequency contours occupy different regions in the spectral plane, i.e., the isofrequency contour corresponding to $9\,kHz$ displays contours that are localized around $k_x = k_y = \pm\pi$, while the isofrequency contours corresponding to $18\,kHz$ are localized around $(\pm\pi, 0)$ and $(\,0 \pm \pi)$. The directivity of the lattice at these frequencies are determined from the group velocity contours, which are also depicted in fig. 5.14, where it is observed that the two frequencies display complementary directionality patterns.

In order to verify the spatial directivity patterns of the unit cell, a finite periodic lattice is considered and the system of equations are numerically solved using a $3D$ Linear Transient Finite Element routine, where the time integration is performed using

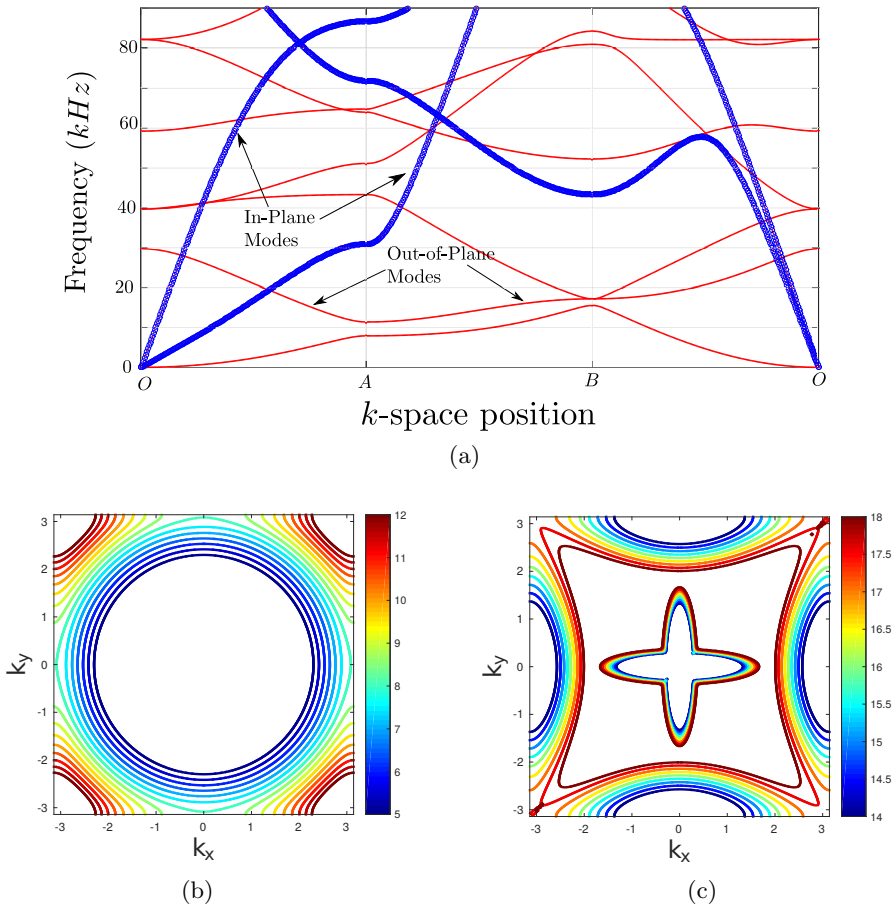

Figure 5.13: (a) The in-plane band structure obtained from 2-D Bloch analysis is superimposed on to the $3D$ band structure of the Aluminum sheet to distinguish the in-plane and out-of-plane wave modes. (b-c) Isofrequency contours of the first two branches of the $3D$ dispersion curve.

the Newmark-Beta algorithm. Snapshots of the resulting wavefield for displacement in the Z-direction for the two considered frequencies[3] are plotted in fig. 5.15, and it is observed that the spatial wave profiles are consistent with the group velocity contours obtained from Bloch analysis.

[3]The higher frequency is chosen to be slightly lesser than twice the fundamental frequency to facilitate experimental acquisition of data. Nevertheless, the characteristics of the propagating wave at $17\,kHz$ does not drastically differ from that at $18\,kHz$ as they belong to the same mode of wave propagation.

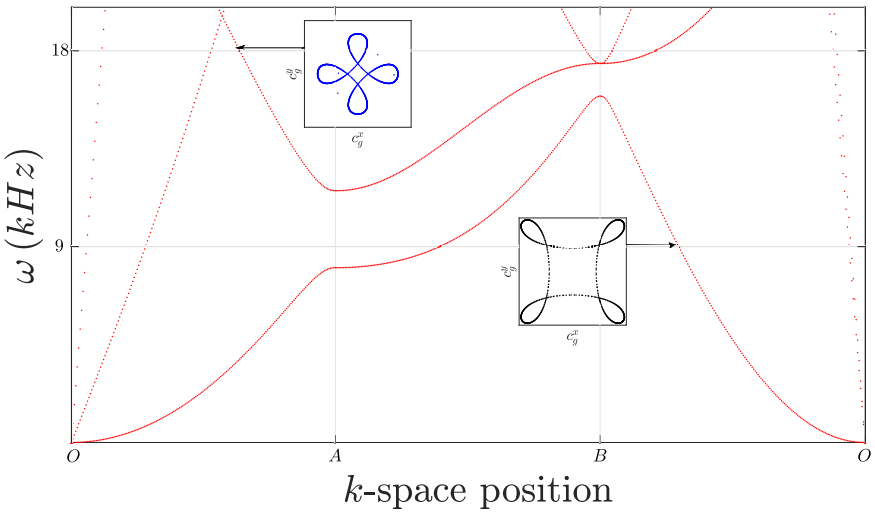

Figure 5.14: Choice of hopping frequencies and group velocity contours of the first two out-of-plane modes at excitation frequencies (a) $\omega = 9\,kHz$ and (b) $\omega = 18\,kHz$ respectively.

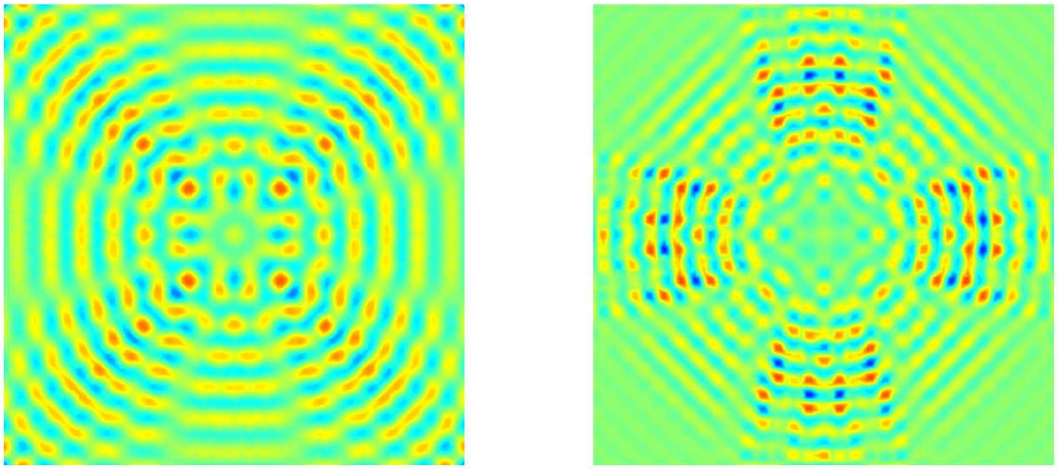

(a) (b)

Figure 5.15: Z-component of spatial wave profile in the Aluminum sheet for excitation frequencies (a) $\omega = 9\,kHz$ and (b) $\omega = 17\,kHz$ respectively.

Since the two frequencies chosen on the first two out-of-plane modes show complementary spatial directivity, by exciting the fundamental harmonic in a nonlinear lattice and appealing to the concept of mode hopping, the spatial directivity associated with the

second mode can be activated for excitations belonging to the first out-of-plane mode. This will be illustrated numerically for the Aluminum sheet in the next subsection.

5.3.4 Wave Propagation in Nonlinear Lattice

Transient finite element simulation of wave propagation in the nonlinear lattice is carried out by employing an energy and momentum conserving algorithm [53, 118]. Two different simulations are carried out: one considering only linear elastic material properties of Aluminum (the finite-deformation effects observed are attributed to geometric nonlinearity), and the other with the third-order constants of elasticity also included in the constitutive relation (finite-deformation effects are attributed to a combination of material and geometric nonlinearity). While the effect of third-order elastic constants is non-negligible in practical scenarios (has been experimentally determined for Aluminum), the inclusion of third-order constants only affects the amplitude of the nonlinear features and does not qualitatively change the characteristics of wave propagation. Since the motive of this study is to analyze the qualitative effect of nonlinearity, the results corresponding to the linear material properties are only reported here[4].

Unlike the granular crystal examples presented before, the nonlinearly-generated harmonics cannot be separated from the fundamental harmonic as the finiteness of the specimen does not allow considering long enough intervals for wave propagation without cascades of reflections from the boundaries. Furthermore, the finite element discretization also plays a limiting role as the number of degrees of freedom required to obtain a converged solution increases exponentially with increasing structure size[5]. Therefore, a simple high-pass filter is applied to the time-series data to filter the nonlinearly-generated second-harmonic (using nodal data from the finite element simulation). The filtered second-harmonic is shown for one particular time instant in fig. 5.16a, where the spatial characteristics of the second-harmonic are observed to be consistent with the characteristics determined from the Bloch analysis of the unit cell (see fig. 5.14). Due to the constraints of computation time, the results reported here are for a structure smaller

[4]The choice is also partly motivated by computational cost constraints.

[5]The optimum size of each element is determined from the dispersion analysis by refining the mesh of the unit cell such that a finer resolution does not produce a significant change in the dispersion relations

in size than that considered for the linear analysis. In order to verify the spectral characteristics of the nonlinearly-generated harmonic, the spatial Fourier transform of the propagating wavefield (from numerical simulations) is compared with the isofrequency contours obtained from unit cell analysis (figs. 5.16(b-c)). Since the burst excites a band of frequencies, some nonlinear contributions also lie on the first out-of-plane mode of wave propagation, a feature which is indeed observed in the spectral contours clustered around $k_x = k_y = \pi$. However, the major contribution is due to the second out-of-plane mode of wave propagation, which is indeed localized around $(\pm\pi, 0)$ and $(0 \pm \pi)$.

It is important to note that this specific choice of frequencies was made to utilize the complementary spatial characteristics associated with the first two out-of-plane modes. However, the phenomena of mode hopping and modal mixing are more generic and can be observed for any choice of frequency. However, the manifestation of nonlinearity could be very different from that observed for the choice of frequencies illustrated here.

Nonlinear Lattice structures provide an ideal testing ground to experimentally verify mode hopping and modal mixing phenomena as the physical realization of specimen and their testing are considerably more agile than for the granular system counterpart. Therefore, in the next subsection, experimental investigation of mode hopping in nonlinear lattices is considered and preliminary results are reported.

5.3.5 Preliminary Experimental Characterization of Nonlinear Wave Propagation

The perforated Aluminum sheet shown in fig. 5.11 was obtained pre-cut to a size of to a size of $2\,ft \times 2\,ft$ (40×40 unit cells) from McNichols Company (Part No. 1796003241). Flexural out-of-plane wave motion in this sheet is monitored by exciting the middle of the structure with a seven-cycle hann-modulated sine-burst using an electrodynamic shaker (Bruel & Kjaer Shaker Type 2809), and measuring the structural response using $3D$ Scanning Laser Doppler Vibrometer (SLDV).

Laser Doppler Vibrometry (LDV) is a non-contact measurement technique which employs high fidelity lasers to measure the velocity of a vibrating object by employing principle of Doppler effect, i.e., the shift in frequency of a laser impinging on a vibrating object is proportional to the velocity of vibration of the vibrating object. Since the velocity of the vibrating object is determined along the line of incidence of the laser,

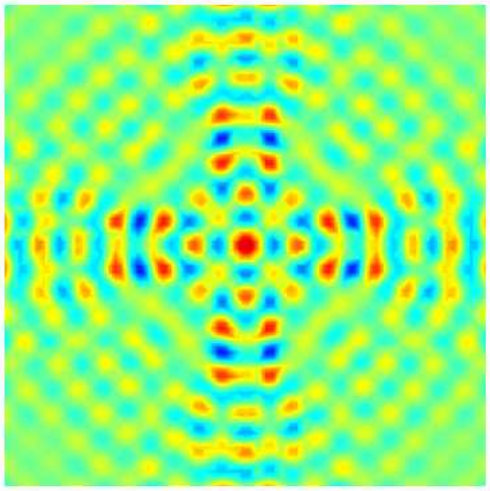

(a)

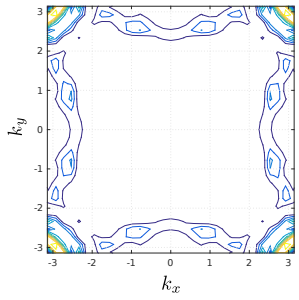

(b)

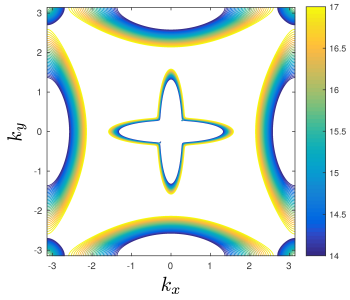

(c)

Figure 5.16: Nonlinear wave propagation in Aluminum sheet - (a) Filtered nodal data corresponding to the nonlinearly-generated higher harmonic plotted for one particular time instant, (b) The spatial DFT of the wavefield for the chosen time instant, (c) Analytical isofrequency contours of the first and second out-of-plane branches of the band structure, sampled around twice the excitation frequency.

a $3D$ LDV utilizes concurrent measurement by three lasers at a single point on the object of interest to compute the complete vibration characteristics of the chosen point (fig. 5.17). Additionally, the $3D$ LDV system supplied by Polytec Inc. (PSV 400-$3D$) features the capability to sequentially determine the vibrations at multiple points of interest on the object, thereby rendering it the ability to scan and measure the response of the entire object. Scanning of the entire object is facilitated by specifying points

of interest apriori to the acquisition. Since the accuracy of velocity measurement is dependent on the quality of the laser reflected back to the scanning head (which in turn is used to determine the shift in frequency of the laser) from the object of interest, the Aluminum sheet is coated with a layer of reflective paint to improve laser reflectance. The accuracy of velocity measurements using the $3D$ SLDV also depends on the ability to direct all the three lasers at the same point on the measurement object. This is achieved by a process called triangulation, where the coordinates of the scan point supplied to the system (prior to the measurement) are used to direct all the lasers simultaneously to each scanning point. A loss of accuracy in specifying the scan points leads to the failure of convergence of lasers on to a single point, thereby voiding the measurement. Therefore, a number of scan point definitions are supplied to the laser, and after acquisition, only the scan points with valid data are considered for the analysis.

First, linear wave propagation in the lattice is considered by supplying very small amplitudes of excitation through the electrodynamic shaker. Wave motion is monitored for two excitation frequencies ($\omega = 9\,kHz$ and $17\,kHz$) and the spatial wave profile obtained by integrating the experimentally measured velocities is plotted in fig. 5.18, where it is seen that the experimental results match the analytical results obtained from Bloch analysis, and the numerical results obtained from finite element simulations.

In order to measure nonlinear wave propagation in the Aluminum sheet, the amplifier (Bruel & Kjaer Type 2718) which powers the electrodynamic shaker is set to maximum gain, and the initial amplitude supplied to the sheet is increased to the limit such that the maximum current supplied to shaker does not exceed its operating limit. In addition, the distortion or lack thereof of the input signal is also verified by monitoring the output of the amplifier using the reference channel of the $3D$ SLDV.

The experimentally obtained data is then filtered using a high-pass filter to monitor the nonlinearly-generated harmonic components. The filtered spatial profile for the high-amplitude excitation ($\omega = 9\,kHz$) is plotted in fig. 5.19, where the wave profile displays a striking similarity to the linear wave profile obtained by operating at twice the excitation frequency. However, spurious features that contaminate the wave profile are also observed in the filtered wave profile.

While fig. 5.19 seems to confirm the numerical observations made in the case of

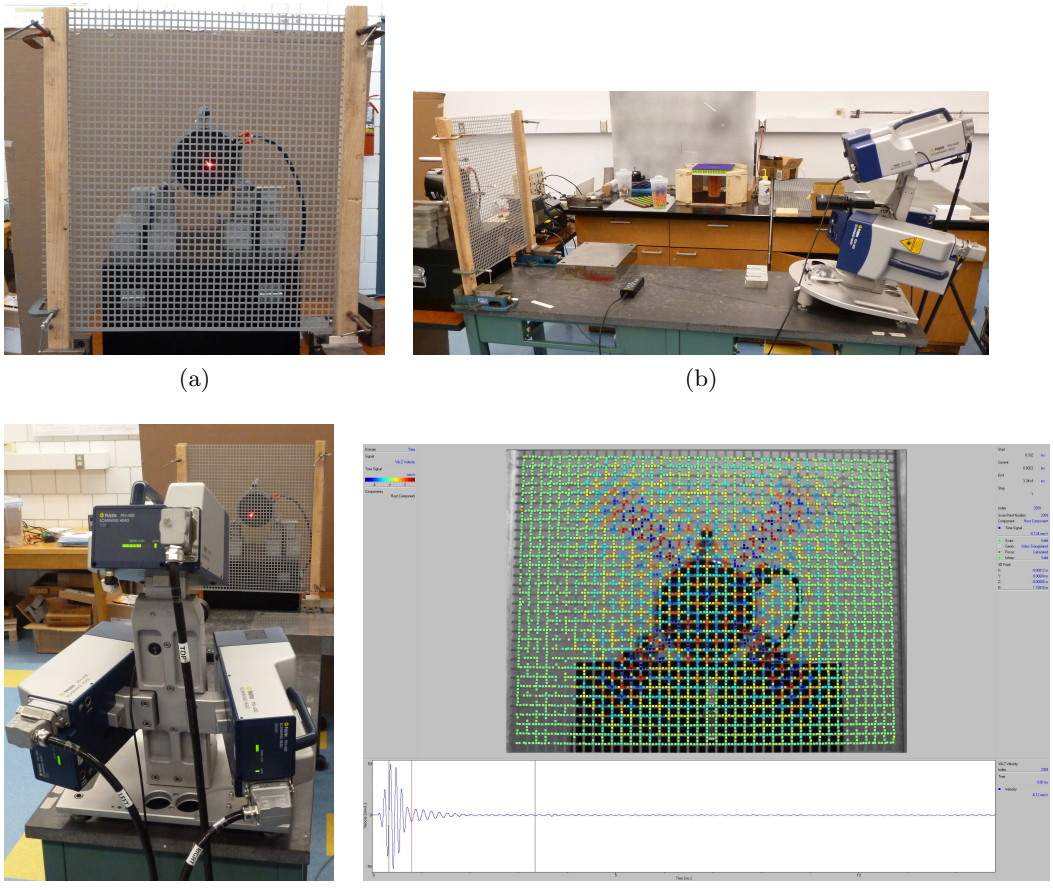

(a) (b)

(c) (d)

Figure 5.17: Scanning Laser Doppler Vibrometer setup to measure wave propagation in $3D$ Aluminum sheet - (a) Front view of the Aluminum sheet attached to the electrodynamic shaker, (b) Side view of the experimental setup, (c) Strength of the reflected laser as observed on the scanning heads of PSV 400-$3D$, (d) Velocity profile in the Z-direction superimposed on to the scan points in the PSV software.

nonlinear lattices, it is necessary to assert that the second-harmonic generation is due to the nonlinearity of the specimen, and not due to non-idealities in the experimental setup. While the nonlinear distortion of the input signal can be easily monitored, the contact between the electrodynamic shaker and the specimen could also be a source of nonlinearity. Therefore, additional details about the mechanics of transfer of the applied excitation need to be studied before categorically claiming proof of experimental evidence of mode hopping and modal mixing in nonlinear lattices.

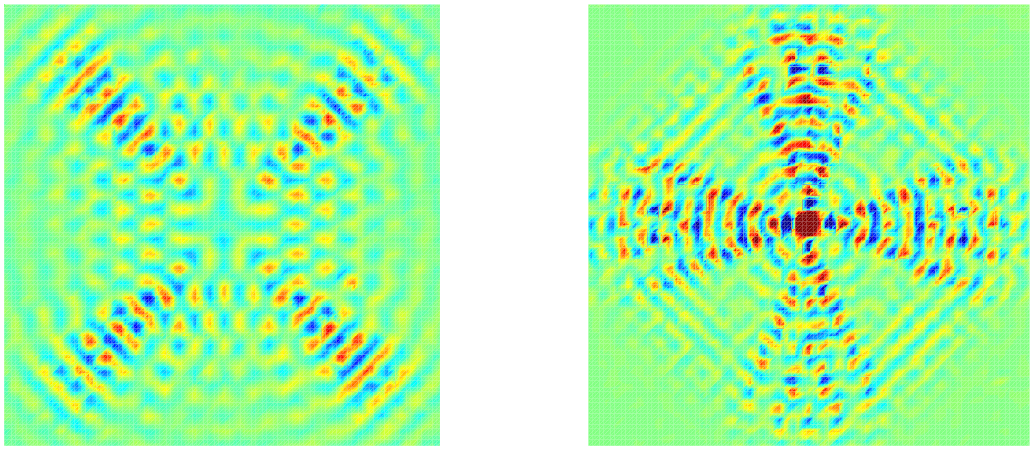

(a) $\omega = 9\,kHz$ (b) $\omega = 17\,kHz$

Figure 5.18: Linear spatial wave profile in the Z-direction obtained from SLDV measurements for two different excitation frequencies.

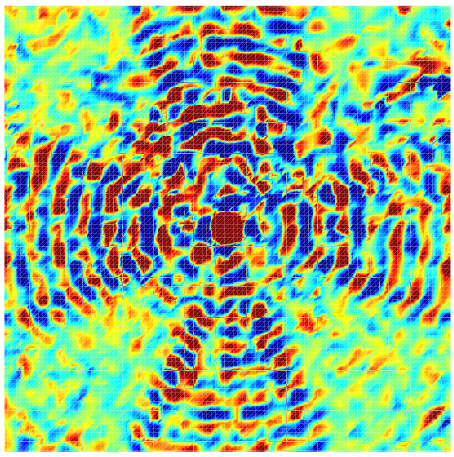

Figure 5.19: Filtered nonlinear spatial wave profile obtained from SLDV acquisition corresponding to high-amplitude excitation at $9\,kHz$.

5.4 Conclusion

In conclusion, a strategy to obtain spatial and modal wave manipulation in granular phononic crystals and nonlinear lattices using the concepts of mode hopping and modal mixing has been proposed. The generation of higher harmonics induces jumps in the response across the available propagation modes, thereby giving rise to a response with a mixture of modes and the simultaneous activation of complementary functionalities. As

a result, functionalities that are normally associated with high-frequency modes can be activated in the response even while applying low-frequency excitations. The design of engineering materials capable of supporting such tunable and switchable functionalities can be achieved by working entirely with the linearized periodic structure and then incorporating mechanisms to introduce finite-deformation effects.

Chapter 6

Summary

In this dissertation, the characteristics of wave propagation in nonlinear periodic structures have been investigated. The nonlinear effects considered in this work are much smaller in magnitude than the linear response of the system, which allows for a perturbative expansion of the governing equations of motion. Since the emphasis is on compact traveling wave packets, a multiple scale expansion in terms of spatiotemporal variables is carried out to reduce the nonlinear equations to a set of cascading linear equations, where the solution at every order of expansion is dependent on the solution obtained at all the previous orders of expansion.

First, the effect of nonlinear terms at the fundamental order of perturbation expansion are examined. When the nonlinear terms can be expressed to the leading order by an equivalent quadratic nonlinear term, the effect of nonlinearity is observed as a modulation of the envelope of the wave packet. Specifically, a non-harmonic modulation is observed to develop in the system in conjunction with the harmonic propagating wave packet. The characteristics of this non-harmonic modulation can be derived analytically for any system, however, are cumbersome and seldom carried out. Therefore, a numerical technique is considered to explore the effect of envelope modulation in a wide variety of nonlinear periodic structures. It is observed that by monitoring the characteristics of the propagating excitations, topological wave packet descriptors that quantitatively capture the effect of nonlinearity and excitation parameters can be determined. Furthermore, these topological wave packet descriptors can be used to setup inverse problems,

by which, the nonlinearity in the system can be determined from experimental or numerical data. The inverse problem is validated for the case of precompressed monoatomic and diatomic granular chains numerically.

At the higher orders of the perturbation expansion, the effect of nonlinearity is observed in the generation of higher harmonics. However, the interplay of dispersion and nonlinearity leads to the generation of higher harmonics with multiple spatio-spectral characteristics. Particularly, a component of the second-harmonic that conforms to the dispersion characteristics of the linearized system is observed. As a result, the characteristics of the generated harmonic can be determined from a simple linear analysis of the corresponding periodic structure. Therefore, by analyzing the linear characteristics of any periodic structure, and appealing to the various sources of nonlinearity realizable in elastic solids (geometric, material, and contact nonlinearity), complementary functionalities that are normally associated with high-frequency modes can be activated in the response even while applying low-frequency excitations. In addition, this reversible activation and deactivation of complementary functionalities can be obtained either as a spontaneous response to changes in the amplitude of excitation or due to external parameter tuning. The ability to design periodic structures capable of supporting these complementary functionalities is demonstrated by considering Granular Phononic Crystals (GPCs), where the nonlinearity manifests due to Hertzian contacts, and Nonlinear Lattices, where finite-deformation displacements are induced by considering the nonlinearities associated with the strain-displacement (geometric) and stress-strain (material) relationships.

In conclusion, the interplay of dispersion and nonlinearity in periodic structures can be exploited in a wide variety of engineering problems. One avenue is to use periodicity as a means to measure nonlinear constants of materials, thereby providing an alternate route to existing methods in published literature such as acoustoelasticity and guided-wave-testing. The other avenue is in the promising field of metamaterials, where adaptive and tunable spatial wave manipulation can be used as a route to induce and control the characteristics of propagating excitations, leading to features seldom observed in the corresponding continuum counterparts.

Bibliography

[1] Mohammad H. Abedinnasab and Mahmoud I. Hussein. Wave dispersion under finite deformation. *Wave Motion*, 50(3):374–388, 2013.

[2] M.F. Ashby. The mechanical properties of cellular solids. *Metallurgical Transactions A*, 14(9):1755–1769, 1983.

[3] A. Askar. Dispersion Relation and Wave Solution for Anharmonic Lattices and Korteweg De Vries Continua. *Proceedings of the Royal Society A: Mathematical, Physical and Engineering Sciences*, 334(1596):83–94, July 1973.

[4] Christian Bermes, Jin-Yeon Kim, Jianmin Qu, and Laurence J. Jacobs. Experimental characterization of material nonlinearity using lamb waves. *Applied Physics Letters*, 90(2):021901, 2007.

[5] K Bertoldi and MC Boyce. Wave propagation and instabilities in monolithic and periodically structured elastomeric materials undergoing large deformations. *Physical Review B*, 78(18):184107, 2008.

[6] S. Bickham, S. Kiselev, and A. Sievers. Stationary and moving intrinsic localized modes in one-dimensional monatomic lattices with cubic and quartic anharmonicity. *Physical Review B*, 47(21):14206–14211, June 1993.

[7] N. Boechler, G. Theocharis, S. Job, P. G. Kevrekidis, Mason A. Porter, and C. Daraio. Discrete Breathers in One-Dimensional Diatomic Granular Crystals. *Physical Review Letters*, 104(24):244302, June 2010.

[8] N Boechler, G Theocharis, and C Daraio. Bifurcation-based acoustic switching and rectification. *Nature materials*, 10(9):665–8, September 2011.

[9] N. Boechler, J. Yang, G. Theocharis, P. G. Kevrekidis, and C. Daraio. Tunable vibrational band gaps in one-dimensional diatomic granular crystals with three-particle unit cells. *Journal of Applied Physics*, 109(7):074906, 2011.

[10] CE Bradley. Time-harmonic acoustic bloch wave propagation in periodic waveguides. part iii. nonlinear effects. *The Journal of the Acoustical Society of America*, 98(5):2735–2744, 1995.

[11] MA Breazeale and Joseph Ford. Ultrasonic studies of the nonlinear behavior of solids. *Journal of Applied Physics*, 36(11):3486–3490, 1965.

[12] L. Brillouin. *Wave Propagation in Periodic Structures*. Dover Publications Inc., 1953.

[13] Kurt Busch, Guido Schneider, Lasha Tkeshelashvili, and Hannes Uecker. Justification of the nonlinear Schrödinger equation in spatially periodic media. *Zeitschrift für angewandte Mathematik und Physik*, 57(6):905–939, nov 2006.

[14] Jérémy Cabaret, Vincent Tournat, and Philippe Béquin. Amplitude-dependent phononic processes in a diatomic granular chain in the weakly nonlinear regime. *Physical Review E*, 86(4):041305, October 2012.

[15] Luyao Cai, Jinkyu Yang, Piervincenzo Rizzo, Xianglei Ni, and Chiara Daraio. Propagation of highly nonlinear solitary waves in a curved granular chain. *Granular Matter*, 15(3):357–366, 2013.

[16] DK Campbell. Localizing energy through nonlinearity and discreteness. *Physics Today*, (January):43–49, 2004.

[17] R. Carretero-González, D. Khatri, Mason a. Porter, P. G. Kevrekidis, and C. Daraio. Dissipative solitary waves in granular crystals. *Physical Review Letters*, 102(2):1–4, 2009.

[18] Paolo Celli and Stefano Gonella. Low-frequency spatial wave manipulation via phononic crystals with relaxed cell symmetry. *Journal of Applied Physics*, 115 (10):103502, 2014.

[19] Paolo Celli and Stefano Gonella. Tunable directivity in metamaterials with reconfigurable cell symmetry. *Applied Physics Letters*, 106(9):091905, 2015.

[20] Paolo Celli and Stefano Gonella. Manipulating waves with lego bricks: A versatile experimental platform for metamaterial architectures. *Applied Physics Letters*, 107(8):081901, 2015.

[21] G Chakraborty and A.K. Mallik. Dynamics of a weakly non-linear periodic chain. *International Journal of Non-Linear Mechanics*, 36(2):375–389, March 2001.

[22] A Chatterjee. Asymptotic solution for solitary waves in a chain of elastic spheres. *Physical review. E, Statistical physics, plasmas, fluids, and related interdisciplinary topics*, 59(5 Pt B):5912–5919, 1999.

[23] Martina Chirilus-Bruckner, Christopher Chong, Oskar Prill, and Guido Schneider. Rigorous description of macroscopic wave packets in infinite periodic chains of coupled oscillators by modulation equations. *Discrete and Continuous Dynamical Systems - Series S*, 5(5):879–901, 2012.

[24] C. Chong and G. Schneider. Numerical evidence for the validity of the NLS approximation in systems with a quasilinear quadratic nonlinearity. *ZAMM - Journal of Applied Mathematics and Mechanics / Zeitschrift für Angewandte Mathematik und Mechanik*, 93(9):688–696, 2013.

[25] C. Coste, E. Falcon, and S. Fauve. Solitary waves in a chain of beads under Hertz contact. *Physical Review E*, 56(5):6104–6117, November 1997.

[26] C. Daraio and V. F. Nesterenko. Strongly nonlinear wave dynamics in a chain of polymer coated beads. *Physical Review E - Statistical, Nonlinear, and Soft Matter Physics*, 73(2):1–7, 2006.

[27] C. Daraio, V. F. Nesterenko, E. B. Herbold, and S. Jin. Strongly nonlinear waves in a chain of Teflon beads. *Physical Review E - Statistical, Nonlinear, and Soft Matter Physics*, 72(1):1–9, 2005.

[28] C. Daraio, V. F. Nesterenko, E. B. Herbold, and S. Jin. Tunability of solitary

wave properties in one-dimensional strongly nonlinear phononic crystals. *Phys. Rev. E*, 73:026610, Feb 2006.

[29] Thierry Dauxois and Michel Peyrard. Energy localization in nonlinear lattices. *Physical Review Letters*, 70(25):3935–3938, June 1993.

[30] W. J N de Lima and M. F. Hamilton. Finite-amplitude waves in isotropic elastic plates. *Journal of Sound and Vibration*, 265(4):819–839, 2003.

[31] C. M. de Sterke and J. E. Sipe. Envelope-function approach for the electrodynamics of nonlinear periodic structures. *Physical Review A*, 38(10):5149–5165, November 1988.

[32] Mingxi Deng. Cumulative second-harmonic generation of lamb-mode propagation in a solid plate. *Journal of Applied Physics*, 85(6):3051–3058, 1999.

[33] Mingxi Deng and Junfeng Pei. Assessment of accumulated fatigue damage in solid plates using nonlinear lamb wave approach. *Applied Physics Letters*, 90(12): 121902, 2007.

[34] Mingxi Deng, Ping Wang, and Xiafu Lv. Experimental observation of cumulative second-harmonic generation of lamb-wave propagation in an elastic plate. *Journal of Physics D: Applied Physics*, 38(2):344, 2005.

[35] Carly M. Donahue, Paul W. J. Anzel, Luca Bonanomi, Thomas A. Keller, and Chiara Daraio. Experimental realization of a nonlinear acoustic lens with a tunable focus. *Applied Physics Letters*, 104(1):014103, January 2014.

[36] Egor V. Dontsov, Roman D. Tokmashev, and Bojan B. Guzina. A physical perspective of the length scales in gradient elasticity through the prism of wave dispersion. *International Journal of Solids and Structures*, 50(2223):3674 – 3684, 2013.

[37] O.A. Druzhinin and L.A. Ostrovskii. Solitons in discrete lattices. *Physics Letters A*, 160(4):357–362, November 1991.

[38] D.B. Duncan and J.A.D. Wattis. Approximations of solitary waves on lattices using weak and variational formulations. *Chaos, Solitons & Fractals*, 2(5):505–518, September 1992.

[39] D.B. Duncan, J.C. Eilbeck, H. Feddersen, and J.A.D. Wattis. Solitons on lattices. *Physica D: Nonlinear Phenomena*, 68(1):1–11, September 1993.

[40] J.C. Eilbeck and R. Flesch. Calculation of families of solitary waves on discrete lattices. *Physics Letters A*, 149(4):200–202, September 1990.

[41] E. Fermi, J. Pasta, and S. Ulam. *Studies of nonlinear problems. I.* Amer. Math. Soc., Providence, R.I., 1955.

[42] S Flach and A Gorbach. Discrete breathers in Fermi-Pasta-Ulam lattices. *Chaos (Woodbury, N.Y.)*, 15(1):15112, mar 2005.

[43] N Flytzanis, S Pnevmatikos, and M Remoissenet. Kink, breather and asymmetric envelope or dark solitons in nonlinear chains. I. Monatomic chain. *Journal of Physics C: Solid State Physics*, 18(24):4603–4629, August 1985.

[44] Gero Friesecke and Jonathan A D Wattis. Existence theorem for solitary waves on lattices. *Communications in Mathematical Physics*, 161(2):391–418, March 1994.

[45] Y. Gaididei, R. Huß, and F.G. Mertens. Envelope solitary waves on two-dimensional lattices with in-plane displacements. *The European Physical Journal B*, 6(2):257–271, 1998.

[46] R. Ganesh and S. Gonella. Spectro-spatial wave features as detectors and classifiers of nonlinearity in periodic chains. *Wave Motion*, 50(4):821–835, June 2013.

[47] R. Ganesh and S. Gonella. Invariants of nonlinearity in the phononic characteristics of granular chains. *Phys. Rev. E*, 90:023205, Aug 2014.

[48] R Ganesh and S Gonella. From modal mixing to tunable functional switches in nonlinear phononic crystals. *Physical review letters*, 114(5):054302, 2015.

[49] J. Gazalet, S. Dupont, J.C. Kastelik, Q. Rolland, and B. Djafari-Rouhani. A tutorial survey on waves propagating in periodic media: Electronic, photonic and

phononic crystals. perception of the bloch theorem in both real and fourier domains. *Wave Motion*, 50(3):619 – 654, 2013.

[50] A. L. Gonçalves and V. V. Konotop. Second harmonic generation in a two-dimensional diatomic lattice. *Physical Review B - Condensed Matter and Materials Physics*, 62(21):14105–14112, 2000.

[51] Stefano Gonella and Massimo Ruzzene. Analysis of in-plane wave propagation in hexagonal and re-entrant lattices. *Journal of Sound and Vibration*, 312(1-2): 125–139, April 2008.

[52] Stefano Gonella, Albert C. To, and Wing Kam Liu. Interplay between phononic bandgaps and piezoelectric microstructures for energy harvesting. *Journal of the Mechanics and Physics of Solids*, 57(3):621 – 633, 2009.

[53] O. Gonzalez. Exact energy and momentum conserving algorithms for general models in nonlinear elasticity. *Computer Methods in Applied Mechanics and Engineering*, 190(13-14):1763–1783, 2000.

[54] F. Karl Graff. *Wave Motion in Elastic Solids*. Dover Publications Inc., 1991.

[55] Sébastien Guenneau, Alexander Movchan, Gunnar Pétursson, and S Anantha Ramakrishna. Acoustic metamaterials for sound focusing and confinement. *New Journal of Physics*, 9(11):399–399, 2007.

[56] Mark F Hamilton, David T Blackstock, et al. *Nonlinear acoustics*, volume 427. San Diego, CA: Academic Press, 1998.

[57] Anne-Christine Hladky-Hennion and Michel de Billy. Experimental validation of band gaps and localization in a one-dimensional diatomic phononic crystal. *The Journal of the Acoustical Society of America*, 122(5):2594–2600, 2007.

[58] G Huang, V V Konotop, H W Tam, and B Hu. Nonlinear modulation of multidimensional lattice waves. *Physical review. E, Statistical, nonlinear, and soft matter physics*, 64(5 Pt 2):056619, 2001.

[59] Guoxiang Huang and Bambi Hu. Asymmetric gap soliton modes in diatomic lattices with cubic and quartic nonlinearity. *Physical Review B*, 57(10):5746–5757, March 1998.

[60] Guoxiang Huang, Zhu-Pei Shi, and Zaixin Xu. Asymmetric intrinsic localized modes in a homogeneous lattice with cubic and quartic anharmonicity. *Physical Review B*, 47(21):14561–14564, June 1993.

[61] D. S. Hughes and J. L. Kelly. Second-order elastic deformation of solids. *Physical review*, 92(5):1145–1149, 1953.

[62] Mahmoud I. Hussein, Michael J. Leamy, and Massimo Ruzzene. Dynamics of Phononic Materials and Structures: Historical Origins, Recent Progress, and Future Outlook. *Applied Mechanics Reviews*, 66(4):040802, 2014.

[63] K. R. Jayaprakash, Yuli Starosvetsky, and Alexander F. Vakakis. New family of solitary waves in granular dimer chains with no precompression. *Physical Review E - Statistical, Nonlinear, and Soft Matter Physics*, 83(3):1–11, 2011.

[64] K. R. Jayaprakash, Alexander F. Vakakis, and Yuli Starosvetsky. Solitary waves in a general class of granular dimer chains. *Journal of Applied Physics*, 112(3), 2012.

[65] Kenneth Langstreth Johnson. *Contact mechanics*. Cambridge university press, 1987.

[66] A. Khelif, A. Choujaa, S. Benchabane, B. Djafari-Rouhani, and V. Laude. Guiding and bending of acoustic waves in highly confined phononic crystal waveguides. *Applied Physics Letters*, 84(22):4400–4402, 2004.

[67] Yuri S. Kivshar and Michel Peyrard. Modulational instabilities in discrete lattices. *Phys. Rev. A*, 46:3198–3205, Sep 1992.

[68] V. Konotop. Second-harmonic generation in diatomic lattices. *Physical Review E*, 54(4):4266–4270, 1996.

[69] V. V. Konotop. Small-amplitude envelope solitons in nonlinear lattices. *Physical Review E*, 53(3):2843–2858, March 1996.

[70] M. S. Kushwaha, P. Halevi, L. Dobrzynski, and B. Djafari-Rouhani. Acoustic band structure of periodic elastic composites. *Physical Review Letters*, 71(13): 2022–2025, September 1993.

[71] Philippe Langlet, Anne-Christine Hladky-Hennion, and Jean-Noel Decarpigny. Analysis of the propagation of plane acoustic waves in passive periodic materials using the finite element method. *The Journal of the Acoustical Society of America*, 98(5):2792, 1995.

[72] R.S. Langley. The response of Two-dimensional periodic structures to point harmonic forcing. *Journal of Sound and Vibration*, 197(4):447–469, October 1996.

[73] A. N. Lazaridi and V. F. Nesterenko. Observation of a new type of solitary waves in a one-dimensional granular medium. *Journal of Applied Mechanics and Technical Physics*, 26(3):405–408, 1985.

[74] Changgu Lee, Xiaoding Wei, Jeffrey W. Kysar, and James Hone. Measurement of the elastic properties and intrinsic strength of monolayer graphene. *Science*, 321 (5887):385–388, 2008.

[75] A Leonard, C Chong, P G Kevrekidis, and C Daraio. Traveling waves in 2D hexagonal granular crystal lattices. *Granular Matter*, 16(4):531–542, April 2014.

[76] Andrea Leonard, Laurent Ponson, and Chiara Daraio. Wave mitigation in ordered networks of granular chains. *Journal of the Mechanics and Physics of Solids*, 73: 103 – 117, 2014.

[77] Feng Li, Paul Anzel, Jinkyu Yang, Panayotis G Kevrekidis, and Chiara Daraio. Granular acoustic switches and logic elements. *Nature Communications*, 5:1–6, 2014.

[78] Qiming Li, St. Pnevmatikos, E. Economou, and C. Soukoulis. Lattice-soliton scattering in nonlinear atomic chains. *Physical Review B*, 37(7):3534–3541, March 1988.

[79] B Liang, XS Guo, J Tu, D Zhang, and JC Cheng. An acoustic rectifier. *Nature materials*, 9(12):989–992, 2010.

[80] Zhengyou Liu, Xixiang Zhang, Yiwei Mao, Y. Y. Zhu, Zhiyu Yang, C. T. Chan, and Ping Sheng. Locally resonant sonic materials. *Science*, 289(5485):1734–1736, 2000.

[81] J. C. Luke. A Perturbation Method for Nonlinear Dispersive Wave Problems. *Proceedings of the Royal Society A: Mathematical, Physical and Engineering Sciences*, 292(1430):403–412, May 1966.

[82] Martin Maldovan. Sound and heat revolutions in phononics. *Nature*, 503(7475): 209–217, nov 2013.

[83] Felicia S. Manciu and Surajit Sen. Secondary solitary wave formation in systems with generalized Hertz interactions. *Physical Review E - Statistical, Nonlinear, and Soft Matter Physics*, 66(1):1–11, 2002.

[84] Kevin Manktelow, Michael J. Leamy, and Massimo Ruzzene. Multiple scales analysis of wave-wave interactions in a cubically nonlinear monoatomic chain. *Nonlinear Dynamics*, 63(1-2):193–203, 2011.

[85] Kevin Manktelow, Raj K. Narisetti, Michael J. Leamy, and Massimo Ruzzene. Finite-element based perturbation analysis of wave propagation in nonlinear periodic structures. *Mechanical Systems and Signal Processing*, 39(1-2):32–46, 2013.

[86] Kevin L. Manktelow, Michael J. Leamy, and Massimo Ruzzene. Weakly nonlinear wave interactions in multi-degree of freedom periodic structures. *Wave Motion*, 51(6):886–904, sep 2014.

[87] R. Martínez-Sala, J. Sancho, J. V. Sánchez, V. Gómez, J. Llinares, and F. Meseguer. Sound attenuation by sculpture. *Nature*, 378(6554):241–241, November 1995.

[88] Kathryn H. Matlack, Jin Yeon Kim, Laurence J. Jacobs, and Jianmin Qu. Experimental characterization of efficient second harmonic generation of Lamb wave modes in a nonlinear elastic isotropic plate. *Journal of Applied Physics*, 109(1): 1–6, 2011.

[89] D M Mead. Wave propagation in continuous periodic structures: Research contributions from Southampton, 1964-1995. *Journal of Sound and Vibration*, 190 (3):495–524, 1996.

[90] F. D. Murnaghan. Finite Deformations of an Elastic Solid. *American Journal of Mathematics*, 59(2):235–260, 1937.

[91] R. K. Narisetti, M. Ruzzene, and M. J. Leamy. A Perturbation Approach for Analyzing Dispersion and Group Velocities in Two-Dimensional Nonlinear Periodic Lattices. *Journal of Vibration and Acoustics*, 133(6):061020, 2011.

[92] Raj K. Narisetti, Michael J. Leamy, and Massimo Ruzzene. A Perturbation Approach for Predicting Wave Propagation in One-Dimensional Nonlinear Periodic Structures. *Journal of Vibration and Acoustics*, 132(3):031001, 2010.

[93] Raj K. Narisetti, Massimo Ruzzene, and Michael J. Leamy. Study of wave propagation in strongly nonlinear periodic lattices using a harmonic balance approach. *Wave Motion*, 49(2):394–410, March 2012.

[94] V. F. Nesterenko. Propagation of nonlinear compression pulses in granular media. *Journal of Applied Mechanics and Technical Physics*, 24(5):733–743, 1984.

[95] AN Norris. Finite amplitude waves in solids. *Nonlinear acoustics*, pages 263–277, 1998.

[96] Masayuki Oikawa and Nobuo Yajima. A Perturbation Approach to Nonlinear Systems. II. Interaction of Nonlinear Modulated Waves. *Journal of the Physical Society of Japan*, 37(2):486–496, aug 1974.

[97] Michel Peyrard. The pathway to energy localization in nonlinear lattices. *Physica D: Nonlinear Phenomena*, 119(1-2):184–199, August 1998.

[98] A. Srikantha Phani, J. Woodhouse, and N. A. Fleck. Wave propagation in two-dimensional periodic lattices. *The Journal of the Acoustical Society of America*, 119(4):1995, 2006.

[99] St Pnevmatikos, N Flytzanis, and M. Remoissenet. Soliton dynamics of nonlinear diatomic lattices. *Physical Review B*, 33(4):2308–2321, 1986.

[100] Mason A. Porter, Chiara Daraio, Ivan Szelengowicz, Eric B. Herbold, and P.G. Kevrekidis. Highly nonlinear solitary waves in heterogeneous periodic granular media. *Physica D: Nonlinear Phenomena*, 238(6):666–676, April 2009.

[101] Michel Remoissenet. *Waves Called Solitons*. Advanced Texts in Physics. Springer Berlin Heidelberg, Berlin, Heidelberg, 1999.

[102] J.-F. Robillard, O. Bou Matar, J. O. Vasseur, P. A. Deymier, M. Stippinger, A.-C. Hladky-Hennion, Y. Pennec, and B. Djafari-Rouhani. Tunable magnetoelastic phononic crystals. *Applied Physics Letters*, 95(12):124104, 2009.

[103] M Romanoni, S Gonella, N Apetre, and M Ruzzene. Two-dimensional periodic actuators for frequency-based beam steering. *Smart Materials and Structures*, 18 (12):125023, December 2009.

[104] Philip Rosenau. Dynamics of nonlinear mass-spring chains near the continuum limit. *Physics Letters A*, 118(5):222–227, October 1986.

[105] M. Ruzzene and A. Baz. Control of Wave Propagation in Periodic Composite Rods Using Shape Memory Inserts. *Journal of Vibration and Acoustics*, 122(2): 151, 2000.

[106] Massimo Ruzzene, Fabrizio Scarpa, and Francesco Soranna. Wave beaming effects in two-dimensional cellular structures. *Smart Materials and Structures*, 12(3):363, 2003.

[107] V. J. Sánchez-Morcillo, I. Pérez-Arjona, V. Romero-García, V. Tournat, and V. E. Gusev. Second-harmonic generation for dispersive elastic waves in a discrete granular chain. *Physical Review E*, 88(4):043203, October 2013.

[108] Francisco Santibanez, Romina Munoz, Aude Caussarieu, Stéphane Job, and Francisco Melo. Experimental evidence of solitary wave interaction in Hertzian chains. *Physical Review E - Statistical, Nonlinear, and Soft Matter Physics*, 84(2):1–5, 2011.

[109] G Schneider. Justification and failure of the nonlinear Schrödinger equation in

case of non-trivial quadratic resonances. *Journal of Differential Equations*, 216 (2):354–386, 2005.

[110] Guido Schneider, P.G. Kevrekidis, and Christopher Chong. Justification of leading order quasicontinuum approximations of strongly nonlinear lattices. *Discrete and Continuous Dynamical Systems*, 34(9):3403–3418, 2014.

[111] S Sen and M Manciu. Solitary wave dynamics in generalized Hertz chains: an improved solution of the equation of motion. *Physical review. E, Statistical, nonlinear, and soft matter physics*, 64(5 Pt 2):056605, 2001.

[112] A Shabat and V Zakharov. Exact theory of two-dimensional self-focusing and one-dimensional self-modulation of waves in nonlinear media. *Soviet Physics JETP*, 34(1):62, 1972.

[113] Sicong Shan, Sung H. Kang, Pai Wang, Cangyu Qu, Samuel Shian, Elizabeth R. Chen, and Katia Bertoldi. Harnessing Multiple Folding Mechanisms in Soft Periodic Structures for Tunable Control of Elastic Waves. *Advanced Functional Materials*, 24(31):4935–4942, August 2014.

[114] A. Sievers and S. Takeno. Intrinsic Localized Modes in Anharmonic Crystals. *Physical Review Letters*, 61(8):970–973, August 1988.

[115] M. M. Sigalas and E. N. Economou. Comment on acoustic band structure of periodic elastic composites. *Physical Review Letters*, 75(19):3580, 1995.

[116] Mihail Sigalas, Manvir S. Kushwaha, Eleftherios N. Economou, Maria Kafesaki, Ioannis E. Psarobas, and Walter Steurer. Classical vibrational modes in phononic lattices: Theory and experiment. *Zeitschrift fur Kristallographie*, 220(9-10):765–809, 2005.

[117] Ole Sigmund and Jakob Søndergaard Jensen. Systematic design of phononic band-gap materials and structures by topology optimization. *Philosophical transactions. Series A, Mathematical, physical, and engineering sciences*, 361(1806):1001–1019, 2003.

[118] J. C. Simo and N. Tarnow. The discrete energy-momentum method. Conserving algorithms for nonlinear elastodynamics. *ZAMP Zeitschrift für angewandte Mathematik und Physik*, 43(5):757–792, 1992.

[119] Alessandro Spadoni and Chiara Daraio. Generation and control of sound bullets with a nonlinear acoustic lens. *Proceedings of the National Academy of Sciences of the United States of America*, 107(16):7230–4, April 2010.

[120] Alessandro Spadoni, Massimo Ruzzene, Stefano Gonella, and Fabrizio Scarpa. Phononic properties of hexagonal chiral lattices. *Wave Motion*, 46(7):435–450, November 2009.

[121] Yuli Starosvetsky and Alexander Vakakis. Traveling waves and localized modes in one-dimensional homogeneous granular chains with no precompression. *Physical Review E*, 82(2):1–14, August 2010.

[122] William C. Swope, Hans C. Andersen, Peter H. Berens, and Kent R. Wilson. A computer simulation method for the calculation of equilibrium constants for the formation of physical clusters of molecules: Application to small water clusters. *The Journal of Chemical Physics*, 76(1):637, 1982.

[123] T. Taniuti and N. Yajima. Perturbation method for a nonlinear wave modulation. I. *Journal of Mathematical Physics*, 10:1369, 1969.

[124] C. Tchawoua, T. C. Kofane, and A. S. Bokosah. Asymmetric envelope and dark solitons in diatomic chains. *Physical Review B*, 50(6):4189–4192, 1994.

[125] Morikazu Toda. Studies of a non-linear lattice. *Physics Reports*, 18(1):1–123, May 1975.

[126] V. Tournat, V. E. Gusev, and B. Castagnède. Self-demodulation of elastic waves in a one-dimensional granular chain. *Physical Review E - Statistical, Nonlinear, and Soft Matter Physics*, 70(5 2):1–14, 2004.

[127] Akira Tsurui. Wave Modulations in Anharmonic Lattices. *Progress of Theoretical Physics*, 48(4):1196–1203, 1972.

[128] Akira Tsurui. Wave Modulations in Anharmonic Diatomic Lattices. *Progress of Theoretical Physics*, 49(4):1121–1129, 1973.

[129] Miki Wadati. Wave Propagation in Nonlinear Lattice. I. *Journal of the Physical Society of Japan*, 38(3):673–680, March 1975.

[130] Pai Wang, Filippo Casadei, Sicong Shan, James C. Weaver, and Katia Bertoldi. Harnessing Buckling to Design Tunable Locally Resonant Acoustic Metamaterials. *Physical Review Letters*, 113(1):014301, July 2014.

[131] Liang-Yu Wu, Mei-Ling Wu, and Lien-Wen Chen. The narrow pass band filter of tunable 1D phononic crystals with a dielectric elastomer layer. *Smart Materials and Structures*, 18(1):015011, 2008.

[132] Jinkyu Yang, Claudio Silvestro, Sophia N Sangiorgio, Sean L Borkowski, Edward Ebramzadeh, Luigi De Nardo, and Chiara Daraio. Nondestructive evaluation of orthopaedic implant stability in tha using highly nonlinear solitary waves. *Smart Materials and Structures*, 21(1):012002, 2012.

[133] N. Zabusky and M. Kruskal. Interaction of "Solitons" in a Collisionless Plasma and the Recurrence of Initial States. *Physical Review Letters*, 15(6):240–243, August 1965.

[134] Norman J. Zabusky and Gary S. Deem. Dynamics of nonlinear lattices I. Localized optical excitations, acoustic radiation, and strong nonlinear behavior. *Journal of Computational Physics*, 2(2):126–153, November 1967.

[135] LK Zarembo and VA Krasil'Nikov. Nonlinear phenomena in the propagation of elastic waves in solids. *Physics-Uspekhi*, 13(6):778–797, 1971.

Appendix A

Dispersion Relation for Weakly Nonlinear Periodic Structure

One of the important features of nonlinearity is the amplitude-dependence of the dispersion relation. For weakly nonlinear structures, any perturbation technique such as the $Lindstedt - Poincaré$ method or the multiple scale perturbation expansion can be employed. In the multiple scale method, the excitation is assumed to be a continuous, constant monochromatic excitation such that the slower multiple scale variables are only a function of the temporal variable, i.e.,

$$u_n(t) = A(\varepsilon t, \varepsilon^2 t, \cdots) e^{i(kn-\omega t)}.$$

Under this assumption, the multiple scale expansion can be written using the total derivative as

$$\frac{d()}{dt} = \frac{\partial()}{\partial T_0} + \varepsilon \frac{\partial()}{\partial T_1} + \varepsilon^2 \frac{\partial()}{\partial T_2},$$

where $T_0 = t$, $T_1 = \varepsilon t$, and $T_2 = \varepsilon^2 t$. The equations of motion for the nonlinear spring-mass chain considered in chapter (2) are

$$\epsilon^0 \quad : \quad m\,\frac{\partial u_n^0}{\partial T_0^2} + K_2\,(2u_n^0 - u_{n-1}^0 - u_{n+1}^0) = 0 \tag{A.1}$$

$$\epsilon^1 \quad : \quad m\,\frac{\partial u_n^1}{\partial T_0^2} + K_2\,(2u_n^1 - u_{n-1}^1 - u_{n+1}^1) = F^1 \tag{A.2}$$

$$\epsilon^2 \quad : \quad m\,\frac{\partial u_n^2}{\partial T_0^2} + K_2\,(2u_n^2 - u_{n-1}^2 - u_{n+1}^2) = F^2 \tag{A.3}$$

where, F^1 and F^2 are given as

$$F^1 = -2m\frac{\partial^2 u_n^0}{\partial T_1 \partial T_0} + K_3\,[(u_{n+1}^0 - u_n^0)^2 - (u_n^0 - u_{n-1}^0)^2] \tag{A.4}$$

$$\begin{aligned} F^2 = {} & -2m\frac{\partial^2 u_n^0}{\partial T_2 \partial T_0} - m\frac{\partial^2 u_n^0}{\partial T_1^2} - 2m\frac{\partial^2 u_n^1}{\partial T_1 \partial T_0} \\ & + K_3\,[(u_{n+1}^1 - u_{n-1}^1)(u_{n+1}^0 + u_{n-1}^0 - 2u_n^0)] + K_3\,[(u_{n+1}^0 - u_{n-1}^0)(u_{n+1}^1 + u_{n-1}^1 - 2u_n^1)] \\ & + K_4\,[(u_{n+1}^0 - u_n^0)^3 - (u_n^0 - u_{n-1}^0)^3]. \end{aligned} \tag{A.5}$$

At $\mathcal{O}(1)$, the solution can be written as

$$u_n^0 = A_0(T_1, T_2) + A(T_1, T_2)\,e^{i(kn - \omega_0 T_0)} + A^*(T_1, T_2)\,e^{-i(kn - \omega_0 T_0)}, \tag{A.6}$$

where ω_0 satisfies the linear dispersion relation. Enforcing the requirement of non-secularity of solutions at $\mathcal{O}(\varepsilon)$, the constraint on A can be derived as

$$\frac{\partial A}{\partial T_1} = 0 \quad \rightarrow \quad A = A(T_2) \tag{A.7}$$

Eqn. (A.7) implies that the amplitude is not dependent on the slow time-scale $T_1(\varepsilon t)$. The particular solution at $\mathcal{O}(\varepsilon)$ is

$$u_n^1 = i\frac{K_3}{K_2}\cot\frac{k}{2}A^2(T_2)\,e^{i2(kn - \omega_0 t)} + c.c. \tag{A.8}$$

At $\mathcal{O}(\varepsilon^2)$, the constraint on A can be derived as

$$i2m\omega_0\frac{\partial A}{\partial T_2} - K_3\left[8\sin^2 k|A|^2A\right] + K_4\left[48|A|^2A\sin^4\frac{k}{2}\right] = 0 \tag{A.9}$$

Since the excitation is assumed to be a continuous constant excitation, the amplitude can be written as

$$A(T_2) = re^{-i\omega_2 T_2} \tag{A.10}$$

Substituting eqn. (A.10) in eqn. (A.9),

$$\begin{aligned} 2m\omega_0\omega_2 - \frac{K_3^2}{K_2}\left[8\sin^2 kr^2\right] + K_4\left[48r^2\sin^4\frac{k}{2}\right] &= 0 \\ \omega_2 &= \left(\frac{K_3^2}{K_2^3}(4K_2 - m\omega_0^2) - \frac{3K_4}{2K_2^2}m\omega_0^2\right)\omega_0 r^2 \end{aligned} \tag{A.11}$$

Using eqn. (A.11), the harmonic solution at $\mathcal{O}(1)$ can be written as

$$u_n^0 = r\cos(kn - (\omega_0 + \varepsilon^2\omega_2)t). \tag{A.12}$$

If the higher order terms in the multiple scale expansion can be neglected, the dispersion relation for the weakly nonlinear periodic structure can be written as

$$\omega(k) = \omega_0(k) + \varepsilon^2\omega_2(k), \tag{A.13}$$

where

$$\omega_0 = \sqrt{K/m}\sqrt{2 - 2\cos(k)} \tag{A.14}$$

$$\omega_2 = \left(\frac{K_3^2}{K_2^3}(4K_2 - m\omega_0^2) - \frac{3K_4}{2K_2^2}m\omega_0^2\right)\omega_0 r^2 \tag{A.15}$$